Final report

Prepared for:

Deltares

Viability study of a prototype windstorm for the Wadden Sea surges

WTI 2011

Project A2239

May 2009

Client **Deltares**

Title **Viability study of a prototype windstorm for the Wadden Sea surges**

Abstract

This study investigates whether and how a windstorm prototype can be used to simulate the severe surges and associated currents in the Wadden Sea realistically. This prototype is inspired to the measurements of the overhead wind due to atmospheric cyclonic circulation in the North Sea. Prototype-like synthetic profiles of wind speed and direction prescribe the peak wind speed, the durations of rising speeds and of a subsequent plateau, and the compass sector swept by the wind while turning clockwise. The wind fields are uniform over the entire computational domains, and tidal effects are omitted to concentrate on wind-driven surges. A 270-strong set of synthetic windstorm-surge events is simulated with the WAQUA solver. Six historical events are also simulated with synthetic wind profiles fitted to measurements. It is argued that uniformity is still too a restrictive condition on the wind field to simulate realistic surges in the Wadden Sea; that more than one windstorm prototype may be relevant to the area; and that the construction of synthetic weather events should be connected to their probability of occurrence.

References Offer A2239, d.d. 27 August 2008
Overeenkomst Prototype Storm. HYE-34231/H5100_20/JG/rr

Rev.	Originator	Date	Remarks	Checked by	Approved by
0	G. Lipari	29 Sep 2008	Preliminary report	G.Ph. v Vledder	G.Ph. v Vledder
1	G. Lipari	17 Oct 2008	Preliminary report	G. v Banning	G.Ph. v Vledder
2	G. Lipari G.Ph. v Vledder	21 Nov 2008	Draft report	J. Adema G.Ph. v Vledder	H.J. Steetzel
3	G. Lipari G.Ph. v Vledder	4 Feb 2009	Revised draft report	J. Adema G.Ph. v Vledder	H.J. Steetzel
4	G. Lipari	13 May 09	Final report	G.Ph. v Vledder	H.J. Steetzel

Document Control		Contents	Status
Report number:	A2239R1	text pages : 58	☐ preliminary
Keywords:	Wadden Sea, WAQUA, synthetic winds, storm surges	tables : 10	☐ draft
		figures : 75	☑ final
		appendices : 1	
Project number:	A2239		
File location:	A2239R1r4.doc		

Alkyon
Hydraulic Consultancy & Research

postal address
PO Box 248
8300 AE, Emmeloord
The Netherlands

visiting address
Voorsterweg 28, Marknesse
tel : 0527 24 81 00
fax: 0527 24 81 11

e-mail
info@alkyon.nl
internet
http://www.alkyon.nl

Contents

List of tables

All tables are in the body of the text.

List of figures

All figures are grouped at the end of the report.

Executive summary

This study aims at investigating whether and how a prototype for windstorms can be used to realistically simulate severe surges and associated currents in the Wadden Sea. This prototype is inspired to the wind associated with atmospheric cyclonic circulation in the North Sea. Prototype-like synthetic profiles of wind speed and direction prescribe the peak wind speed, the durations of rising speeds and of a subsequent plateau, and the compass sector swept by the wind direction while turning clockwise. The wind fields are uniform over the entire computational domains, and tidal effects are omitted to concentrate on wind-driven surges.

In the first part of this study, the real-world storms typical to the Dutch weather are briefly outlined, and a conceptual framework to categorise synthetic as well as historical windstorms is developed. In the second part, a test set of 270 synthetic windstorms is defined and applied to the flow simulations for the Wadden Sea using the WAQUA solver on the nested CSM-ZuNo domains. In the third part, the surge results at the stations Den Helder, Lauwersoog and Delfzijl are discussed and put in relation with the overall strength of the surge as well as, tentatively, with the defining parameters of the synthetic windstorms. In addition, selected historical storms were fitted with the synthetic prototype-like model in order to infer the amount of realism in the corresponding surges. The criterion to assess the viability of the schematisation of a prototype windstorm was based on simply comparing the predicted surges with the observed ones for the selected historical storms.

The results indicate that the chosen set of parameters is necessary to model a prototype windstorm through a uniform unsteady wind, although more realistic models allowing for the parent pressure field can be devised. The coverage of parameter values proved to be sufficient to determine a large number of different surge scenarios, but probably not yet large enough to infer systematic connections between windstorms and surges. Several surges in the Wadden Sea that possibly belong to another hydrodynamic ‘regime’ were found that differ from some recent historic severe storms.

Several recommendation for further advancement follow, regarding the number of windstorm prototypes, spatially varying wind fields, surge-tide interaction, and so forth. The construction of the synthetic storms needs to be linked to both driving physical processes and their probability of occurrence. The latter requirement is necessary for inclusion in a probabilistic environment for the regulatory Hydraulic Boundary Conditions.

This study was performed in the framework of WTI-2011 as a step in developing applicable methods for determining the Hydraulic Boundary Conditions in the Wadden Sea with realistic surges and associated currents, while accounting for the dynamic behaviour of wind storms. Unfortunately, the present schematisation of a prototype wind storm is still not ready as an operational tool for WTI-2011 because the complexity of the problem cannot be resolved with the proposed schematisation, which proved to be more complex than expected at the start of this study.

1 Introduction

1.1 Context

The present study aims at unravelling whether the concept of a `prototype' windstorm can be used as a basic as well as a general scheme to model the storm/surge events in the Wadden Sea (WS, hereinafter) for application in the determination of the Hydraulic Boundary Conditions (HBC). This study was performed in the framework of WTI-2011 as a step in developing applicable methods for determining the Hydraulic Boundary Conditions in the Wadden Sea with realistic surges and associated currents, while accounting for the dynamic behaviour of wind storms.

As ascertained in Alkyon (2008a), historical storms with a consistent pattern have generated the recent most severe surges in the eastern WS. This pattern consisted of winds with rising speed and clockwise rotation from near-south to near-north. The underlying insight is that the generation and propagation of extreme water levels in the Wadden Sea are strongly dependent on the temporal variability of the storms.

1.2 Problem description

Previous studies (e.g. Alkyon, 2007, 2008a) proved that modelling the dynamical storm behaviour is necessary. One of the outcomes of Alkyon (2008a) was that the oversimplification of wind fields made steady resulted in unrealistic surges. Instead, it was recognised that a parameterisation of the windstorms allowing for dynamic behaviour was required to produce more realistic results of peak water levels and associated currents. We became, therefore, at want of non-oversimplifying schemes that can be used to determine severe surge conditions on the shore, and include their dynamics accurately enough to produce realistic results. If this approach is viable, it might open the way to include the dynamics of storms in the probabilistic determination of the HBC for the WS area.

In Alkyon (2007) it was found that currents significantly affect the wave conditions in the Wadden Sea during severe storms. This finding implied that current effects are certainly relevant to the HBC for the Wadden Sea. The present methodology to determine the HBC uses steady wind fields, and current effects are disregarded therein.

Alkyon (2008a) performed an investigation to find physically-based procedures to simplify the wind fields that generate severe surges and use them as forcing on the WS basin. The main benefit of such an approach is that the current fields associated to the storm surges can be accurately simulated, and reliable, physically-based estimates can be determined.

Conveniently, such a prototype shape seems to be expressible through the rate at which the wind speed increases to a maximum; the maximum wind speed itself; the duration of this maximum; the initial wind direction; the rate of turning; and the final direction. **The suitability and reliability (i.e. viability) of a schematisation in terms of those parameters is studied here**. Based on that recommendation, we have tested the parameterisation of a 'prototype storm' with the above-mentioned six parameters as a start. This choice should only be considered as a working assumption; since it may well be that additional parameters are required.

We also made other working assumptions, like performing tide-free computations and applying a uniform wind field. Those are presented afterwards, and their likely impact commented when appropriate.

1.3 Objective

The primary objective of this study is to verify if the duration, initial and final conditions, and rates of change of a windstorm are "a necessary and sufficiently complete set of parameters to describe a prototype storm". This investigation, additionally, has the character of a feasibility study to identify remaining knowledge gaps as well as to indicate possible adaptations to the methodology with which the regulatory Hydraulic Boundary Conditions (HBC, hereinafter) are currently computed. The second aim is to include a more accurate description of the physics.

1.4 Approach

The core question is approached in several steps.

The first step is to understand whether the structures of the wind speed and direction in the prototype windstorm (PW, hereinafter) are consistent with typical and relevant atmospheric processes occurring in the Netherlands. This task provides physical backing and perspective for the PW concept, and is discussed in Chapter 2.

The PW concept provides an indication on the general behaviour of surge-generating windstorms, but it is not able to determine a unique shape having one all-purpose rising and rotating wind. Therefore, a number of shapes and adequate ranges of variability for the shape parameters need to be chosen to represent different heavy stormy conditions. Each realisation is thus one synthetic windstorm that generates its own surge. This approach yielded a number of problems; firstly, how to distinguish and classify such a population of storms; secondly, how to connect those and their effects on the shore; and thirdly how to single out the windstorms that have a potential to bring hazard on to the coast in the form of high surges. This is an essential problem of data recognition and management.

In Chapter 3 we propose a physically-based presentation model that is able to `frame' the storms based on their duration, peak speed and energy content, with respect to speeds; and on the rate of rotation, with respect to direction. Their handling is worked out to a certain degree of detail, and it requires further attention to be fine-tuned, especially considering that the physical connection between windstorms and water flow is complex and therefore elusive to intuitive schematisations.

Once a framework to present and interpret a high number of storm/surge events is available, we turn to the choice of the speed and direction parameters that define a test set of 270 temporal profiles, chosen of triangular and trapezoidal shape. In addition, we applied the current prototype-storm schematisation to the six historical year-record storms of Alkyon (2008a) to further investigate its capacity of reproducing realistic surges. The synthetic windstorms are presented in Chapter 4.

In Chapter 5 we discuss the flow simulations carried out with Rijkswaterstaat's WAQUA-in-SIMONA solver on the nested domains of the Model Train.

The flow simulations are carried out in a number of phases. Firstly, high-resolution calculations, like those from the Kuststrook domain, are carried out for just a few cases on the grounds of the high number of runs and computational economy. The likely impact of this working assumption is discussed. Further, because the windstorm is defined as a given uniform wind field, rather than a travelling atmospheric system, the arbitrary extension of the windblown area may have an impact on the local circulation that is assessed. All these considerations also provide interesting insights on the hydrodynamic behaviour of the Wadden Sea.
Secondly, the complete set of surge results obtained on the (nested) ZuNo domain after a uniform wind field applied on the same area is discussed. A bird's eye view over the results is given by relating the surge peaks at the stations of Den Helder, Lauwersoog and Delfzijl with the local exceedance levels and with the volume of water that the windstorm has driven into the Wadden Sea. This approach condenses information about the onshore water levels and the general hydrodynamic behaviour of the whole basin with the through-flux across the tidal inlets. The results show that a wide range of surges is simulated, also including rather extreme events.

In Chapter 6 a connection between surges and storms is discussed based on the results of our test set. This is done with the tone of an exploratory exercise by seeking simple monovariate and bivariate relations between the strength of the surge and the parameters of the windstorm.

Lastly, conclusions and recommendations are given in the closing Chapters 7 and 8. Here, attention is also paid to knowledge gaps that have been identified regarding the need for further investigation and to the relation with the determination of the Hydraulic Boundary Conditions for the Wadden Sea.

1.5 Scope limitations

In this phase we do not attempt to assign a probability of occurrence to each windstorm, as would be required in the probabilistic approach of determining the HBC. Such an assignment can only be made, once sufficient confidence is obtained in the procedures of prototype-storm parameterisation. Other working assumption concerning the wind fields are listed in Section 2.3.1.

Because we are primarily interested in wind-generated storms, the astronomical forcing is not considered in this study. Including such a forcing is not a trivial exercise because the interplay between tides and surges is still not fully understood. By omitting tides we could better focus on the hydro-dynamic interplay between windstorms and surges.

Tides are not considered. This would lead to an extra complication to test the viability of the windstorm concept, especially because we know that **a non-linear coupling exists between tides and surges** – see, for example, Dillingh et al (1993). For instance, in Alkyon (2008a) the potential hazard of historical storms was determined by subtracting the astronomical tide from the total water levels for the sake of progress. Close inspection of those results also indicated that the tide-free surge signal shows oscillations, especially during low wind speeds, which could also be due to unresolved tidal constituents.

Waves also are not modelled.

Conclusions are based on numerical-modelling results with their inherent calibration and resolution limitations. In line with the project's original plan, only briefly in Sections 4.2 and 5.3 do we compare computed with measured water level histories for the purpose of description and not for validation.

Lastly, during the execution of this project, we resorted to some working assumptions for the sake of progress. They are introduced as relevant. Those are further mentioned among the conclusions and recommendations only as and if they resulted in concerns about serious knowledge gaps.

1.6 Team

This study has been conducted by Giordano Lipari and Gerbrant van Vledder of Alkyon Hydraulic Consultancy and Research BV for Deltares.

Giordano Lipari has developed the viability study, and Gerbrant van Vledder has dealt with the link to the HBC. The simulations have been run by Giordano Lipari with contributions of Jeroen Adema (wind field) and Mattijs Wakker (post-processing). The project has been managed by Gerbrant van Vledder.

The report has been controlled by Gijs van Banning, Jeroen Adema, Joost Hoekstra and Gerbrant van Vledder (for parts he has not written).

Jacco Groeneweg of Deltares has led the project. The external reviewers were Herman Gerritsen and Joost Beckers of Deltares.

2 Bases of the prototype windstorm

2.1 Definitions

Prototype windstorm (PW) is the term introduced in Alkyon (2008a) to define some essential features of the storm winds recorded at Huibertgat during the most six severe year-record surges at Delfzijl in the period 1981-200Huibertgat is the only wind station covering the eastern area of the Wadden Sea, with the earliest measurements taken in 1981. Delfzijl was chosen a station statistically representative of the eastern Wadden Sea (WS) in surge conditions. By eastern WS, here, we mean the part broadly corresponding to the coasts of the eastern part of the province of Friesland and of the province of Groningen.

The term 'windstorm' is preferred over the term 'storm', as the latter includes the entirety of wind, currents, waves, tide and surge that can be seen in episodes of tumultuous weather. Although windstorm precisely refers to storms with heavy winds and little precipitation, we use the term as a name of convenience for the atmospheric forcing only. In this study we are interested in finding and testing a synthetic form of the *storm winds* that can realistically replace a wide class of hazardous historical storms – from which to simulate surges with a numerical flow solver.

Figure 2.1 reproduces the wind histories for the above surges reviewed in Alkyon (2008a), with values grouped into 6-hour averages. Those storm winds approached Huibertgat with clearly common trends for speed and direction that appeared in the last few days before the day of the highest surge at Delfzijl – indicated by the horizontal interval (0,1). Although with different paths for each individual storm, the speed increased up to Beaufort force 9 and the direction turned from S-SW to NW-N sectors. The arrows can be read as indicators of the behaviour of the PW.

Section 2.1 shows that this behaviour of the airflow's is very likely the footprint of cyclones travelling eastwards across the southern North Sea, which are thought to be responsible for most of the major stormy events in the area.

Section 2.2 shows what we can, or cannot, expect from an a priori specification of the PW.

2.2 Weather systems in the North Sea

2.2.1 Generalities about cyclonic air circulations

Unless otherwise stated, the information in this subsection is based on the notions of general meteorology reported in the Admiralty Sailing Direction, 1959; and from Parker 1988.

It is well known that the conventional *synoptic charts* visualise a *depression* as a series of closed isobars around an area (*low*) where atmospheric pressure is lower than in the surroundings. Pressures values are given at the mean sea level. A pressure low implies that the air is locally rising from ground level and cooling in the updraft. Circulating horizontal air flows develops in the larger area around the low.

Depressions are not, by any means, the only pressure patterns that generate wind. However, it is acknowledged that they are responsible for "most of the occasions of strong winds and unsettled weather" in mid latitudes (ASD 1959). One depression can be distinguished from any other by:

- Shape (enclosed by a chosen isobar, and more or less oval in shape);
- Size (radii of a few hundreds to a few thousands of kilometres);
- Depth (the difference in pressure between centre and boundary of the depression, defined in some way);
- Lifetime (the duration over which an individual character holds, in the scale of 4-6 days);
- Path (the trajectory that the low follows on the Earth's surface); and:
- Rate of travel (the instantaneous speed at which the centre of a mobile depression moves, in the region of 5-20 m/s and with peaks up to 30 m/s).

The horizontal air flow in the upper atmosphere associated with a depression is called *cyclone*. As the friction due to the Earth's surface is negligible in the upper atmosphere, the motion of those air masses is driven by the dynamical balance of pressure and Coriolis forces only. This entails that cyclonic air flow is anticlockwise in the northern hemisphere, approximately along the isobars with a slight inclination towards the low. Lower near to the Earth's surface, friction tends to further steer the wind direction toward the direction of the pressure's downward slope, increasing the cross-isobar speed component.

Shape, size and depth of the depression are reflected by the distribution of isobars and associated pressure gradients. Regardless whether the air flow belongs to the near-surface or the upper layer, the air speed increases as the local pressure gradient does. An increase of pressure gradients is displayed by closer isobars – narrowing isobars indicate a spatially increasing wind speed.

The development of a depression is influenced by a number of features. A more or less wide *warm sector* can be present in the equatorward flank of the low, because of intrusion of neighbouring air masses having warmer temperatures in comparison. Depressions generally travel approximately in the direction of the wind along the isobars of the warm sector. A warm sector is delimited by an upwind, faster *cold front* and a downwind, slower *warm front*, both moving anticlockwise (in our hemisphere). As and if, at some point and place, the cold front behind manages to catch up with the warm front ahead, the air in the warm sector is lifted up, and the two cold masses that once delimited the sector meet there (*occlusion*). After the first point of occlusion, this process progresses so that the pressure low is filled up by the colder air and the warm sector is displaced upward. This process promotes the extinction of the depression. Alternatively, a persisting warm sector may deepen and accelerate the depression, as well as enhance the associated wind speeds. Moreover, a parent depression may also shed a secondary depression that occasionally produces gale-force winds (Bft 8) unseen in the primary depression. All those conditions, of course, vary according to the characteristics of the different air masses at play (such as temperature and humidity), on the interaction with the neighbouring weather systems and, at large, on the state of overall atmospheric circulation.

2.2.2 On weather systems that are important for the Netherlands

Unless otherwise stated, the information of this subsection is based on Admiralty Sailing Direction, 1999 – covering the eastern part of the North Sea from Scheveningen to Skagen in Denmark.

The weather in the southern North Sea is mostly determined by the Azores and Scandinavian anticyclones (high-pressure areas) and by the Atlantic depressions.

The relatively stationary or slow-moving Scandinavian anticyclone can bring NE to SE winds occasionally reaching gale force (Bft 8). The Atlantic depressions, by contrast, are commonly secondary offshoots of larger systems, and sweep the northernmost quarters of the North Sea with rates of travel of up to 10-20 m/s. An extreme low value for pressure is 950 mb, and pressure changes of up to 40 mb in 24 hours are possible. Such depressions have seldom an erratic path and mostly travel eastwards, although they may be deflected more often northwards than southwards if a stationary Scandinavian anticyclone happens to obstruct their transit. Winter depressions are deeper than summer ones and lead to stronger winds, all other conditions being equal. Depressions can also occur in groups of 3 and 4 with similar tracks at intervals of 1 to 2 days.

Based on this description, the Atlantic depressions are the weather systems most likely to bring heavy winds over the Dutch coast, which is therefore exposed to their southern flank. As a depression travels eastwards, the first winds to make landfall blow from within the south-to-west quadrant, whereas the last ones to leave the coast behind do so from within the west-to-north quadrant. The precise headings of the wind during a storm, of course, depend on the path and shape of the depression, but a transiting cyclone, regardless of its intensity, produces the clockwise rotation of the wind (also said *veer*) on the Dutch coast. Gale force winds (force 8) are expected in the 15% of occasions in the southern North Sea. With regards to duration, the records at the stations of Helgoland and Die Elbe in Germany show that 64% of gales last for less than 4 hours, 20% for 4 to 6 hours, 10% for 6 to 12 hours and 4% for 12 hours or more.

The flatness of the Dutch coast is unlikely to play a major steering effect on the approaching wind. Variations can be expected due to the increased roughness above land over that above sea. For instance, this may result either in a perturbed offshore wind past the Wadden Islands, or in a mild funnelling effect into the Eems-Dollard estuary as a corridor of reduced friction compared to land.
The analysis of the Climatic Tables compiled on a period over 13 years (past 1961) shows that the annual number of days of gale-force winds is 8 at Den Helder and 28 at Terschelling, in the westernmost and central WS area respectively. This suggests that an internal variability does exist, although such aggregated data cannot make it clear whether this is due to different weather systems or to different sheltering at either station for the same weather systems. Additionally accounting for such effects requires wind fields defined to a suitably small scale, arguably more refined that those of the customarily used HIRLAM fields (11-km spaced grid). On the other hand, the eight wind histories at Texelhors and Huibertgat examined in Alkyon (2008a) were at least qualitatively related, so that those weather events were encompassing the entire WS.

We leave those remarks on a qualitative basis, referring to other specific studies for quantitative determinations. In any case, we can safely assume that, for the level of detail required by this investigation, the changes of the wind field in the WS due to the sheltering of the barrier islands is an effect that can be accounted for at any later stage. Land effects on the overall wind flow become (at least relatively) weaker as the wind speed increases. So, we may expect that for the present practical purposes we can omit such effects of land roughness. To account for such effects, additionally, high-resolution wind fields would be appropriate.

2.3 Assumptions and potentialities of the PW

The fundamental knowledge on the weather systems in the North Sea discussed above seems sufficient to lend credibility to the scope of the PW schematisation. If this approach yields acceptable results, it can be regarded as a first advancement towards the inclusion of storm dynamics in the HBC. Further, it will be improvable by as much refinement on physical and statistical grounds as necessary. Whether our approach is sufficient for the purposes will be determined in the subsequent chapters in which the results of the simulations are discussed.

2.3.1 Working assumptions

The setup of the concept of the six-parameter windstorm was a logical step in view of preceding studies (e.g. Alkyon, 2008a). However, during the course of this study we realized, firstly, that the identification of surge-generating windstorms suffers from a lack of complete knowledge in many respects – and, secondly, that an all-encompassing modelling approach is not realistic. This awareness led to a list of working assumptions which can also be considered as potential improvements for further studies.

In particular, with regards to the wind modelling, this study makes **no attempt** to determine:

- In which proportions of frequency and intensity the heavy winds generated by depressions prevail over those generated by other weather systems. Here, **we are assuming without proof that depressions represent the entirety of the stormy-weather events**. Other studies in the past have touched this topic: Kruizinga (1978) produced, for example, a classification of the pressure fields according to four different basic patterns combined in a way to generate up to 30 derived patterns. Dillingh et al. (1995) then determined the connection of the surges at Hoek van Holland and such basic patterns for 30 year worth of data.
- How the wind parameters used to describe a PW model relate to the features of the real-world depressions and, additionally, to their probability of occurrence. In the meantime, we can assume that two subsets of depressions exist; the ones that cause storm winds for which the PW-based schematisation is a fair representation; the others that result in histories of wind speed and direction for which the synthetic temporal profiles of the PW type are insufficient. Here, **we assume without proof that the PW-type synthetic winds represent, at the very least, all the storms with severe surges in the WS**;
- How the lifecycle of the depression affects the temporal wind (speed and direction) profiles on the WS area. In reality, the pressure and velocity fields are coupled. Assuming that the pressure is purely an external force is an approximation, because the displacement of air masses brings about an obvious continuous rearrangement of the pressure field that drives them. As will be seen in Chapter 5, any correspondence between air pressure and velocity needs to be broken anyway as soon as a uniform artificial wind is applied to a limited area. However, **a higher-level schematisation of the windstorm scenarios could be obtained by modelling the transit of synthetic depressions over the southern North Sea and taking the wind field as a result to force the waters with**. Of course, investigating the physical connection between a depression's different features and its associated wind is an extension of the present study. This is tantamount to modelling synthetically the causes one grade up in the chain of consequences (the atmospheric forcing is the cause of the wind which is a cause of the surge, and can directly cause additional sea level rises by pressure action);

- How the spatial variability of the wind field is important. For the purpose of description, we may think of a depression that has an unchanged circular shape while transiting over the WS. Even if the pressure gradient is uniform (depression with uniform slope), the wind speed and direction are non-uniformly distributed because air rotates at different distances around the pressure low. The wind, however, will be steady when seen from the pressure low. A distance of 160 km (a rough estimate for the length of the Dutch WS as well as a lower size for a depression) is covered at 20 m/s (the rate of travel of a fast cyclone) in little more than 2 hours. So, at any time during the transit, every location in the area will experience conditions different from neighbouring points, since the cyclone's size is comparable with the scale of the basin. Conversely, when a whole sector of the depression is wide enough to cover the WS, there is some likelihood that the wind field is to a greater degree uniform (while unsteady) over the basin. However, the change of wind direction will be narrower, because the coast is covered by isobars with a larger radius of curvature along which the air flows. This first-order analysis unveils a possible inconsistency between the assumption of wind uniformity and its rotational character: **a cyclonic wind that changes in time may entail spatial changes in most of realistic cases at the expense of the uniformity assumption**.

2.3.2 What the PW can explain

Based on the derivation of Alkyon (2008a), the PW is best seen as a skeleton structure around which each historical storm acts with specific characteristics. The individual characteristics of the storms inspected in Alkyon (2008a) differed for the storm's durations; for speeds rising with different rapidity and (non-linear and/or piecewise) progressions; and for the directions rotating with different angular speeds over wider or narrower sectors. Chapter 5 of Alkyon (2008a) contains a detailed description of these. The extent of such differences is already apparent from Figure 2.1 and, later from Figure 3.16.

However, in spite of the natural wind variability, the PW description appears to account for the major wind features that drive water from the North Sea into the WS through the tidal inlets, accumulate it into the WS itself and then displace it against different stretches of the coast, thus creating a surge. This is the motivation and ultimate aim of the current task of research. Alkyon (2008a) also contains several series of numerical experiments that suggested that **synthetic windstorms with suppressed temporal variability do not predict surges with any acceptable realism. Thus, it appears that the synthetic profiles based on the PW concept is the natural first step to overcome the steady-state limitation when devising synthetic windstorms**.

It is important to emphasise that the PW concept can be considered as an element in a sequence of weather events. Here, it represents the last wind conditions ahead of a surge high. In particular, it is assumed that the water levels prior to the onset of the PW are undisturbed (that is driven by the tide alone) or, equivalently, that the PW is a lone event. As soon as a historical event is a complex sequence of sub-storms, the PW might be considered as a 'modular' element, like a self-contained unit that can be combined with other units to create different shapes.

Therefore, the PW description is an insightful blueprint to design 'concept windstorms' by specifying suitable temporal profiles for the wind speed and direction that generate the flow and water-level fields of significant surges. It is important to realise that the strength of this project is not about finding the perfectly nature-fitting synthetic storm,

but about thoughtfully connecting any storm (synthetic of a chosen type, in the first instance; but also natural) with its hydrodynamic effects in the interior of the Wadden Sea.

3 Parameterisation of storms

In this study we assume to work with a uniform wind field. So, spatial variations are not considered here. The wind field is unsteady, and the ways the wind speed and direction change needs to be specified. In this Chapter, in particular, we try to define a way to characterise the temporal variation of the wind and distinguish any one windstorm from another. This is important because many synthetic windstorms will be created later in this study; commenting and comparing them is a pointlessly difficult exercise without a **conceptual framework** that supports a classification.

The definition of such a framework is, indeed, the content of the following subsections. We note here that such a framework is not only limited to the application to synthetic storms, but can also host information extracted from whatever storm, including historical ones. **This conceptual framework, in its first conception, aims at making presentation possible and informative**.

The histories of wind speed and direction are the elements of the temporal evolution of the wind storms. The profiles of wind speed and direction, therefore, describe such a temporal variation. The question at stake here is: is it possible to condense the extended information contained in those histories into a smaller number of parameters that describe certain essential features of the wind storms? 'Essential' is intended here, of course, with regards to the wind seen as a mechanical action that can generate currents and surges. **Such a smaller number of informative quantities are the elements of the conceptual framework** that we referred to just earlier. **The conceptual framework is therefore a relation that connects them**.

If one is derived, tabulation and graphical representation enable us to classify the steps taken in pursuit of the artificial (or real) connection between synthetic (or historical) storm winds and surges in the WS area. The similar efforts related to the surge parameterisation are discussed in Chapter 5.

Moreover, the conceptual framework may also turn out to be a validating tool **as and if there is some physically-based *equivalence* between synthetic and historical windstorms that are able to generate similar surges**. This may help to establish a rational connection – either sufficient, necessary, or just complete enough – between synthetic and historical events.

An important consequence of having decoupled the wind from a parent pressure distribution is that the wind speed and direction are separated quantities, the temporal variations of which need to be devised independently. The only gain that we take from the PW profile is that, while the wind veers, its speed increases to a peak or a plateau value. The information contained in the PW only suggests a strong physical connection between speed and direction, but this insight does not yield a mathematical relation. Therefore, the profiles of direction and speed need to be discussed and prescribed separately, albeit in consideration of the PW blueprint (Figure 2.1). The only feature common to both speed and duration profiles is, obviously but importantly, the overall duration of the windstorm. The schematisations used in the current study are described hereinafter and in Chapter 4.

With respect to historical time signals, the wind speed and direction are available from the anemometrical stations. The measurements are continuous, and data may be measured and published at different intervals.

In general, well-established techniques for signal processing, both in the time and frequency domains, may be used to derive a number of shape parameters that condense certain descriptive features of the signal. Once this is done, the synthetic storms may be generated so as to have the same parameters as a set of historical storms.

In this connection, it is clear that **the current PW modelling approach is a somewhat raw and unsophisticated description of the parent historical storms.** However, we do not take the avenue of an elaborate signal processing for the time being. Rather, **we start from a schematisation of the temporal behaviour that is already advancement with respect to the present methodology where steady-state wind fields are only considered**. For the moment, we will use the PW model to generate a simple arithmetical shape for the time profile of wind speed and duration.

The methodology that we propose aims at being as much upgradeable to better physics and modular as possible. We suggest that such a method will be able to host more refined handlings as need be, once it stands the testing against a basic windstorm description. In fact, the PW is informative and close to reality enough to justify its usage the whole way until a first methodology is constructed and evaluated. Only at the point, we can understand whether the methodology embeds a 'complete enough' description of the windstorm. After assessing its sufficiency (or insufficiency), we need to think about how much the good (or bad) results depend either on physics not included, or on a poor description of the physics.

Before we turn to the description of those profiles in Chapter 4, we develop the conceptual framework in which the synthetic will be set and described afterwards.

3.1 Conceptual framework for speed

The PW concept suggests that the following aspects should be at least considered to define a parametric form: the duration of the windstorm; how rapidly and steadily it reaches the peak; and whether the peak value is a point or a plateau.

In the first place, information on the duration of the storm is to be included, as it is conceivable that lower (or upper) temporal threshold exists for the wind to generate a surge (or sustain a gain in water levels on the coast). A minimum duration is related to the time needed to move and drive the waters toward the coast (fetching and accumulation); a maximum duration is connected to the attainment of a steady-state flow when resistive forces from the bottom balance the active forces from the wind drag.

It is already convincing on intuitive grounds that ramping-up speeds are necessary to generate a surge, because otherwise the water would lack strong enough a forcing to drive increasing volumes of piled-up water against the coast. This is obviously favoured by the semi-enclosed structure of the WS. **The underlying view here, gained from Alkyon (2008a), is that the WS surge is an unsteady process of local water accumulation.**

As also shown in Alkyon (2008a), **the peak speed alone is not representative of the capability of a storm to generate a surge**: in fact, historical surges sorted by the peak wind did not rank like when sorted by the corresponding (tide-free) surge. This is because the temporal variability is important to generate surges in the WS, no one storm exactly behaved like another, and similar wind-induced peak water levels could be obtained by different wind histories – recall Figure 2.1.

Finally, it is assumed here that the way in which the speed decreases from the peak to the after-storm values is unimportant because, as the wind forcing terminates, the disengagement from the most critical conditions occurs. Then, the flow driven by the surface slope will move the water away from the shore. The inclusion of a final period, though, can become relevant for studying long-period offshore swells, which often occur

in the tail of a storm and may take advantage of high water levels to penetrate into the Wadden Sea. But this is not crucial for the present purposes.

The information above can be summarised in a verbal equation where an unspecified function *f* connects the storms' speed history and the defining features that we deduced from the temporal profile:

Surge-generating speed = f(duration, ramp-up behaviour, peak value, peak duration)

The number of parameters at the right-hand side is however too large for representation in tabular form on a two-dimensional chart. In particular, as felt necessary, the above verbal equations might even be set on more rigorous grounds by applying the tools of dimensional analysis, which would lead to a parameterisation in terms of fewer dimensionless variables. This is altogether customary in many engineering applications. For the moment, we prefer to work using dimensional quantities that are more readily understandable.

While searching for a scale for the wind speed alternative to the peak value, Alkyon (2008a) proposed that the **average power of the windstorm** (rate of transfer of kinetic energy per unit area) can be used to derive a more insightful speed scale than peak values. A wind blowing at average-power speed transfers the same amount of energy as the real storm over the same period. However, the average-power speed is lower than the peak value and, when used as a replacement value for steady synthetic storms, in Alkyon (2008a), proved to be of two to three Beaufort forces weaker than the peak.

At any rate, energy information must be included since we ultimately aim at describing a process of momentum transfer from the air flow to the water flow, which occurs because the wind does work on the free surface. Therefore, we propose a conceptual framework in the form

Surge-generating speed = f(duration, speed information, energy information).

Once we choose the quantities containing the speed and energy information, the above conceptual framework lets the windstorms be represented graphically as geometrical entities (surfaces – or isolated points referred to as placemarks) in a three-dimensional space. As shown later, the choice of two main parameters to plot in a chart (say speed versus duration or energy information) implies no real loss of information, as we resort to contours for the third quantity. This can also be put in tabular form.

The general formulation of the mechanics of momentum exchange at the air-water interface is reviewed here.

The shear stress exerted by the wind over the water surface is the rate of momentum transferred per unit area, τ_{wind}. This is commonly parameterised by the expression

$$\tau_{wind}/\rho_a = C_D\, u_{10}^{\,2},$$

where the dimensionless drag coefficient C_D depends on the sea-surface state and wind speed in a complex manner, and u_{10} is the wind speed at 10 meter height above the mean sea level. The ρ_a symbol indicates the density of air. As the surface water is set in motion by the wind, the wind does a work on the unit water surface at a rate given by

$$P_{wind} = \tau_{wind}\, u_{water},$$

where P_{wind} is the *wind power per unit area* (in W/m^2 units) and u_{water} is the surface water velocity. This neglects the angle of 30 deg expected between the downwind direction and the drifted water in steady conditions (Admiralty Sailing Direction, 1999) – also discounting the wind and current adjustment in rapidly varying conditions, which further complicates the picture. The integral over time of the above power is the kinetic energy that is transferred from the wind into the drift current (E) – to which we will refer as 'transferred energy' or '**energy content**' leaving it understood that it is an amount 'transferred from the airflow into the water across a portion of interface and depending on its state'.

Approximate scaling arguments can be introduced by considering that $\tau_{wind} \sim u_{10}^2$, and assuming that $u_{water} \sim u_{10}$, whereby $P_{wind} \sim u_{10}^3$. The resulting scale for the energy E per unit mass of air transferred across the unit area of interface in a period T from a speed signal starting at time t is, therefore,

$$E \sim \int_t^{t+T} u_{10}^3 \, dt = e(t,T), \qquad [E] = [e] = L^3/T^2. \tag{1}$$

The quantities E and *e* can be measured in m^3/s^2 as well as in Jm/kg, or any multiple thereof. For speeds in the order of tens of m/s and durations in the scale of days, the e quantity at the right-hand side takes values of order of 10^8 in meter-and-second units. Using km^3/s^2 or kJ·km/kg the order of magnitude of the values reduces to a handier 10^{-1}.

It is important to realise that the quantity, e, at the left hand side is just a scale for E, and that the relationship of proportionality (~) holds with allowances being made, because the drag and skin friction coefficients are far from being linearly dependent on the wind speed. In fact, a more complete and general form for the same quantity would be

$$E(x,y;t,T) = \int_t^{t+T} \alpha \, \beta \, u_{10}^m \, dt, \tag{2}$$

where α is a function resulting from the parameterisation of the drag coefficient and skin-friction factor, also producing an exponent m different from 3; and β is a unknown function introduced as repository of uncertainty – in particular, accounting to the whole range of large-scale process that may affect the intensity of local energy transfer (say, long-fetched waves). The physical dimension of the integral at the right-hand side is, of course, unchanged by the new combination of factors – so as to give L^3/T^2 at all times.

In this work, however, upon referring solely to the cubed wind velocity, u_{10}^3, rather than to the specific expressions for the wind power P_{wind} and surface velocity u_{water}, **we assume the coefficients for some particular, unspecified sea state hold at all times, whether sustained by the actual wind speeds or not**. This is an important limitation that can be removed at a later stage.

From Formula (1), the energy content relates to the area of the wind signal in the time-speed plane, whereby time is implied in it as a measure of its horizontal extension, and so is the average-power speed (u_{ap}) as a measure of its vertical extension, namely

$$u_{ap} = \sqrt[3]{(e/T)}. \tag{3}$$

Formula (3) states the definition of **average-power speed**. So, the e-scale allows for a meaningful comparison between different events, even at the price of levelling out important differences – and it is open to subsequent refinements when better physics

are included. In the following, we will refer to e as just the 'energy content' rather than 'scale for the transferable energy', leaving it understood that, for the time being, we only deal with approximations based on scaling arguments.

The energy information is thus conveyed by the energy content *e* defined by (1). Because the duration T is another basic parameter and the average-power speed u_{ap} is just a result of both e and T via relationship (3), we need an independent speed scale that conveys some information on the speed profile's shape. This scale for speed can then be given by the peak speed u_p.

Therefore, if the temporal speed profile can be parameterised as a product of u_p and a shape function, and if this is plugged into (1), Equation (1) gives the relationship $f=f(T,u_p,e)$ to use as a **framework equation for the windstorm speed**. Its arguments are therefore the **framework variables for the speed profile.**

If the wind is uniform the area of the water body is immaterial, otherwise delimiting the area becomes important, and several specific issues grow relevant – this is noted without further discussion in this study.

3.1.1 Speed-based framework chart for a windstorm

Thanks to the framework equation, each windstorm can be located, or framed, in a chart with either the energy content or the duration in the abscissas, and the peak speed in the ordinates. Figures 3.2 and 3.3 illustrate two fictional scenarios of four events, where either the duration or the energy content is used as horizontal axis respectively. Each event is represented by a bullet point. **Either chart thus works as a speed-based diagram of state for the windstorms.** That is tantamount to saying that the framework variables help define the speed history in terms of its potentiality to transfer energy into the waters.

As we will show shortly, both charts contain the same amount of information, so which of either representation is better is mostly a matter of preference. Of course, it is possible to define a (duration, energy content) chart with contours and gradients of the peak speed – although this is not pursued here for the sake of brevity.

The annotations in the boxes drawn in help connect the data positioning of different windstorms with qualitative information that is also recognisable at a glance. Moreover, in both charts it is possible to plot the contours of the quantity left out, once the shape of the speed profile is known – which is impossible for historical storms, but readily made for constructed ones.

The shape of the contours, we recall, is a result of the shape function of the speed profile. In each of the Figures 3.2 and 3.3, three contours are drawn from a constant-speed signal, that is to say a rectangular temporal profile. This is, of course, the simplest shape. Also note that the values associated to the curves in the charts are only a measure of relative magnitude.

In case of a rectangular signal, the instantaneous value, the peak value and any average are the same, so that $u_p=u_{ap}=u$. So the laws for the iso-energy and iso-duration curves are embedded in the function $u(e,T)=\sqrt[3]{(e/T)}$ of Formula (1). We will refer to those loci as **e-contours** and **T-contours**. Expectedly, this formula is the same of the average-power speed for any generic profile – having its own state (T,u_p,e) –, since the average-power windstorm is a steady equivalent event by construction. The green-amber-red colour coding of the bullet points indicate increasing intensity of the contoured parameter.

The dashed lines, finally, are the gradient curves for the contoured quantities. At each point those lines are always perpendicular to the contour in that same location. In

particular, as a point moves about on the chart, they indicate the direction along which the maximum change of the contoured quantity occurs. We shall refer in brief to those lines as **e-gradients** and **T-gradients** – making allowance for a slight misuse of terminology, since gradients are in fact point vector quantities.

In case the signals are not defined by a well-defined profile function – because of being historical, or because of being synthetic and generated with several functions – the contour lines for the group must be interpolated from the durations/energy contents associated with each data point. The gradient curves would need to be determined point-wise.

Moreover, in case of historical signals, each event is determined by its own triplet of peak speed, energy content and duration; because of the haphazardness inherent in natural events, there is no a priori connection between the three values, as is the case when a shape function is set a priori instead. However, this is not a limitation to using those plots for historical events too – as shown later in Figure 3.17.

Chapter 4 of this study is dedicated to the definition of a number of synthetic speed profiles and their application as forcing terms on the WS waters. Here, we introduce a few basic shapes (rectangular, triangular, and trapezoidal) and comment on their representation in the framework charts.

We work with a parameterisation of the speed profile in the form $u(t) = u_p F(t,T)$, where $F=F(t,T)$ is a shape function that defines the approach to the peak value u_p in a duration T. We assumed that the initial time is always t = 0. The shape function takes dimensionless values in the interval [0,1]. A shape function can also be defined piecewise, but we consider two parts only, of durations T1 and T2 with T=T1+T2.

In particular, we consider four shape functions tabulated in Table 3.1 and shown in Figure 3.1.

Shape	*Meaning*	*Shape function*
Rectangle	Steady speed	$F(t,T) = 1 \quad 0 \le t \le T$
Right-angled triangle	Rising speed	$F(t,T) = t/T \quad 0 \le t \le T$
Acute triangle	Rising and dropping speeds	$F(t,T) = \begin{cases} t/T & 0 \le t \le T1 \\ (T-t)/T & T1 \le t \le T1+T2 \end{cases}$
Rectangular trapezium	Rising and steady speeds	$F(t,T) = \begin{cases} t/T & 0 \le t \le T1 \\ 1 & T1 \le t \le T1+T2 \end{cases}$

Table 3.1 Shape functions for basic synthetic speed profiles

It is important to recall that the peak value u_p becomes the natural scale for the wind speed, that is to say the required `speed information'. **This is not in contradiction with the previous finding of Alkyon (2008a) that peak speeds should not be used for scaling as long as the following distinction is clearly kept in mind. Peak speeds are, of course, a scale of the windstorm. But they are not a scale of the surges that they generate – especially if those peaks are not achieved at the end of a process that approaches the steady state (see Section 5.3 later)**. A connection based on work done/energy transferred is the essential information that must be included to link what happens in the air flow and in the water flow. These anticipations are critically discussed in Chapter 6.

3.1.2 Speed-based framework chart: non-rectangular signals

In the case of a non-rectangular speed profile, either synthetic or historical, each triplet (T,u_p,e) places (frames) a windstorm on a representing placemark point of the speed `diagram of state', or framework chart. However, the rectangular-profile contours still help the interpretation, because their defining equation is $u(e,T) = \sqrt[3]{(e/T)} \equiv u_{ap}$. Therefore, the point of the rectangular-profile contour corresponding to a generic pair (T,e) helps determine the average-power speed of that generic storm.

This is best explained by Figures 3.4 and 3.5, where the point P – shown as a black bullet – indicates an input windstorm whatsoever having peak speed $u_p(P)$, duration T(P), and energy content e(P).

In the plan (duration, speed) of Figure 3.4, the vertical line down point P obviously shows the duration T(P). This line crosses the rectangular-profile e-contour with parameter e(P) at the point Q.

The ordinate of point Q is thus the average-power speed of the windstorm P, since it refers to a rectangular storm with same duration and energy – this is the definition of average-power speed. Of course, Q is below P, because an average is bound to be lower than a (absolute) peak.

The e-contour of a rectangular profile passing exactly through point P, rather, indicates the energy content of another windstorm steadily blowing at the peak value of the first storm, and it is no surprise that such content is much larger than e(P).

In general, the vertical distance $\overline{PQ}$ between any one storm point and the e-contour of a profile with a reference shape indicates the degree of difference between the actual and reference conditions. The ratio of the segment lengths $\overline{PQ} : \overline{PR}$ indicates the degree of 'dissimilarity' of the storm profile from whatever reference profile used for the contours. The dissimilarity is larger, the more the index departs from zero. Moreover, when using the rectangular speed as reference profile, such index of dissimilarity is also expressed in terms of significant speeds as $1 - u_{ap}/u_p$.

In the plan (energy content, speed) of Figure 3.5, the vertical line down point P obviously shows the duration e(P). This line crosses the rectangular-speed T-contour with parameter T(P) at the point O.

The ordinate of point O is thus the average-power speed of the windstorm in P. Of course, O is found below P, because of the relative position of any average and peak.

The T-contour passing through point P indicates the duration of another rectangular windstorm steadily blowing at the speed $u_p(P)$ and with same energy content. It is no surprise that it should blow for much shorter than T(P) to build up the same energy content as e(P).

The ratio of the vertical segment length $\overline{PO} : \overline{PN}$ measures $(1 - u_{ap}/u_p)$, and that is the index of dissimilarity between the storm profile of P and the rectangular-speed model that generated the contours.

3.1.3 Time tracks of a developing windstorm

Other than for placing points representative of complete windstorms, **the same framework charts can be used to monitor the temporal evolution of each windstorm**. **This is done by tracking the position of the points (t,u_p,e) as the speed develops in time.** Each point in the track, in other words, represents the state that the windstorm has achieved until a moment t (`partial duration') of its whole duration T.

Time tracks are shown in the plots of Figure 3.6 and 3.7, where a generic rectangular speed is tracked in the (t,u_p) and (e,u_p) charts. The line dotting shows data taken at an equal time interval. While the equal spacing in the (t,u_p) chart has an obvious reading, an equal spacing in the (e,u_p) chart means that the energy content increases by equal amounts over each time interval – thus giving an indication of how dynamic a storm is (this is too discussed later in the test application to historical storms).

It is important to emphasise that **there is a difference between the time history of a speed, u=u(t), and the time history of the points that represent the evolving state of the windstorm**. They may look like each other under the condition of non-decreasing speed (also viewed next), but they are quite different objects from the outset.

Both in Figure 3.6 and 3.7 the progress of the windstorm is marked by a sequence of track points that moves away from the initial position on the vertical axis (green point at/for t=0). Here, they do so along a horizontal line, since the peak value does not change on account of the particular speed profile chosen.

In the first chart, the track line crosses different e-contours at an angle with them. Smaller angles with the e-gradient curves indicate that the windstorm evolves so as to face larger increases of energy content. This leads to the concept of a 'potential' maximum increase of energy, which is resumed in Section 3.1.6 – however, we note already at this point that the time track and the gradient curves are both originated by the speed profile.

In the second chart, the track line crosses T-contours of increasing value, and those can be conveniently used to place the track points in their own temporal sequence. The T-gradient curves, however, are not as insightful as the e-gradient curves. Nominally they indicate the direction of maximum increase of duration, which is normally an independent variable and is not subject to options.

Finally, the last points of the time tracks (in red) are representative for the complete event. Naturally, each lays on the final e- and T-contours relative to the entire windstorm.

3.1.4 Framework charts for triangular speed profiles

We already pointed out that the contour and gradient curves are results of the speed profile. This is, in fact, a corollary of a more general, and perhaps obvious, statement that the framework function $f=f(T,u_p,e)$ that describes a windstorm is a result of how the windstorm itself develops in time.

The rectangular profiles discussed so far are only suitable to represent the average, steady value of a real storm. Windstorms, however, approach with a period of rising speed that can be schematised, in the simplest form by setting a right-angled triangular profile for the function u=u(t) – as shown in red in Figure 3.1.

The shape function for a windstorm rising linearly up to speed u_p in a time T is

$$u/u_p = t/T, \tag{4}$$

while the framework formula takes the expression

$$e = u_p^3 T/4. \tag{5}$$

Some calculus shows that the e- and T-contours of a triangular profile always are above the corresponding contours of a rectangular profile, while the contours for either speed profiles are similar in shape, and the gradient curves are the same for both. It is therefore appropriate to see how the two families of profiles compare one to another when presented in terms of (T,u_p,e) framework values.

Four figures are commented next with a colour association where blue indicates rectangular profiles, and red does triangular ones. The differences regarding the windstorm points are shown in Figures 3.8 and 3.9. The differences in the time tracks are shown in Figures 3.10 and 3.11.

Firstly, the point P in Figure 3.8 places a rectangular windstorm having e=1 (the value is indicative) on the (T,u_p) plane. Point P lays on an e-contour in blue. On the e=1 contour for triangular windstorms (in red), there are two triangular storms worthy of comment, namely points Q and R. As said earlier and now shown, either profile's contours have similar shapes.

Point Q (point R) says that a triangular windstorm with the same duration (peak speed) can achieve the same energy content as a rectangular one only if its peak speed (duration) increases – as one can firstly guess from the proportion of the areas of a triangle and of a rectangle.

Also, the index of dissimilarity, $1-u_{ap}/u_p$, for the triangular windstorm Q is given by the quantity $\overline{QP} : (\overline{QP} + \overline{PN}) = 0.58$This value is constant for any pair of contours with the same e and, therefore, is a property of the triangular profile. Therefore, **a rule of thumb follows: to achieve the same amount of energy content in the same time, any triangular windstorm must have either the peak speed that is 59% higher than a rectangular windstorm**. This is, again, a criterion of area equivalence between a triangle and a rectangle, with the difference from 50% (area ratio) due to the cubic power in Formula (1).

Point R, instead, shows that to achieve the same amount of energy content with the same peak speed, any triangular windstorm must last four times longer than a rectangular windstorm. This too is, of course, contained in Formula (5).

Secondly, the point P in Figure 3.9 places a rectangular windstorm having T=10 (indicative value) on the (e,u_p) plane. Points S and T indicate two notable triangular storms with the same duration, as indicated by their position on the red T=10 contour. In particular, point S (point T) indicates that a triangular windstorm that lasts just as long as a rectangular one with the same peak speed (energy content) comes with lower energy content (higher peak speed). As before, the index of dissimilarity for the triangular windstorm T is given by the quantity $\overline{TP} : (\overline{TP} + \overline{SN}) = 1.587$ that applies everywhere in the plot. Also in this application, therefore, the framework charts plotted on the (T,u_p) and (e,u_p) planes convey equivalent information.

Turning from the windstorm points to the time tracks, Figure 3.10 shows the time tracks of rectangular and triangular profile in the plane (T,u_p). As neither profile's speed ever decreases, both time tracks look like the speed profiles themselves. The windstorms P and Q have the same duration and final peak speed, but the energy content of the triangular storm is lower because the peak speed builds up gradually.

After the same duration, while both windstorm points collapse on the chart (T,u_p), they fall on two overlapping e-contours: one relates to the rectangular profile (e=1, blue), the other relates to the triangular one (e=0.25, red). **This means that the triangular profile transfers into the water one fourth of the energy that a rectangular profile does in the same period and for the same peak wind** – consistently with Formula (5).

On the one hand, either profile's e-contours collapse because their shape, as already mentioned, is similar. Note, in passing, that the ratio between the two energy contents (0.25) does not reflect the triangle-to-rectangle area ratio (0.5) on account of the third power in Formula (1).

On the other hand, either profile's contours taken at the same value of energy content do differ, here shown by the curves (e=0.25, blue) and (e=0.25, red). Moreover,

the speed at point R is the average-power speed of the triangular windstorm P, smaller in the proportion of 1:1.587 as seen earlier on.

Also interesting to note, the triangular track cuts across the e-gradient curve at smaller angles that the rectangular tracks does at the same time. Those angles are shown only at the points P and Q, conveniently coinciding. Note that angles can be properly visualised if the chart's axes are isometric, which is not always possible when their ranges are set by the circumstances (for example Figure 3.16 later on). **Such angles suggest that, in spite of a lower energy content, the triangular profile builds up its energy content at a faster rate than the steady rectangular profile does – precisely, by a fourth-power against a linear law of growth**. The windstorm development can be viewed in a three-dimensional fashion by saying that the point of a triangular windstorm climbs the hill of increasing energy transfer through a steeper path, although reaching a lower elevation. Although less energy-giving in the end, **the triangular shape provides the water body with more power (time rate of energy) than the rectangular profile – of course, in otherwise identical conditions**.

Finally, Figure 3.11 shows the same time tracks in the (e,u_p) plane. As both windstorms have the same duration, each final point lays on its own T-contour at the same value (T=10 here).

The one-fourth proportion in the energy content seen in Figure 3.10 appears in the ratio of the segment lengths $\overline{OP} : \overline{OQ}$. These lengths are the abscissas for the rectangular and triangular profile points P and Q. Naturally, the same amount of energy $\overline{OP}$ is reached earlier by rectangular profile than the triangular one, as seen from the fewer dots (instants of time) in the track from the start to P. In particular, the blue T=10 collapses with the red T=4 contour – recall that energy content and duration are proportional for the current profiles.

Finally, point R denotes the rectangular windstorm at the average-power speed of the triangular windstorm P.

In case the synthetic profile is chosen to represent the linear growth to a speed peak and a linear decay afterwards, an acute triangle would follow according to Table 3.1 and Figure 3.1 (in orange). In this case it is noteworthy that the framework formula becomes

$$e = u_p^3(T1+T2)/4. \qquad (6)$$

Since T=T1+T2, this is exactly the same expression as Formula (5). This means that the amount of energy content transferred in the period T by a triangular profile is the same irrespective of when the peak is achieved. Therefore, the same framework formula – (5) or (6) – covers triangular profiles, whether right-angled or acute. Contours and gradient curves are the same for both subgroups.

By the same token, we gain that there are chances that different shape profiles are masked behind a single framework formula, so long as they produce the same overall effect. This is not an entirely undesired occurrence provided it is noted, because it conveys the fact that similar speed histories may produce the same general effects. Of course whether they produce the same surge is another facet of the problem.

The difference between the two aliasing profiles would become evident again once we look at the time tracks. Therefore, an added value of time tracks as indicators of the windstorm identity comes into evidence. Here, this is welcomed as a relevant point of caution, although it will not be subject of further study because the synthetic profiles discussed in the following chapters will be right-angled triangles and trapeziums.

3.1.5 Framework charts for trapezoidal speed profiles

In case of trapezoidal shape functions, like those of Figure 3.1 and Table 3.1, the framework formula reads:

$$e = u_p^3 \left(\frac{T1}{4} + T2\right) = u_p^3 T \left(1 - \frac{3}{4}\frac{T1}{T}\right), \quad (7)$$

which depends on an additional shape parameter T1/T, that is the fractional duration of the triangular/rising period. We indicate the shape parameter of the trapezium as *c* = T1/T. When c = 0, the speed profile and framework formula become those of the rectangular profile (T1=0, T=T2). Otherwise, when c = 1 the triangular profile is recovered (T2=0, T=T1). The parameter c indicates how much of the overall duration a triangular shape occupies.

Also, the formulation of the trapezoidal profile includes the previous one as particular cases. We note that Geerse (2006), for example, used an isosceles trapezoid to fit data of storm winds measured at Schiphol.

For the above temporal shape functions, the relation between T,u_p and e takes the general form valid for a triangular, trapezoidal and rectangular profile alike

$$\mathbf{e = b\, u_p^3 T}, \quad (8)$$

where *b* is a shape factor that takes the values given in the following Table 3.2. Also, since $u_p^3 T$ is the energy content of a rectangular profile, the shape factor is $b = e/e_{c=0}$, and the index of dissimilarity, here given in percentage, can be also derived. As a result, the contour lines of triangular, rectangular and trapezoidal profiles are all similar in shape, and have the same gradient curves.

	Rectangle					*Trapezium 50/50*					*Triangle*
C=T1/T	0	0.1	0.2	0.3	0.4	0.5	0.6	0.7	0.8	0.9	1
B=1-0.75*c*	1	0.925	0.85	0.775	0.7	0.625	0.55	0.475	0.4	0.325	0.25
ID=1-$\sqrt[3]{b}$	0	3%	6%	9%	13%	17%	22%	28%	36%	44%	59%

Table 3.2 Coefficients of the framework formula for different shape functions. (The values of the ID are rounded off to the nearest percent unit.)

As an illustrative application of this general case, six windstorms with the same duration and speed but shapes varying from a rectangle to triangle via trapezia (as the parameter *c* increases from 0 to 1 in steps of 0.2) are plotted in the (T,u_p) chart of Figure 3.12 and in the (e,u_p) Figure 3.13. The colour association is consistent with the remainder of the chapter (also shown in an inset for convenience).

In Figure 3.12, the time track coincides with the temporal profile, so the shape is easily recognisable. All time tracks eventually reach one single placemark P, which lays on one single contour. Such one e-contour, however, comes with different readings for each shape; namely, the energy content decreases from 1 (rectangular shape) to 0.25 (triangular shape) in proportion with increasing c's.

Figure 3.13, instead, shows the same events in the (e,u_p) chart. As the peak speed is the same but the final energy contents differ, all placemarks lie on the same horizontal line but at different positions. They are spaced apart in proportion to the difference in

shape factor. Each event's placemark lays on its own distinct T-contour relative to the same duration. Only the triangular and rectangular T-contours are drawn, and those of the trapezoidal profiles lay in between.

Next, six windstorms with same duration and energy content as well as the shapes of the previous application are plotted in the (T,u_p) chart of Figure 3.14 and in the (e,u_p) Figure 3.15.

Firstly, in Figure 3.14, it is obvious that to achieve equal energy content within the same time, the peak speeds need to be different, which results in the different heights of the final placemarks. The peak speed for c=0 is the average-power speed for all other profiles (placemarks), as they come with equal energy content. Here again, the speed profile can be read from the time track. Each windstorm's placemark lays on its own -contour at the common final energy value: unlike Figure 3.12 earlier, the contour is different while the parameter value is the same, because of the different shape.

Secondly, in Figure 3.15, the same events are plotted in the (e,u_p) chart. There we loose the visual correspondence with the speed profile, but the windstorm placemarks will lie each on its own T-contour (at the same duration value), vertically aligned (same energy content) and at different heights (different peak speeds). Note that, while the T-contours are the same of Figure 3.13 earlier (same duration and shape), now the final points are spaced apart in the vertical rather than in the horizontal direction (the speed rather than the energy changes). This vertical spacing is not proportional to c, though, but follows the differences in the index of dissimilarity – last row of Table 3.2.

In both of last two charts, the windstorms' placemarks all fall in the band between the e- or T-contours of the rectangular and triangular profiles having the same parameter. This is because the trapezium is an intermediate shape. Therefore, the contours of those limiting shapes help positioning windstorms in the chart and visualise their similarity to/departure from the rectangular (only steady speeds) and triangular (only rising speeds) behaviours.

Also, if any set of contours for rectangular storms is drawn at a fourfold increase of the parameter, each pair of next curves can be read by keeping either a shape or a parameter value fixed in mind. In the first, more obvious case, the contours simply indicate the chosen increase of the parameter (say 1, 4, 16 and so forth); in the second case, though, they will represent the contours for a rectangular (lower curve) and triangular (upper curve) shape profile having the same value of the rectangular profile, and therefore the band within which trapezoidal shapes will also be found.

The contours for a trapezoidal profile will lie in the band between the rectangular (lower) and triangular (upper) contours having the same parameter. Such a band is the area where all trapezoidal profiles with the given e- or T-parameter fall while their shape factor change.

3.1.6 The maximum-effect speed profile

An interesting side remark follows from the above conceptual framework. Given the group of windstorms that have a certain duration T and terminal peak speed u_p, **it could also be possible to anticipate the speed profile giving a time track that experiences the maximum increase of energy content**. In this case, the speed profile is such that both its time track and e-gradient curve coincide on the (T,u) chart. The interest of such a profile is that, while the final state (T,u_p) is the same as any other speed profile, the maximum increase of energy content is reached while the windstorm progresses. So, the energy transfer from wind to the water over the duration is maximised, all other conditions being equal. Each windstorm, of course, will reach the energy content that is associated

to its own profile. This concept can be useful to point out history effects, although it is only outlined in the present study. It might be used as more sophisticated approaches grow relevant.

3.1.7 Representing historical storms on framework charts for the speed

Given the above conceptual framework and its representation on charts, it is interesting to explore how such knowledge can be used when the windstorm data belong to **historical records**. Embarking on a detailed analysis of this facet is beyond the intended plan of work. However, we deemed it illustrative to present an application and point to possible developments.

Figure 3.16 shows the measured signals of the wind speed for the same six year-record storms as Figure 2.1, plus the two storms of 12 and 18 Jan 2007 included in the hindcasts of Alkyon (2008a). The wind was measured at Huibertgat.

A 4-day long time window starts two days before and finished one day after the highest surge at Delfzijl, and is given here in 0 to 96 hours. The time window is thus nearly the same from which the PW behaviour could be derived – see the arrows of Figure 2.1. Such a fixed-size time framing is blind, in the sense that it cuts each signal off its own history disregarding the storm development as a whole. Those 96 hours should not be intended as the duration of the storm's speed proper. This is clearly shown by the varying initial values of speed. This crude delimitation, however, prompts a few useful notes of caution discussed next.

The time tracks of the above measured signals are plotted on the plane (e,u_p) in Figure 3.1The corresponding chart in the plane (T,u_p) will not be shown.

As before, line dots mark regular time intervals, hourly in this case. Triangular symbols are used there to mark a 24 hour period, while the larger bullet point indicates the end of the time track that is the windstorm placemark. Dots that are narrowly spaced apart indicate slow dynamics, that is little increase of the energy content (transferred energy) in the same time interval. Conversely, the wider the spacing is, the more active the dynamics is, as the energy content leaps forward by larger amounts.

We recall here that the peak speed on the vertical axis is the largest speed achieved since the beginning of the screening until a point in time, so that the track-points move higher only as the previous peak value is exceeded. The peak speed of the entire storm is the highest value of the entire track, and its moment in time corresponds to the first storm point of the last horizontal line. Especially for historical signals, the horizontal segments in a time track may hide periods of decreasing as well as increasing speeds – this, of course, applies to synthetic profiles with decreasing sections too. Therefore, **active dynamics are best inferred from the dot spacing rather from the steepness of a time track**.

Also, as shown by signal of the 1981 storm in amber, the time track is highly sensitive to the value of speed at start, which sets the height over which the ensuing curve builds up. **It is, therefore, important to use a separate time window for each storm that starts from a suitably low speed**. This would be the nominal beginning of the storm. Any low threshold speed is good, provided it does not create a surge set-up (this can be inferred by cross-checking with a surge signal, having in mind that the wind and water stations are far apart and a time lag follows).

Further, the excess peak speed from such an initial value may be more significant parameter than the peak speed as such – this issue does not occur in synthetic profiles starting from zero.

Finally, as shown by the signal of the 1983 storm in pale green, the measured signal need to be complete, as missing information reduce the amount of energy that is eventually attributed to the windstorm during its effective duration.

If all these caveats are met, the final point in the chart will then be a fair representation of each event's intensity and allows for a meaningful comparison between different historical storms. However, taking advantage of the 'blind' 96-hour window for the time being, the average-power speeds is easily visualised by the intersection points of the same T=96h contour with the verticals from each windstorm placemark.

For example, the top-to-bottom ranking in the average-power scale for this 'as is' application would be 1990, 1994, 1981, 2007 (12 Jan), 2006, 1995, 2007 (18 Jan) and 1983. (This is the same ranking as that based on energy content, as the duration is equal and $e=u_{ap}^3 T$ by definition.) The more customary ranking according to the peak speeds is different, and namely: 1990, 1983, 1995, 1994, 1981, 2006, 2007 (18 Jan) and 2007 (12 Jan).

Most importantly, this opens to the possibility of comparing synthetic and historical events on quantitative grounds that, additionally, can be connected to a qualitative description like in Figures 3.2 and 3.3.

3.2 Conceptual framework for wind direction

The creation of a framework relation for wind direction is somewhat simpler than for the wind speed. **This is simpler, however, solely because it is assumed that the effects of wind direction, and especially of its temporal and spatial rate of change, on the wind-driven flow are neglected.** In effect, a wind that rotates 'too quickly' may be not able to effectively impart momentum to the waters so much as to create a current. We probably lack sufficient physical insight for such an extreme condition**. Here, the description of the wind direction becomes a purely kinematical matter, and it is assumed to have no dynamical impact**.

It is therefore easy to recognise that the simplest framework equation to use is the definition of the rate of rotation for the storm direction. This is

$$\omega = (\alpha 2 - \alpha 1)/ T1,$$

where α1 and α2 are the initial and final directions respectively, ω is the temporal rate of rotation (angular speed), and T1 is the duration of the veering windstorm. Note, that in this parameterisation the change of wind direction coincides with the change in wind speed. Decoupling of these moments is possible, but it will lead to an additional parameter (see for instance the suggestion of Gerritsen, 2008). For the moment we keep this as a working assumption.

Turning to the chart representation, it is clear that the parameters to be represented on a 2-d chart are T1, ω and $\Delta\alpha = \alpha 2 - \alpha 1$ (the windswept compass sector). Of course, one of the three parameters needs to appear as contour lines in the chart plane of the remaining two. In particular, in the plane (T1,Δα) the ω-contours are hyperbolas (the farther away from the origin, the faster the rotation), while in the plane (T1,ω) the Δα-contours are straight lines departing from the origin (the steeper, the wider the sector).

Because T1= cT, we also note that c acts as a hidden parameter. If the total duration were chosen in the time axis, then the contours would have been representing the cω or cΔα values. Alternatively ω- or Δα-contours could be still used in the (T, Δα/c) or (T,cω) charts respectively. Because the choice of the best presentation is rather arbitrary, the charts of the Figures 3.18 and 3.19 show indicative storm placemarks in the (T, Δα/c) or (T,cω) planes. We recall here that the framework equations and charts for speed and

direction are different because we chose to parameterise them in a decoupled way (an outcome of having disregarded the transiting low-pressure distribution that generates the whole wind vector).

4 Temporal profiles for the storm winds

4.1 The test set

As already discussed in Chapter 3, we apply synthetic profiles of trapezoidal/triangular shapes for both the wind speed and direction. The wind rises and veers in the first triangular part of duration T1, and remains constant in speed and direction in the second rectangular part of duration T2. As a special case considered here, the wind can rise in speed while remaining steady in its initial direction. **It is emphasised that we lock together the times over which the speed raises and the direction veers. This is done to limit the number of parameters; in general, however, those timescales are distinct**. The initial speeds are invariably zero, because we are mainly interested in isolated surges, i.e. not adding to previously risen or lowered water levels.

The parameters for the synthetic profiles are the following:

- Three total durations (T1+T2) of 1, 2 and 4 days;
- Two peak speeds of 25 and 37 m/s (9 and 12 Bft) ;
- Veering in the SW-to-NE sector on a 8-point compass (for a total of 15 sweeps of amplitudes from 0 to 180 degrees, thus including 90 cases with steady direction);
- Three triangular fractions: c=T1/T= 0.33 (long plateau), 0.66 (short plateau) and 1.00 (fully triangular).

Overall, 270 synthetic storms are generated. They can be qualitatively described as of short/long duration, high/low power, fast/slow rotation, wide/narrow sweep, and sharp/flat peak period. Their features, including the remaining framework parameters (the energy content for the speed, and the rate of rotation for the direction), are tabulated in Table 4.1.

The duration, triangular fraction, peak speed, initial and final direction are also used to derive the run codes for each storm in the form, for example, t24-c33-s370-225315 for a 24h storm with c=33/100=0.33, peak speed of 37 m/s (note that the speed is coded in dm/s) and veering from SW to NW (the nautical convention is followed for the wind direction). The corresponding wind fields are generated with an ad hoc program that feeds the WAQWND tool of the SIMONA suite; WAQWND creates the binary file that eventually sets the forcing on the water domain.

All test-set storms, of course, have their own placemarks in the framework speed and direction chart. Figure 4.1 is the speed framework chart, and blue objects are related to rectangular profiles, red ones to triangular profiles and green ones to trapezoidal ones. As noted, the T-contours of the 1h/rectangular and 4h/triangular profiles overlap, and the placemarks of trapezoidal windstorm lay between the triangular and rectangular T-contours with the same duration. The energy content values cover a range one order of magnitude wide. It is also interesting to note that a few placemarks collapse or are very close: this means that those storms have same energy, peak speed, but their profile shapes and durations are different: for example, the windstorms with the (T, u_p, c) triplets of (48h, 25 m/s, 0.33), (24h, 37 m/s, 0.66) and (48h, 37 m/s, 1.00) come with energy content of 2.03, 2.19 and 2.21 km^3/s^2. Because speed and direction are treated separately, the placemark corresponding to a certain triplet of speed framework parameters refers to all sorts of directions.

The framework direction charts for the test set already appear in Figures 3.18 and 3.19. The surge results are commented from Chapter 5 onwards.

4.2 Synthetic approximate hindcasts ('eyecasts')

Here, we applied the above prototype-windstorm schematisations to the individual historical storms originally used to infer the prototype windstorm itself (Figure 2.1). Gerritsen (2008), in particular, suggests that the parameters of a general synthetic prototype storm could be best-fitted so as to minimise the differences between simulated and observed peak surges at a number of stations and for a number of important surges. The optimal parameter settings would then be determined iteratively using a least-squares event. This would produce a WS-fitted prototype storm. Each of the iterations requires performing a set of wind-driven simulations to obtain the surges in the Wadden Sea.

The above approach, however, comes with drawbacks that, as it stands now, make it less suitable for answering the basic question of this study. As it will become evident in the following chapters, the uniform-wind assumption limits the capability of the flow solver to predict historical surges accurately. In addition, subjective choices are still to be made about the starting moment and the duration for each parameterised storm (recall Section 3.1.7). Further, a model for prototype storm cannot be calibrated based by minimising errors on water levels (and currents) that are inclusive of tide (the topic of tide-and-surge interaction, in fact, still deserves much attention). Then, any fitting method could result in an optimal surge prediction in the least-squares sense, but it may produce unrealistic storm profiles as well as badly-matching predictions of water levels and current fields, which are both essential for the wave climate. The historical data, finally, also suggest that a similar surge could be created by different storms, and the issue of multiple solutions (however realistic) in the fitting procedure could grow relevant.

For sure, some of these limitations apply to the present study as well (as noted in the Conclusions). Therefore, we rather opted for a 'low-profiled' approach where one synthetic storm is constructed around each historical storm from the year-record set of Alkyon (2008a). **In such a simpler approach, we found a synthetic alias for each historical storm profile 'by eye', followed by a computation of the WS surges. We named this approach 'eyecast'** to distinguish it from the concepts of hindcast and forecast**. The 'eyecast' term, therefore, refers to numerical experiments that have the tone of synthetic approximated hindcasts.**

4.2.1 Eyecast windstorms

The same synthetic models for the wind speed and direction has been applied to the year-record storms studied in Alkyon (2008a) and shown here in Figures 2.1 and 3.16. Those windstorms, presented in decreasing order of surge severity (as total water level) at Delfzijl, are the year records of 2006, 1994, 1995, 1990, 1981 and 1983. We recall that those are six of the most severe storms in the period 1981-2006 for which wind measurements at Huibertgat are available, and not the most severe six on records (barring the well-known 2006 storm).

The synthetic wind profiles have been fit to the historical wind records 'by eye', and used to hindcast the surges and currents. (The only difference with the synthetic windstorm of the test set is that the initial wind speed in not set to zero by default.) **The wind field is thus fully uniform and unsteady.**

We noted that Alkyon (2008a) already contained some numerical experiments in which either the wind speed or the wind direction was given a steady value while the other followed the recorded history. Those resulted in insufficiently high surges, although steady speeds lower than the peak value were applied on equal-energy

grounds. Here, instead, the peak wind speed will be used as the reference substituting value.

The purpose of this exercise is to test the current implementation of the prototype storms against historical events, and sufficient accuracy is attained by eye-fitting as shown in Figures 4.2 to 4.7, which compare the measurements at Huibertgat with the adopted profiles. It is emphasised that **the eyecasts do not test the validity of the prototype storm concept (based on historical measurements and, so, not dismissible) but rather the modelling assumptions used to design the synthetic forcing**. The surge results are commented separately in Chapter 5.

Figures 4.2 to 4.7 show that, at times, only fractions of the real windstorms have been modelled. This is to guarantee a fair amount of closeness between the real-world events and the model's synthetic shape profiles. We also note that, for the eyecasts, having locked together the speed-varying and direction-varying periods is a reasonable assumption.

For the storms of 1990 (27 Feb) and 2006 (1 Nov), in particular, we tested two variants where a 'rectangular period' was added to the ramping period. There, the steady speed was set either at the peak value of the measurements or at the (arithmetic) average over the steady-wind period. (The surge results will show to which extent the peak speed is a scaling variable for the surge.) The positioning and duration of the periods T1 and T2 was chosen using the wind direction as a primary guideline – in a way that the direction is always realistic. However, this could not always guarantee that the measured initial surge level at the beginning of the modelled windstorm is negligible.

The two variants relative to the 1990 storm are shown in Figure 4.9 and 4.10, and those relative to 2006 are shown in Figures 4.11 and 4.12.

T(h)	C(%)	u_*(dm/s)	α1 (deg)	α2 (deg)	α2-α1 (deg)	ω (deg/h)	e (km²/s²)
24, 48, 96	33	250	45	45	0	0	1.02, 2.03, 4.06
24, 48, 96	33	250	225	225	0	0	1.02, 2.03, 4.06
24, 48, 96	33	250	225	270	45	5.7	1.02, 2.03, 4.06
24, 48, 96	33	250	225	315	90	11.4	1.02, 2.03, 4.06
24, 48, 96	33	250	225	360	135	17	1.02, 2.03, 4.06
24, 48, 96	33	250	225	45	180	22.7	1.02, 2.03, 4.06
24, 48, 96	33	250	270	270	0	0	1.02, 2.03, 4.06
24, 48, 96	33	250	270	315	45	5.7	1.02, 2.03, 4.06
24, 48, 96	33	250	270	360	90	11.4	1.02, 2.03, 4.06
24, 48, 96	33	250	270	45	135	17	1.02, 2.03, 4.06
24, 48, 96	33	250	315	315	0	0	1.02, 2.03, 4.06
24, 48, 96	33	250	315	360	45	5.7	1.02, 2.03, 4.06
24, 48, 96	33	250	315	45	90	11.4	1.02, 2.03, 4.06
24, 48, 96	33	250	360	360	0	0	1.02, 2.03, 4.06
24, 48, 96	33	250	360	45	45	5.7	1.02, 2.03, 4.06
24, 48, 96	33	370	45	45	0	0	3.29, 6.59, 13.17
24, 48, 96	33	370	225	225	0	0	3.29, 6.59, 13.17
24, 48, 96	33	370	225	270	45	5.7	3.29, 6.59, 13.17
24, 48, 96	33	370	225	315	90	11.4	3.29, 6.59, 13.17
24, 48, 96	33	370	225	360	135	17	3.29, 6.59, 13.17
24, 48, 96	33	370	225	45	180	22.7	3.29, 6.59, 13.17
24, 48, 96	33	370	270	270	0	0	3.29, 6.59, 13.17
24, 48, 96	33	370	270	315	45	5.7	3.29, 6.59, 13.17
24, 48, 96	33	370	270	360	90	11.4	3.29, 6.59, 13.17
24, 48, 96	33	370	270	45	135	17	3.29, 6.59, 13.17
24, 48, 96	33	370	315	315	0	0	3.29, 6.59, 13.17
24, 48, 96	33	370	315	360	45	5.7	3.29, 6.59, 13.17
24, 48, 96	33	370	315	45	90	11.4	3.29, 6.59, 13.17
24, 48, 96	33	370	360	360	0	0	3.29, 6.59, 13.17
24, 48, 96	33	370	360	45	45	5.7	3.29, 6.59, 13.17
24, 48, 96	66	250	45	45	0	0	0.68, 1.36, 2.73
24, 48, 96	66	250	225	225	0	0	0.68, 1.36, 2.73
24, 48, 96	66	250	225	270	45	2.8	0.68, 1.36, 2.73
24, 48, 96	66	250	225	315	90	5.7	0.68, 1.36, 2.73
24, 48, 96	66	250	225	360	135	8.5	0.68, 1.36, 2.73
24, 48, 96	66	250	225	45	180	11.4	0.68, 1.36, 2.73
24, 48, 96	66	250	270	270	0	0	0.68, 1.36, 2.73
24, 48, 96	66	250	270	315	45	2.8	0.68, 1.36, 2.73
24, 48, 96	66	250	270	360	90	5.7	0.68, 1.36, 2.73
24, 48, 96	66	250	270	45	135	8.5	0.68, 1.36, 2.73
24, 48, 96	66	250	315	315	0	0	0.68, 1.36, 2.73
24, 48, 96	66	250	315	360	45	2.8	0.68, 1.36, 2.73
24, 48, 96	66	250	315	45	90	5.7	0.68, 1.36, 2.73
24, 48, 96	66	250	360	360	0	0	0.68, 1.36, 2.73
24, 48, 96	66	250	360	45	45	2.8	0.68, 1.36, 2.73
24, 48, 96	66	370	45	45	0	0	2.21, 4.42, 8.84
24, 48, 96	66	370	225	225	0	0	2.21, 4.42, 8.84
24, 48, 96	66	370	225	270	45	2.8	2.21, 4.42, 8.84
24, 48, 96	66	370	225	315	90	5.7	2.21, 4.42, 8.84
24, 48, 96	66	370	225	360	135	8.5	2.21, 4.42, 8.84
24, 48, 96	66	370	225	45	180	11.4	2.21, 4.42, 8.84
24, 48, 96	66	370	270	270	0	0	2.21, 4.42, 8.84
24, 48, 96	66	370	270	315	45	2.8	2.21, 4.42, 8.84
24, 48, 96	66	370	270	360	90	5.7	2.21, 4.42, 8.84
24, 48, 96	66	370	270	45	135	8.5	2.21, 4.42, 8.84
24, 48, 96	66	370	315	315	0	0	2.21, 4.42, 8.84
24, 48, 96	66	370	315	360	45	2.8	2.21, 4.42, 8.84
24, 48, 96	66	370	315	45	90	5.7	2.21, 4.42, 8.84
24, 48, 96	66	370	360	360	0	0	2.21, 4.42, 8.84
24, 48, 96	66	370	360	45	45	2.8	2.21, 4.42, 8.84
24, 48, 96	100	250	45	45	0	0	0.34, 0.68, 1.35
24, 48, 96	100	250	225	225	0	0	0.34, 0.68, 1.35
24, 48, 96	100	250	225	270	45	1.9	0.34, 0.68, 1.35
24, 48, 96	100	250	225	315	90	3.8	0.34, 0.68, 1.35
24, 48, 96	100	250	225	360	135	5.6	0.34, 0.68, 1.35
24, 48, 96	100	250	225	45	180	7.5	0.34, 0.68, 1.35
24, 48, 96	100	250	270	270	0	0	0.34, 0.68, 1.35
24, 48, 96	100	250	270	315	45	1.9	0.34, 0.68, 1.35
24, 48, 96	100	250	270	360	90	3.8	0.34, 0.68, 1.35
24, 48, 96	100	250	270	45	135	5.6	0.34, 0.68, 1.35
24, 48, 96	100	250	315	315	0	0	0.34, 0.68, 1.35
24, 48, 96	100	250	315	360	45	1.9	0.34, 0.68, 1.35
24, 48, 96	100	250	315	45	90	3.8	0.34, 0.68, 1.35
24, 48, 96	100	250	360	360	0	0	0.34, 0.68, 1.35
24, 48, 96	100	250	360	45	45	1.9	0.34, 0.68, 1.35

continued

24, 48, 96	100	370	45	45	0	0	1.09, 2.19, 4.38
24, 48, 96	100	370	225	225	0	0	1.09, 2.19, 4.38
24, 48, 96	100	370	225	270	45	1.9	1.09, 2.19, 4.38
24, 48, 96	100	370	225	315	90	3.8	1.09, 2.19, 4.38
24, 48, 96	100	370	225	360	135	5.6	1.09, 2.19, 4.38
24, 48, 96	100	370	225	45	180	7.5	1.09, 2.19, 4.38
24, 48, 96	100	370	270	270	0	0	1.09, 2.19, 4.38
24, 48, 96	100	370	270	315	45	1.9	1.09, 2.19, 4.38
24, 48, 96	100	370	270	360	90	3.8	1.09, 2.19, 4.38
24, 48, 96	100	370	270	45	135	5.6	1.09, 2.19, 4.38
24, 48, 96	100	370	315	315	0	0	1.09, 2.19, 4.38
24, 48, 96	100	370	315	360	45	1.9	1.09, 2.19, 4.38
24, 48, 96	100	370	315	45	90	3.8	1.09, 2.19, 4.38
24, 48, 96	100	370	360	360	0	0	1.09, 2.19, 4.38
24, 48, 96	100	370	360	45	45	1.9	1.09, 2.19, 4.38

Table 4.1 Test set. Columns 1 to 5: main parameters (T, durations; c, triangular fraction; u_p, peak speed; a1 and a2, initial and final wind directions). Columns 7-8: derived parameters (windswept compass sector; rate of rotation; energy content). Note that elements in the triplets of duration and energy content correspond.

5 Surge simulations

The surges generated by the test windstorms are simulated with the WAQUA solver for the depth-averaged equations of motion in a water body with free surface. **No astronomical forcing is considered, because the present aim is to simulate the wind-generated effects, and interaction with the tidal cycle is not relevant to the purpose**. Astronomical forcing will be appropriate when synthetic storms are treated in a probabilistic approach to derive the HBC, but investigations on these effects are only applicable if the present study leads to results that can be amplified.

The WAQUA solver has been run on the CSM-ZuNo nested domains, since the results in Alkyon (2008a) suggest that, for the purpose of this project, the 15-fold increase of computational time does not justify the increase of accuracy in running the Kuststrook domain. A few flow fields are run with the Kuststrook domain to test the impact of this working assumption. Kuststrook results are discussed in Section 5.1.1 and 5.3.

The synthetic time-varying profiles are applied as a uniform field. More insight was needed to determine the area over which to apply such wind. In Alkyon (2008a), synthetic winds were applied unchanged over the CSM-to-Kuststrook domains; there, it was recommended to check whether the uniform wind artificially applied over each larger domain generates biasing surge and currents that affect the flow and free surface in the smaller domain through the open boundaries. This is discussed in Section 5.1.2.

We also point out that, **because the wind is set as a time-varying and uniform forcing over a limited area, it is unnecessary to devise an atmospheric pressure field that drives the wind**. Pressure gradients would be needed along the boundary of a region to sustain the wind inside of it, while they should vanish outside the domain where no wind blows. The pressure field may undergo discontinuities. The change of pressure across the boundary of the windblown area would generate some unphysical effect on the water. There should also be a physical model for the atmospheric motion, however simple, that connects the pressure field and air motion, say a geostrophic-speed or, even better, gradient-speed estimate (see Parker, 1988). Bijl (1995), for example, used a geostrophic estimate (not accounting for the centripetal acceleration acting on trajectories along curved isobars) to hindcast the 1953 flood through the wind speed associated to a moving cyclone. That said, neglecting the presence of atmospheric pressure field and setting the wind speed directly are fully consistent with the scope of this study.

In such an approach another boundary anomaly may occur related to the sudden change in the wind speed across the windblown area. This is relevant because, in this study, we consider the extent of the windblown area as a parameter of the uniform-wind schematisation. A wind blowing with uniform speed and direction over as large an area as the CSM is certainly unrealistic, and in Section 5.1.2 we test the effect of the reduction of the windblown area on nearshore flow field. To avoid the occurrence of spurious effect we set a buffer zone of one-degree width around the windblown area, where the speed increases from zero outside to the non-zero value in the interior.

5.1 Preliminary tests on uniformly applied winds

Here, we comment on the numerical simulations of two windstorms: the first is a slowly-varying event, and the second is a rapidly-varying event. The aim is to make clear which

differences arise in the simulated flow in consequence of two of our working assumptions outlined earlier.

The assumptions under check are, firstly, the choice of running the Model Train only down to the resolution of the ZuNo (Southern North Sea) domain; and, secondly, the arbitrary selection of the extension of sea to be uniformly blown by the synthetic wind.

The motivation of choosing such two storms is explained soon afterwards. Here, we emphasise that this is not a sensitivity analysis. Within the scope of the current project, it is sufficient to carry out just two exercises and become aware of the differences in the results. This project aims at developing a framing tool to better understand the connection between air and water flows in the WS surges. While it provides proper bearing for the relevant (modelled) physics, it takes no responsibility for, and should function regardless of, the degree of accuracy that is put in either the forcing or the solver (i.e. in the physical and numerical modelling).

Firstly, the choice of carrying out serial computations devoid of the Kuststrook domain is motivated by computational economy, since the corresponding CPU time would take 15 times longer than the time required by the ZuNo. The approximate 15-fold increase in the computational time follows because the time step and number of active cells in the Kuststrook settings are respectively 5 times smaller and 3 times larger than for the ZuNo domain (0.5 v 2.5 minutes, and 40,621 v 134,444 active cells).

Obviously, the flow processes that take place at those smaller scales, spatially as well as temporally, are not captured by the WAQUA solver on the coarser domain. In a semi-enclosed basin such as the WS, for example, the fluxes through the tidal inlets and some large-scale oscillating processes may be mishandled and/or overlooked with a coarser resolution of the grid and time step. We note that the higher resolution also entails a better positioning of the test stations (the typical width of a CSM cell, for example, is 10 km).

Previously, from the hindcasts of four historical storms in Alkyon (2008a), we have gained that, at a ZuNo-settings resolution, the water levels at selected onshore stations are recognisably affected by differences of magnitude and by phase shifts, although the general surge history is not dramatically altered. Here, therefore, we will add some information based on two synthetic events.

Secondly, **the extent of the windblown area is obviously important, because the volume of water set in motion increases if the wind action is exerted across larger sea areas. Ostensibly, the size, intensity and path of the currents, as well as the free-surface arrangement, are influenced thereby**.

The purpose of this exercise is to show whether the windblown sea area is a crucial parameter, and learn useful indications thereby, to be possibly considered with more attention in the future.

On the one hand, in hindcasts, the spatially- and temporally-varying wind and pressure fields are known through the HIRLAM fields provided by KNMI (Royal Dutch Met Office); those fields can also be scaled up and partly conditioned so as to create a surge of desired magnitude at chosen locations (for example, Alkyon (2007)). Those fields are based on historical measurements, and their spatial and temporal variability is consistent in terms of atmospheric dynamics. In this connection, from the point of view of a one-way coupling with a flow model, they are essentially used as complete enough input

data (although their spatial and temporal resolutions certainly have an effect on the corresponding flow simulation).

On the other hand, in our pursuit of adequate synthetic storms, the wind field has been assigned heuristically (that is by gradual insights and further concepts), and a certain degree of detail is invariably lost while the understanding progresses step by step. The extension of sea over which the constructed wind blows rests on the modeller's hands. In the numerical experiments carried out in Alkyon (2008a), for example, the synthetic winds were applied uniformly over the entire water domains of the Model Train. Two shortcomings were pointed out there: firstly, a wind blowing uniformly over the whole North-Sea continental shelf is certainly unrealistic; secondly, it is not immediate to anticipate how sensitive the nearshore currents and water levels are to the long-fetched, wind-driven flow field. In that study, this was left as a point worthy of further attention.

Therefore, here, we made the two test storms blow with the same temporal profile over four increasingly large areas. Those areas, tabulated in Table 5.1 and shown in Figure 5.1, are defined by decimal degrees of latitude and longitude, and labelled according to the customary small to extra-large grading. The Model Train domains are clearly indicated in the figure. The XL- and L-areas coincide with the CSM and ZuNo computational domains respectively. The M- and S-areas are parts of the southern North Sea; in particular, the former's eastern boundary is placed east of the Dover Strait and the northern one runs at the same latitude of the island of Sylt (Germany); then, the latter's eastern boundary runs along a meridian near Oostende (Belgium; within the Kuststrook domain) and the northern one runs along the 54th parallel (north of the Kuststrook boundary).

Label	*Coverage*	*Latitude E*	*Latitude W*	*Longitude S*	*Longitude N*
S	Quarter-ZuNo	3 (Oostende)	13	49.5	54
M	Half-ZuNo	-1 (Dungeness)	13	49.5	55 (Sylt)
L	ZuNo	-2	13	49.5	57.5
XL	CSM	-12	13	48	62.5

Table 5.1 Extensions of the four test windblown areas for the uniform synthetic winds. The coverage may be intended as at a good approximation. Degrees in decimal values.

Two specific storms have been chosen as test cases for the exploratory purposes described so far. They are a rapidly varying and a slowly varying event, because firstly they can exercise to a different degree the spatial and temporal resolutions of each Model-Train domain; and, secondly, because such windstorms blow for different timescales compared to the time that a current generated in faraway windblown areas may take to approach the shore.

The test storms have been chosen from the extreme ends of the 270-strong broader set. For both, in particular, the wind peak speed is 37 m/s (the highest of our set), and the wind direction veers from SW to NE (the largest compass sector of our range). Therefore, they differ for the duration of the unsteady period (i.e. rising/veering wind) and, on so doing, for the shape. The slow-varying storm is a long storm (96h) with no plateau (whereby fully triangular, c=100), while the rapidly-varying one is a short storm (24h) with a 8h period of changing wind (whereby c=33, the lowest of our range). The run codes are t24-c33-s370-22545 (fast) and t96-c100-s370-22545 (slow).

Upon the achievement of the peak value, the wind keeps on blowing at the peak speed from the last direction. The fast-varying storm can then be seen as an approximation to

the case of a square speed to the extent that the second, steady-wind period prevails. In these applications, however, a northeasterly wind is probably an unusual event for the WS, but we stress again that, at this stage, high closeness to realistic scenarios is relevant to a much limited extent.

The rates of change of the slowly varying storm are 12 times smaller than for the fast varying event. Namely: the winds increase by nearly 0.4 and 4.6 m/s per hour, and veer at a rate of 1.9 and 22.5 (one-octant width) degrees per hour respectively. Also, the energy contents and average-power speeds are tabulated in Table 5.1. The slow-varying, longer and fully-triangular storm has a 30% higher energy content, but the fast-varying, shorter and near-rectangular storm has a 45% higher average-power speed. This means that the same-energy and steady-speed equivalent of the fast-varying storm is a more intense event than that of the slow-varying storm. (We recall that the energy reasoning does not account for wind direction.)

Test storm	*T (h)*	*c (%)*	u_p *(m/s)*	*e* (km^3/s^2)	u_{ap} *(m/s)*
`slowly-varying'	96	100	37.0	4.38	23.3
`fast-varying'	24	33	37.0	3.29	33.7

Table 5.2: Shape and framework parameters of the test-storm speeds used in this chapter (dependence on domain resolution and windblown area).

5.1.1 Effect of computational resolution

Figure 5.2 shows the water-level histories at Den Helder, Harlingen and Delfzijl (covering the western, central and eastern WS) for the **slow-varying windstorm** as computed in the CSM, ZuNo and Kuststrook domains. Colour coding refers to the stations, whereas the thicker the line, the higher the domain resolution. The wind blows over the entire CSM area ('XL-coverage').

At the start-up, a southwesterly wind rises from zero; it grows up to 9+ m/s westerly at 24 hours; then, 18.5 m/s northwesterly at 48 hours; 27.7 m/s northerly at 72 hours; and, finally, 37 m/s northeasterly at 96h. Thereafter, the wind drops to zero (with steady direction) within one more hour (this decay span is merely a requirement of the WAQWIND tool used to work out the wind field). Such an arrangement determines two distinct phase in the histories of the water level: the first is wind-driven; the second is driven by inertia. We will frequently use this distinction in two phases in the following.

Irrespective of the locations and numerical resolution, while the wind blows, all **water levels** build up gradually, reach a peak and decrease more rapidly than they grew. The differences between the results from each model are quite consistent in appearance. In particular, **in the wind-driven phase, the ZuNo results tend to overestimate the Kuststrook ones by limited amounts, so the two are effectively interchangeable for our purposes**. The histories at different stations essentially differ because the surge peaks are achieved earlier or later (in the increasing order Harlingen, Den Helder and Delfzijl) and with different magnitudes (in the increasing order Den Helder, Harlingen and Delfzijl). The peak surge occurs while the wind blows from between NNW and N at Den Helder and Harlingen, and between N and NNE at Delfzijl; a farther veering determines the lessening of the local surge strength and, eventually, surge set-downs. However, this is not tantamount to stating that the local surge is only determined by a particular wind heading, because in Alkyon (2008a) the surge at large (i.e. the wide mound of raised water levels) is seen to develop and travel along the WS.

After the wind speed falls back to zero, inertial oscillations develop, because the free-surface slope is not held up by the wind drag any longer. So, the transfer of potential and kinetic energy between the displaced free surface and the inertia of the inner masses generates a sloshing motion across opposite shores of the WS. Such oscillation is damped by bottom friction and, of course, further affected by any escape/intake of water through the tidal inlets that may occur. Because the free-surface slope adjusts fairly rapidly to the wind direction (that varies gradually here), it is arguable that, at least initially, those oscillations take place along the NE-SW axis. This could be clarified by an analysis of the flow field, but unravelling such details is not pertinent with the current scope. Also in such inertial phase, the ZuNo and Kuststrook models appear to capture the same physics at a comparable level of accuracy. We note that the inertial effects would have been reduced if we had also modelled a decaying phase for the wind speed.

Figure 5.3 shows the **histories of the net mass-flux across the WS tidal inlets**, namely, from east to west: North Holland/Texel (Marsdiep), Texel/Vlieland (Eierlandse Zeegat), Vlieland/Terschelling (Vliestroom), Terschelling/Ameland (Borndiep), Ameland/Schiermonnikoog (Pinkegat), Schiermonnikoog/Rottumeroog (western Eems estuary), Rottumeroog/Juist (eastern Eems estuary). The flux at the westernmost control section, across the shoals from Juist to the German mainland, is not included here. Colours refer to sections, thickness to the solver's resolution. Positive fluxes indicate mass transport that fills the WS, while negative ones indicate transport that empties it. Only the ZuNo and Kuststrook results are plotted. The chart is apparently rich in lines, but for this subsection's purpose it is sufficient to focus on the gaps between lines in the some colour (same location) and different thickness (different numerical settings).

The ZuNo and Kuststrook results are again similar to each other. In the wind-driven phase, the most noticeable differences occur for the Marsdiep and eastern Eems estuary. Concentrating on the Kuststrook results only, all fluxes are initially positive (filling), but they become negative (emptying). The inlets contributing the most to net inflow (in the given wind conditions) are the Vliestroom and the eastern Eems estuary, whereas those doing so to net outflow are the Marsdiep and the western Eems estuary.

For each flux history, three points in time are then particularly meaningful: firstly, when the net flux achieves its positive maximum (flux inwards); secondly, when the net flux is zero; thirdly, at the time of the largest negative flux (flux outwards). The first point represents the moment when the actions driving water into the basin (first and foremost, the wind) begin to be contrasted by those driving water out. The second point represents the moment when this process has led to the inversion of the net flux (possibly because of an inviting surface slope generated by the near-shore surging). The third point indicates the apex of the net outflow, which then begins to be limited by increasing inflow.

We do not embark on a detailed analysis of the basin-wide inflow/outflow patterns. Because of orientation, width, storage area downstream and so forth the temporal sequence of zero-net-flux times follows a non-geographical order (as the wind veers): Marsdiep, western Eems estuary, Pinkegat, Eierlandse Zeegat, Vliestroom, and eastern Eems estuary. Water is still entering the WS through the Borndiep at the end of the storm. **It is perhaps appropriate to emphasise that the most effective direction for the penetration of the wind-driven water is that along the main axes of the outer tidal channel, where bottom friction is the least effective, rather than the one normal to the openings as seen in maps**. The same Figure 5.3 also shows that the fluxes acted on by

the (unlikely) inertial oscillations can be up to one order of magnitude larger than those in the wind-driven phase.

Figure 5.4 shows the histories of the **wind-driven volume** contained inside the WS. This is the result of the overall mass transport through the basin's cross-sections that, by global mass conservation, determines in turn the temporal changes of the (mean) free surface. To recall, the lowering/rising of water levels locally is determined by the spatial distribution of the water divergence/convergence events. Globally, though, **such a wind-driven volume indicates how much water the windstorm loads within the WS, to be possibly displaced against the shore as an effective surge**. This volume can also be called '**surge water**' (resumed in Section 5.2.1).

Whether and where and how severely such a surge becomes noticeable at the shore depends on the flow dynamics, but the total wind-driven volume remains a valid indicator of the capacity of the storm to drive water into the WS in the first place. This concept is soon resumed and used in Section 5.2. The connection between the (modelled) energy content and the wind-driven volume is briefly explored in Chapter 6. Expectedly, the difference between the two resolutions shown by Figure 5.4 is limited.

A note about units and orders of magnitude is in order here. As shown later, the computed wind-driven water volumes cover a range from fractions to tens of billions of cubic meters. For those volumes we use the unit $Gm^3 = 10^9\ m^3 = 1\ km^3$. The WS area over which the mass balance is computed is about 3,400 km^3 wide. (As a dry-land reference, the Province of Overijssel is nearly 3,300 km^2 wide.) Thereby, **1 Gm^3 (km^3) excess volume in the Wadden Sea corresponds to an excess height of about 30 cm uniformly spread over the basin**.

Figure 5.5 shows the water-level histories for the same stations as above and for the **fast-varying windstorm**. The wind grows up to 9+ m/s W at 2 hours; to 18.5 m/s NW at 4 hours; to 27.7+ m/s N at 6 hours; and, finally, reaches 37 m/s NE from 8 to 24 hours. All other settings, as well as the charts' notation, are unchanged. Contrary to the slowly-varying windstorm, the surge patterns are more varied here, which confirms that the water response can be rather complex in spite of the drastically simplified wind forcing.

The differences between ZuNo and Kuststrook **water levels** are small in the rising phase of the windstorm only, i.e. the first 8 hours. Rather, those differences become noticeable at all stations during the steady phase of the windstorm as well as in the first periods of the inertial oscillations. The results then become equivalent again in the long run. While the pairs of peak values are close irrespective of either resolution (which could be valuable information if proved to be a general enough), **in the fast-varying storm some wind-driven processes apparently occur that are not sufficiently well resolved with the coarser ZuNo settings**.

At Delfzijl, for example, a series of fast oscillations develop between 16 and 24 h, while the wind is steadily northeasterly, that are possibly linked to resonance occurring in the Eems-Dollard estuary. Such oscillations, with a period of nearly 80 min, stop when the wind falls and the water levels drop to negative marks, an indication of local emptying flow. The ZuNo model runs with a 5-fold time step of 2.5 min and a 3 time coarser grid and, instead, gives a rapid continuous lowering of water levels from 8 to 16 hours. In the same line, the histories of the water levels from 12 to 24 hours are dissimilar at Den Helder and Harlingen too, with the ZuNo model that misses the extended periods of set-down at either station.

Comparing the two test events at the same Kuststrook resolution, it is interesting to note that for the fast-varying storm the only wind-driven surge worthy of notice occurs at Delfzijl (~240 cm), while Den Helder and Harlingen immediately suffer from set-downs of ~250 cm, more severe than those for the slow-varying event. Such different local outcomes are not entirely surprising, because they are consistent with the kind of storms that have been applied and with the effects that they entail in the local histories of water levels. However, as a general consideration, they clearly suggest that the rotational features of the wind (such as the swept sector and rate of rotation) are capable to determine a variety of impacts on the WS coast.

Then, Figure 5.6 shows the **net-flux** histories across the same control sections as in Figure 5.3. Values in the order of millions of cubic meters per second occur (We may recall that discharges in oceanography are often measured in Sverdrup = 10^6 m^3/s). Said again, to appreciate the difference between the ZuNo and Kuststrook results it is sufficient to focus on the lines in the same colour (sections) and different thickness (domain). The difference between the two resolutions is clear especially in the period from 8 to 36 hours, where **extended quasi-steady periods are missed out with coarser settings**. In addition to the increased temporal resolution noted above, the difference is certainly also explained by a finer spatial resolution, thanks to which the areas and wet perimeter of the tidal inlets are defined more accurately.

Of course, the comparison with Figure 5.3 indicates that **the flow dynamics needs to change at a sufficiently rapid rate before a difference in the results becomes significant. Because such rapidity is within the limits of natural events, additionally, it should be borne in mind for future applications that the substitution of ZuNo results applied in this study is merely a contrivance**. Hereafter, for the sake of progress and without further testing, we will assume that, at least, the loss of accuracy in the pairs of surge peaks computed through ZuNo and Kuststrook is acceptable and nearly insensitive to the rate of change of the windstorms.

Lastly, Figure 5.7 shows the history of the **wind-driven water volume** (surge water) for the fast-varying storm. The net-fluxes differences in the wind-driven phase and the closer agreement in the inertial phase of the windstorm are reflected in the history of the total water volume. Unlike for the slowly-varying windstorm of Figure 5.4, the (first) peak of the surge and the (first) peak of the wind-driven value occur at the same time – we only look at the wind-driven phase here.

5.1.2 Wind forcing on a limited area: the extension of the windblown area

The results shown in this subsection belong to the flow of the fast-varying storm of Table 5.1. The results obtained with the wind blowing over the CSM domain ('XL-coverage') have been shown in the previous Figure 5.2 to Figure 5.Here, we comment on the ZuNo and Kuststrook results obtained with the M- and S-size windblown areas of Table 5.2. Figure 5.8 and Figure 5.9 thus show the water-level histories for the fast-varying windstorm when the wind blows over the S and M-size area respectively and when the flow is resolved on the ZuNo and Kuststrook systems.

The most noticeable feature, specifically in the wind-driven phase, is that (at least in these cases) **the Kuststrook results are to a good approximation insensitive to the windblown area, distinctly unlike the ZuNo results. In other words, the Kuststrook results converge to the same flow description**. During the inertia-driven phase, a

difference between each Kuststrook clearly appears in the amplitudes of the oscillations, more so than in their periods.

Figure 5.10 and Figure 5.11 then show the corresponding net-fluxes. The ZuNo fluxes deviate from the Kuststrook ones by the least amount when the windblown area is the smallest, i.e. for the storm event at a local scale, during both the wind- and inertia-driven phases.

The interpretation of the above behaviour is complex and will be only touched herein. **It seems to indicate that, as and if the flow is accurately resolved (here, Kuststrook), the computed flow in the WS is primarily determined by the wind conditions in force in the near region, because the variations caused by enlarging the windblown area (and therefore by the far-fetched currents that flow in across the open boundaries) are certainly secondary**.

By contrast, a coarser domain (here, ZuNo) bears significant traces of the different flow patterns acted on by wind fields blowing over diversely large areas. Only when the far-field large-scale circulations are completely removed from the outset (because the wind blows on the smaller, nearer domain), do the coarse results collapse with the more refined and robust results – or, at least, follow them more closely.

Disdaining obviousness, we emphasise that the WS basin is represented in both domains (to either's own grid resolution), and that the Kuststrook model is temporally and spatially nested into the ZuNo. Thence, they are the increased temporal and spatial resolutions that lead to a clear and robust distinction between primary and secondary contributions that we are seeing here. This argument, moved at first by numerical considerations, seems to point to a physically-based conclusion that **the entire WS area may have a remarkable modulating effect on the large-scale circulation of the North Sea**.

The behaviours in the inertial phase may also be consistent with this. It looks at first perplexing that the Kuststrook water levels begin to depend on the windblown area as soon as the wind quits (the smaller the windblown area, the narrower the amplitude). This may still be explained upon accepting that the water levels *outside the WS instead* are remnants of the large-scale wind-driven currents that, rather, do not affect the inner basin. Because inertial oscillations are first triggered by the free-surface slopes, the differences in the inertial-phase oscillations may be caused by different slopes between inside and outside the tidal channels in either simulation.

Such speculations would certainly need in-depth studies to be defined more precisely and corroborated more extensively, but they lend some credibility to the view that the WS surges are primarily generated by the regional wind climate. In the remainder of this study we will consider wind fields blowing over the ZuNo area (L-size), on the (not-so-firm) grounds that the peak surges may be predicted well enough (while the net fluxes seemingly are not).

5.2 Surge simulations: The test set

5.2.1 Indicators for the surge strength at a basin-wide scale

In the same way as the energy content aims at representing the grand features of a windstorm, we may find a corresponding quantity that serves the same purpose as far as the surge is concerned. A benefit is that the surges could be ranked by some reference

quantity inherent in the process, that is to say linked to water's actual behaviour and not to the external forcing. In Alkyon (2008a) it was suggested trying to rank the surges by the volume of water that the windstorm loads into the WS through the openings between the barrier islands and the shoals. This was motivated by the observation that, for example, in the surge of 1 Nov 2006 the high water levels at Delfzijl occurred because massive volumes of water appeared to be build up between the barrier islands and the mainland shore, before being funnelled into the Eems-Dollard estuary.

The WS is obviously a semi-enclosed basin which receives the North Sea water across the tidal channels between the barrier islands. Therefore, the processes of filling and emptying are also governed by the capacities of those openings to carry water. Noted in passing, both processes of emptying and filling may in fact coexist at different depths because the local flow is expected to be strongly three-dimensional and also possibly affected to some extent by density effects. In this connection the values computed by the WAQUA solver are depth-averaged net fluxes, whereby much care should be taken when hastily assuming that the flow direction over the whole water columns is unique.

At any rate, the overall volume that is build up inside, or removed from, the WS through the net fluxes across the tidal inlet is accurate to the same extent that the depth-averaged equations approximate the fully-three dimensional and non-hydrostatic ones. By mass conservation, the temporal variation of such a volume contained in the WS is made available to raise or lower the basin-averaged sea level. In general, **it could be easily and credibly anticipated that there can be no severe surge without a considerable excess of water volume that is charged against the coast**. Of course, this statement should be revised while new insight develops.

So, such excess water volume, which we hereafter call the **wind-driven excess volume** (or 'surge water') may be a necessary condition to see rising waters shoreward. We will associate it to the surge's **overall potential strength**. The wind-driven excess volume is not a sufficiently descriptive quantity to infer severe surges for sure, because the effective arrangement of the free surface is non-uniform, time-varying and promptly responsive to the atmospheric forcing. This is to say that **the distribution of the potential hazard 'lumped' in the wind-driven excess volume may need further steering to become an actually hazardous surge (and, even then, not uniformly along the coast). Seen from the side of the atmospheric forcing, an extremely severe windstorm is likely to be one that creates a high wind-driven excess volume (global condition) *and* a definite shoreward rise (local condition). How such a shoreward rise occurs at different stations depends on the particular flow that develops over the extended shoals of the western WS, the narrower stretches of the middle WS and the Eems-Dollard estuary in the east**. An important benefit of using the excess volume as basin-wide surge indicator is that it condenses, at the very least conveniently, the massive amount of information that could be extracted by the time-varying maps of the flow. In this study we will refrain from taking the avenue of commenting on those maps, because they would lead the study towards a direction where the scrutiny of processes at a detailed scale seems unwieldy and premature.

Each storm thus produces its own history of water excess in the WS, i.e. it is a temporal trace of its effectiveness, as seen in Figures 4.4 and 4.Many different patterns are of course possible, while we are in search of one particular value that is representative of the whole history. Here, we chose to use the **maximum wind-driven excess volume** or '**surge water**' (within the surge's wind-driven phase). In principle, there is no guarantee that the time of the maximum excess volume coincides with the time of the highest

surge at any relevant location (because the surge may be a travelling mound of water). In practice, though, this indicator is probably the most immediate and convenient choice for histories having a lone peak. Other more suitable indicators could be devised to account for when the history takes more complex shapes. Importantly, we should emphasise that, **whereas the tide is not considered here, the overall potential surge strength would need to include the water volumes that are acted on by the tide**.

5.2.2 Per-station normalisation of water levels into alert scores

As we have already gained from the hindcasts of Alkyon (2007,2008a) and from the preliminary analysis of Chapter 5, we do not expect that the WS behaves like a completely unitary basin even under uniform wind conditions. Because of the basin's complex geomorphology and the time-varying flow motion, the histories of the surge at different stations are thereby expected to be dissimilar, arguably also under uniform wind forcing. This was also shown to be certainly the case in nature when the year-record water levels across the WS in the period 1933-2005 were compared. There, the stations in the eastern and western basins were correlated with noticeable differences of the coefficient of determination R^2 (0.5-0.9).

Here, we check out this expectation by concentrating solely on the water-level stations of **Den Helder, Harlingen and Delfzijl** in the west, mid and east basin – hereinafter also referred to as **test stations**. Figure 5.12 shows the scatter plot of the peak surges for the same events at paired stations. A definite common trend is clear. The correlation between Delfzijl and Lauwersoog is almost perfectly linear (R^2=0.997), while that between Lauwersoog and Den Helder is the poorest (R^2=0.968). There can be many reasons why the synthetic windstorms behave more consistently than the historical data. First of all, the synthetic profiles have homogeneous shapes, while natural processes are undoubtedly more haphazard. Also the uniformity of the wind field could play a role, but only a comparison between uniform and non-uniform wind fields could lead to a definite conclusion in this respect.

Limiting ourselves to the current set of results, in Chapter 5 we noted that the synthetically-generated surge histories at different stations may differ more than expected based on the wind 'simplicity' because, while the wind is uniform, geography is clearly not so. Here, in particular, it appears that their peak surges behave more closely to each other, which is a convenient circumstance of which we take advantage for the following comparisons.

In addition to the values simulated, Figure 5.12 shows the data point relative to the peak surge levels for the historical surges of Alkyon (2008a). Those levels are reported twice, as the measured water high and as the tide-free surge (approximated as water high minus simultaneous tide). Consistent with the above procedure, those have been normalised with the corresponding design level and with the design level minus the highest high tide respectively. The total-water alert scores are shown by symbols filled in grey, while the tide-free alert scores are shown by symbols filled in white. It is clear, that whether tide-free or not, the surges of Alkyon (2008a) did not impact uniformly over the Wadden Sea (they were chosen as those with the severest impact on Delfzijl). Although already well acknowledged, **the insight is that, in spite of the prototype structure of the windstorms, the hydrodynamic responses were different**.

However, in order to discount for the local differences and to make an unbiased basin-wide comparison, we also opted for normalising the peak values with a suitable local safety water level. As a first choice, this could be the design level (`ontwerppeil') as set by

the Waternormalen service of Rijkswaterstaat. This level normally coincides with the1:4000-year return time for the high water. According to the 'Average 1991.0' values currently available, it takes the values 445, 500 and 600 cm at Den Helder, Harlingen and Delfzijl respectively. The design levels, further, provide the regulatory norm according to which the water defences are designed and maintained. Therefore, it is an appropriate quantity to assess the challenge that the storm poses along the WS coast. Because the current simulations do not take into account the tide, which in fact causes offsets in time and water peaks with the surge (see, for example, Dillingh et al. 1993), we crudely consider the margin between the design level and the high spring tide as a better approximation for the safety level. For our exercise the safety level, therefore, is the difference between the design level and the high spring tide. The latter's values are 66, 117 and 151 cm in Den Helder, Lauwersoog and Delfzijl (Waternormalen). The safety levels are then 379, 383 and 449 cm respectively.

The dimensionless ratio between the **highest water level** and the **safety level** will be named here **alert score** (noted in decimal format). We define those windstorms/surges with an alert score of more than 0.75 as **'alerting'**. Such 0.75 value – an **alert threshold** – is purely conventional in more ways than one. For example, it does not need to be unique for the whole basin, and may weight several local circumstances either of hydraulic nature (say, the additional wave set-up and run-up) or other (say, the local dyke strength). The **safety threshold** is naturally the unity alert score, when the water level equals to the safety level.

We also note that similar quantities could be drawn based on the margin of safety water height that remains dry in the given surge conditions. In this case, the safety threshold would set the zero value, while negative values would indicate a non hazardous situation.

Figure 5.13 shows that the paired alert scores for the test stations now lay on a narrower band across the bisector (unity ratio) than the corresponding water levels in metric units. The worst agreement (that is the slope farthest from unity) occurs, expectedly, for Den Helder and Delfzijl at the opposite sides of the WS. However, the normalisation by the safety level successfully smoothes out the sub-regional differences and will be used throughout in the remainder to discuss the water levels. The orange square in the chart frames in the non-alerting event based on the 0.75-alert threshold.

Like in Figure 5.12 and obtained with the same normalisation criteria, the alert scores for the historical surges of Alkyon (2008a) are added. The alerting events appearing outside the orange square are the year-records of 1983, 1990 and 2006, and only the 1983 event appears to have been concerning in terms of tide-free surges at all three stations. The comparison with the historical measurements, however, points out that the alignment of the test-set data is partly due to the similarity of the windstorm generated out of the prototype mould (so to speak), but also that there may be modelling shortcomings at play (because the prototype windstorm is a deduction from those very historical storms). The eyecast exercise, in effect, aims at separating the issue of dissimilarity of the natural and modelled wind profiles (at Huibertgat) with that of the appropriateness of the model's assumptions (primarily wind uniformity).

Figure 5.14 to Figure 5.16 show the histories of the alert scores at Den Helder, Lauwersoog and Delfzijl for the complete test set of windstorms. The aim is only to give an impression of the variety of surge responses behind the choice of the maximum alert value as overall indicator. Therefore, each individual curve is left undistinguished from the other, but some features like the passage from the wind-driven into the inertial

phases are evident at first sight. The similarity of the alert-score histories at each test station is also striking. Although we did not carry out a quantitative assessment, it is apparent that most differences are of details, rather than of character. (We did not consider here the possibility of all surge profiles being self-similar by normalising with suitable scales for time and water levels.)

We may also note that **the safety level could also be worked out in a 'top-bottom' fashion, based on the simulations of the flow field generated by windstorms having a different return time**. The flow simulations, for example, could then direct towards the windstorm features that generate an extreme surge locally. From there, it could be possible to find out the frequency of occurrence of those weather conditions from the historical records according to standard probabilistic tools. Alternatively, **the same tool could be used to confirm that the expected return times for the local surge are consistent with the return times of the weather system that arguably has the most severe impact on the same location**. It is clear though that every difference between the current and alternative practices, as well as among different possible alternative practices, points to interesting areas of exploration/investigation on the underlying physical processes.

5.2.3 Framing surge events through local alert scores and overall potential strength

Thanks to the concepts of (overall) surge strength and (local) alerting event, we may propose a presentational framework to display the test-set surges as placemarks on a chart, similarly to the windstorms of Chapter 3 (although no framework equation is devised here). If the representations of the maximum water levels through alert scores and of the potential surge strength by the maximum wind-driven volume are accepted, the surges generated by the test-set windstorms can be plotted in the chart of Figure 5.17 (**framework surge chart**), where an amber-coloured line indicates the alert threshold and a red line indicates the safety level (unity value). The highest wind-driven excess volumes are all less than 25 billions of cubic meters (Gm^3), whereas the lowest ones are near to zero (for prevalently emptying events, for which a maximum deficit value would be relevant).

Based on the prototype behaviour, 270 windstorms have been created with different shapes of the temporal profile, peak speeds, durations, initial directions and veering widths – recall Section 4. Those parameters took exploratory values and did not cover the natural ranges of variability densely at all times. Also they were not associated with a probability of occurrence. However, the extreme surges that resulted could cause a much greater hazard than the historical storms events singled out in Alkyon (2008a). We stress that the above 25 billions of cubic meters corresponds to a staggering 7.5 m rise of the average level in the WS (recalling the rule of thumb: $1Gm^3 \sim 0.3$ m). Such a paradoxically high value is due to the fact that the solver assumes that the dykes are infinitely high. In practise, once the water level overtops a dyke's crest and overflow occurs, dam breaching and flood follow catastrophically. In what follows, we will analyse the results keeping this point of realism in the rear of our mind. However, this consideration may provide an important reminder about the fact that critical surge conditions are not necessarily a result of extreme windstorm parameters (the so-called 'superstorms'). **While it is almost trivial that any super-storm worthy of this name will create a super-surge of some sort and arguably helplessly catastrophic, a serious hazard conditions may be generated by windstorms having parameters that are not exceptionally high in themselves but combine in a way to create concerning enough surges**. This suggests that, ultimately, for the issue of water defences, surge simulations and probability of

extremes should not be regarded as altogether alternative approaches. Moreover, the statistics of extreme surges may not be linearly linked to the statistics of the extreme winds.

Same events for different stations are not immediately recognisable, but certainly lie on the same horizontal line because each surge is associated to an own amount of surge water (maximum wind-driven excess volume). The data at the test stations is quite consistent: they show positive correlation, and linear interpolation is appropriate. There, the higher the water excess, the more severe the challenge on the water defences.

However, it is also interesting to note that the events appear to behave somewhat differently for lower and higher alert scores, with decreasing scatter as the score increases. This would suggest, somewhat convincingly, that the more extreme the conditions, the more uniformly the WS would behave, since it will progressively depart from the connotation of a shallow basin. The question whether and to which extent the assigned shape of the WS is conserved, while moving towards more and more severe conditions, is an intriguing one. We emphasise that the quality of the alignment in the figure might adjust to some extent once Kuststrook-, rather than ZuNo, results are used.

The 0.75-alert threshold cuts out 196 (72%), 191 (70%) and 176 (65%) events at Den Helder, Lauwersoog and Delfzijl respectively. All surges with excess volumes larger than 5 Gm^3 can be alerting for Lauwersoog and Delfzijl, while it takes nearly two times more surge water to get equivalent alert conditions at Den Helder (probably a consequence of the larger storage areas in the western Wadden Sea). The fact that the alert scores in the above-unit range are consistently higher at Delfzijl is explained by the funnelling effect of the Eems-Dollard estuary, but also indicates that the (assumed) safety level would be less cautionary there than in the other stations. **So, in this case, the alert score concept can be used 'backwards' to assess the safety requirements against realistic scenarios. The framework surge chart of Figure 5.17 is therefore a successful tool to locate and discuss surge scenarios. The severe surges of the current test set (at least) could be ranked effectively enough by either the (global) wind-driven excess score or any (local) alert score**.

Although a detailed analysis is beyond the scope of this project, in the chart we note that several surge placemarks are more or less closely clustered. Those are possibly a result of similar windstorms that have similar effects; thence a consequence of the test set choice. In particular, we comment on two sets: the clusters near the safety score, and the lead clusters with the highest alert scores. The results are realistic in the first group only, since in reality the dyke's crests stand above the design level and the nearshore boundaries of the flow solver represent factual conditions. In the second group, as already noted, the results are indicative of some kind of disastrous windstorm, the water levels raised by which would have not been withheld by the dykes long since.

Table 5.3 shows the features of 6 windstorms generating surges with a safety score in the range 1-1.1 at Delfzijl (which also gives the sorting column-wise).

It is to be noted that Den Helder, and in a few cases Lauwersoog, are not pushed to the safety score while Delfzijl is. This is worthy of notice because, in principle and ideally, there should be no difference between the alert scores of any stations. Assuming that the reference levels used for normalisation are correctly devised in the first place, **the differences in the results mean that, for those events, the safety levels at Den Helder are more than cautionary, while those at Delfzijl are insufficient – for this kind of windstorms. This, of course, does not amount to saying that any weather event should have the same surge impact everywhere.** Rather it implies that – if an event is so large

to have a basin-wide impact – then all alert scores should fall in the same narrow range, because the local design levels are truly representative of the local risk of overtopping.

Those six storms of Table 5.3, 'hand-picked' from the test set, are all of 37 m/s, relatively short, and, if rotating, they end blowing northerly with no or a short ramp period. The two steady-direction cases are westerly as well as northerly. It is clear that inferences on such a small sample would be short-legged, but they already help gaining a flavour of a connection between windstorms and severity of surges (this is resumed in Chapter 6).

T(h)	c(%)	u_p m/s	α_1	α_2	e (km^3/s^2)	ω (deg/h)	u_{ap} (m/s)	Excess volume (Gm^3)	alert scores Den Helder	alert scores Lauwersoog	alert scores Delfzijl
48	100	37	315	360	2.19	0.9	23.3	9.8	0.72	1.01	1.06
24	100	37	225	360	1.09	5.6	23.3	8.8	0.55	0.93	1.04
24	66	37	270	360	2.21	5.7	29.5	9.9	0.89	1.02	1.03
24	66	37	315	360	2.21	2.8	29.5	9.8	0.87	1.02	1.01
24	66	37	360	360	2.21	0.0	29.5	9.6	0.84	1.01	1.01
24	100	37	270	270	1.09	0.0	23.3	12.6	0.85	0.89	1.01

Table 5.3: The windstorms of 6 surges near the safety score at Delfzijl

Table 5.4 shows that the top-6 surges at all test stations are generated by the same six storms. Their common features are high peak speed, either northwesterly direction or veering to it, long trapezoidal shapes, and same average-power speed. The energy scale alone is not a determining factor. Whether the storm is veering or not does not determine appreciable difference in the maximum peak score (because the triangular part is small in comparison), nor does so the rate of rotation that, in all cases, is low in our range. The insight we gain here is that we should be watchful of strong quasi-steady northwesterly winds. Three final points are worth commenting thereby.

T(h)	c(%)	u_p m/s	α_1	α_2	e (km^3/s^2)	ω (deg/h)	u_{ap} (m/s)	Excess volume (Gm^3)	alert scores Den Helder	alert scores Lauwersoog	alert scores Delfzijl
48	33	37	225	315	6.59	5.68	33.6	24.61	1.76	1.95	2.05
48	33	37	270	315	6.59	2.84	33.6	24.55	1.76	1.94	2.05
48	33	37	315	315	6.59	0.00	33.6	24.49	1.76	1.94	2.04
24	33	37	270	315	3.29	5.68	33.6	23.89	1.73	1.92	2.03
24	33	37	315	315	3.29	0.00	33.6	23.92	1.73	1.92	2.02
96	33	37	225	315	13.17	2.84	33.6	24.23	1.73	1.92	2.02

Table 5.4: The windstorms of the top-6 surges.

Firstly, although this is not sufficient to conclude that rotational features are unimportant, this finding certainly supports the speculation that non-rotating winds are relevant (so another kind of prototype windstorm may turn up to be relevant). In particular, those windstorms clearly lead the basin towards a steady-state flow arrangement, which cannot be established for windstorms changing on rapid enough timescales.

Figure 5.18 shows the history of the alert scores at Delfzijl for a selection of surges with the same features as the top-6 surges of Table 5.3: those are long trapezoidal shape (therefore, extended steady winds) and northwesterly final direction. All other windstorm parameters vary according to the test-set general specifications.

It is important to note that, irrespective of the windstorm's duration, the peak values are achieved earlier than or when the levels have become steady in time. After steadiness is achieved, the hydrodynamic conditions seem to be fully adjusted to the steadiness of the wind. In the case of the 24 h and 48 h windstorms, there is a continuing increase in water level past 8 and 16 hours respectively, when (and because) the wind has stopped rising and veering (whereby the maximum levels occur at the end of the storm). Conversely, in the case of the 96 h windstorms, where the wind becomes steady

at 32 hours, the increase of water level is not indefinite but seems very nearly settled earlier than 48 hours. Admittedly those considerations should be revised when the time is scaled with duration, and the proportions of the results become apparent.

However, **it seems that there is some sort of inherent (probably local) timescale after which the hydrodynamic conditions become steady in turn. The impact on our modelling can be important, because the duration of the steady wind beyond such timescale has no significance in the evaluation of the peak surge** – and rather could make the 'T2' durations of our synthetic profiles misleading. A detailed analysis of when the surge peak occurs for each scenario has not been carried out in this study.

As a matter of fact, to make the picture more complicated, the infamous surge of 1 February 1953, which was a rather steady wind event, is the most severe on record ever at Den Helder, but ranks just 49 among the Delfzijl year records (see Alkyon 2008a). On the other hand, the peak surges of 1 February 1953 at Den Helder and Delfzijl normalised with the current design levels give alert scores of 0.73 and 0.54 respectively. Their placemarks in Figure 5.17 would lie rather far away from the top-6 of the test-set.

Secondly, the likelihood of the natural occurrence of such severe synthetic windstorms is an important topic that deserves attention, because it gives the very ground to practical concerns.

Thirdly, the longer the storm, the more evident the need is to consider the interaction with several tidal cycles.

5.3 Surge simulations: the eyecasts

In this section we turn to commenting on the eyecast surges of 27 Feb 1990 and 1 Nov 2006 by comparing them with the available measurements. The other four eyecasts first introduced in Section 4.2 gave similar results. Further, the chosen ones were repeated for two variants, wherein the simulation period was extended by attaching a steady-wind period (duration T2) at the tail of the initial rising/veering period (duration T1).

We discuss the results at Den Helder and Delfzijl only, because of the availability of 30-constituent accurate tidal information through the Tide Tables (RIKZ, 2009). The 'real-world' surge is estimated by subtraction of the measured water levels (retrieved by the Waterbase service) – the limitation of this best-estimate expedient has already been discussed and acknowledged in Alkyon (2008a).

All eyecast data discussed here have been computed on the Kuststrook domain. In the chart, thick red lines indicate the wind-driven phase, while thin red lines do the inertia-driven one (i.e. the inertial motion caused by the wind turned off artificially).

The comparison of the baseline cases (where the eyecast windstorm is designed with a close match with the measured wind) is presented in Figures 5.19 to Figure 5.22, for the 27 Feb 1990 and 1 Nov 2006 surges respectively, each at Den Helder and Delfzijl. The plotted measurements at Den Helder are jagged more than those at Delfzijl, because all measures are taken at 10-min intervals, whereas the Delfzijl curves are drawn at an hourly rate (by the highest water level within each hour).

The peak surges at Den Helder (at the end of the windblown phase) are underestimated even if we take into account that, in reality, a sizeable set-up was already present at the time when the synthetic wind starts to blow. This is compensated in the plot by the artificial vertical offset of the red line to match the simultaneous tide-free surge (estimated as it is). At any rate, the simulated increase in water level at Den

Helder is smaller than measured. (A note of caution is in order regarding the fact that measured water levels include the wave set-up that has been completely disregarded in the modelling.)

The peak surges at Delfzijl behave similarly. For the 1990 event only, the overall water rise in the eyecast at the end of the wind-driven period compares well with the measured one, but it falls short of the measured surge peak that occurs later by more than 150 cm. Such a large gap indicates a definite deficiency somewhere in the modelling. Alkyon (2008b) has shown that a two-way coupling between wave and currents can account for a sizeable part of that gap, but probably not so much as to completely justify this.

These results indicate that, at the end of the wind-driven phase, not enough water has been displaced to the test stations. In turn, this suggests that a drawback may lay in some insufficiency of forcing terms as we have modelled them – that is, in the current schematisation of prototype storms.

Figures 5.23 to Figure 5.26 show the same plots for the eyecast variant with a steady speed extension. The steady-speed value is the peak speed, here unlike Alkyon (2008a). The first period (T1) is thus the same as before, while the extension (T2) is a fraction of T1 for the 2006 storm and a multiple thereof for the 1990 storm. The duration of the two extensions is chosen such that the synthetic and effective directions stay close (small variance). This choice thus implies that the only eyecast parameter that is effectively 'boosted' is the steady wind speed. By the arguments of Chapter 3, we therefore expect a considerably more energy-giving event than in reality (unlike in Alkyon 2008a, granted the limits of using Formula 8).

The comparison of the water levels is insightful, because the eyecasts' growths to the peak unfold with quite different evolutions from those in nature. Firstly, the measured peaks are completely missed. Secondly, the simulated ones are attained at the end of the wind-driven phase. These considerations mean that the natural peak is not explained by a hydrodynamic system approaching the steady state in the way that the eyecasts do. Commenting on four hindcasts, in Alkyon (2008a) it was already argued that surges in the WS are intrinsically unsteady process, and the present results corroborate this.

Additionally, the causes for the discrepancy that we observe must originate from processes that are already active before the steady-wind period that we have constructed (else, the windstorm extension would have helped to approach the measures to any extent). Therefore, we argue that the modelling deficiency probably lays in the assumption of applying a uniform wind. Said otherwise, **the missing action on the waters that may explain the inability to capture a realistic peak could arise from the basin-scale differences of the wind action over the free surface**.

We note (perhaps redundantly) that, **in the depth-averaged governing equations solved by WAQUA, the wind stress appears only as a scalar and not as a gradient term**: this means that **the non-uniformity of the wind does not affect the flow pattern by direct action on the water column, but rather through the local balance of all the forces and the mass/momentum exchange between columns of water.** This mechanism is certainly complex in a natural body of water. **This seems to suggest that wind non-uniformity can effectively translate into surge unsteadiness by causing flow processes with time scales that are not exactly those of the atmospheric forcing**.

Figure 5.27 to 5.30 show the same eyecast surges for the second variant, i.e. when the steady wind blows with an averaged, rather than peak, speed. The simulated directions are the same as above, but in this case the ramping period of speed is affected too, with

reduced speeds. The results are consistent and unsurprising, since the peak surges are accordingly reduced on account of the lower wind speeds at play.

However, this observation prompts another insightful comment. It suggests that **the lack of any significant connection between measured peak surges and measured peak winds (Alkyon 2008a) is another manifestation of the fact that the surge flow was quite far from steady-state conditions. If a wind had blown long enough to sustain such path (like in the test set windstorms), a connection between peak surges and peak wind speed could have been established. But this has not certainly been the case for the relevant historical events on focus in Alkyon (2008a) and, again, here**.

In addition, we can also warn that the search for the 'best' steady speed value to provide the same peak surge is unconvincing, because the underlying current field would certainly be different. This is especially relevant in the present context, where the ultimate aim concerns the safety of the water defences. It has been ascertained that both water levels and currents are crucial for the determination of the local wave climate (Alkyon, 2007, 2008b). And both need to be modelled consistently and realistically, that is for a unique hydrodynamic scenario.

6 Connecting wind scenarios and surge simulations

This chapter discusses the relationship between wind scenarios and the resulting surges as inferred from this study. Firstly, some general observations are made about the set-up of the study. Secondly, the main results of this study are discussed, although more efforts are needed to identify which features of a windstorm are dominant parameters for the generation of the WS surge.

6.1 General observations

The surge data need to be put in relation with the windstorms that have generated them. This is functional to understanding (or gaining an overview) the physical connection between windstorm and surges when a large number of events are considered. The wished gain of knowledge is twofold. On the one hand, this supports the confidence-building at using synthetic events to model the prototype storm; we can in fact only do so by trusting the flow solver and appreciating how the extent of realism placed in the causes (air flow) is reflected on the response (water flow). On the other hand, thanks to the insight gained by data inspection, **our understanding of the hydrodynamic behaviour during stormy weather of the WS can broaden in spite of the working assumptions which limit this study**.

Since in the test set there is a clear positive correlation between the wind-driven excess volumes and the maximum alert scores at all test stations (Figure 5.17), commenting on either is to a large extent equivalent, especially in the regime of high alert scores where a more clear-cut behaviour seems established. It is to be emphasised that such a tidy arrangement is, certainly, in part due to the fact that the windstorms are similar in shape as a start. A detailed analysis of the whole test set is not relevant to the primary aim of this project, but it is interesting to see whether surges as a whole show any systematic tendency to follow some of the windstorms' features. This might pave the way to investigating a sort of 'spine structure', or 'character', around which the actual unsteady flow tends to arrange itself in (the modelled) stormy conditions. Typical behaviours (if found) would indicate the action of the less ephemeral agencies driving the flow: those could be shape, bathymetry, morphology or, in general, any condition or process that, for example, outlasts the storm period relatively unaffected.

6.2 Generation of the surge strength

As a first step, we rank the surge strength through the maximum wind-driven volume, and evaluate whether and how they relate one-to-one with the speed and direction framework parameters of the test set. In particular, we will focus on the top-50 surges of the set, which have excess volumes larger than about 16 Gm^3. We have already pointed out that this is a regime where the withstanding capacity of the water defences is not modelled realistically.

Figure 6.1 is the scatter plot of the excess volume against the windstorm duration. Top-50 surges can be generated by windstorms lasting for 24, 48 and 96 hours alike, each covering the whole upper range of excess volumes. Table 5.3, indeed, showed that duration is not a determining factor of the top-6 storms. **This is consistent with the fact that long steady winds will drive the flow towards a steady state and, once this is**

achieved, the duration of the wind is not a timescale for the hydraulic processes any longer.

Figure 6.2 is the scatter plot against the triangular fraction, that is to say an indication of the profile shape independently of the parameters that set the magnitude. Top-50 surges can be generated by triangular as well as trapezoidal shapes. This complements Table 5.3 and confirms that **fully-triangular windstorms, where the wind direction veers and is never steady, are a class contributing to severe surges**. Plateaus, however, make the surge more severe, although the increase in excess volume between the short- and long-trapezium shapes is smaller than the increase from the fully-triangular to the short-trapezium shapes. Three values of duration are not enough to infer whether this indicates that there is a tendency sort of 'saturation' (that is: even lower differences) while the profile tends to become fully rectangular. **Fully rectangular profiles (c=0) represent the current way of schematising the storm conditions in the HBC (steady uniform winds)**. Following the analysis of Chapter 3, **fully-rectangular windstorms invariably have higher energy content than profiles with the other shapes, all other conditions being equal. The question about their likelihood is therefore one about which atmospheric conditions can sustain such a windstorm and how likely to occur it is**.

Figure 6.3 shows the scatter plot against the peak speed. Only two peak speeds are used in the test set (25 and 37 m/s), but the lower wind is clearly not strong enough to cause a surge stronger than 10 Gm^3 – less than needed to break the safety score. All top-50 surges are in fact caused by the strongest wind. In retrospect, more values of wind speed would have helped recognise a possible connection between peak speeds and the largest excess volumes that each can deploy (irrespective of the other parameters). This clear-cut connection between the highest surges and the highest peak wind speed would be at variance with the indication gathered in Alkyon (2008a) that measured peak surges did not quite rank as the peak speeds that generated them. This was regarded as a manifestation of the fact that the storm/surge dynamics redistributes the hazard over the WS coast in a way escaping simple schematisations. Some tentative explanations can be given here though. **The non-triangular synthetic storms of the test set, in fact, generate peak surges by steady action, i.e. by driving the flow towards a steady state. The simulated peak surge is invariably attained upon the establishment of a steady-state arrangement, while this is not certainly the only way a peak surge can develop in nature. In such a complex basin as the Wadden Sea, mounds of high water can build up and develop, regardless of whether any steady state is ever attained. We work in completely unsteady hydrodynamic conditions**. This was seen to be the case for the surge of 1 Nov 2006 Alkyon (2008a). The fact that this is not seen in the present test set suggests that the present schematisation for the synthetic windstorms fails somewhere. In the previous discussion on the so-called 'eyecasts' (Sections 4.2 and 5.3), wind uniformity was earmarked as a working assumption in the forcing that could restrict realism (at first order). Whether this is a failure of the present working assumptions or the indication of different hydrodynamic behaviours for very high alert scores is a question for which more attention is needed.

Figure 6.4 shows the scatter plot against the energy content (18 test values in the range 0.35-13.17 km^3/s^2). Top-50 surges occur for all values in the range above 2 km^3/s^2, but this is quite not a necessary condition. Therefore, the energy content alone is not a determining factor. We acknowledge that here **the energy content is worked out based on scaling arguments, whereas the solver implements a specific equation for the wind-stress coefficient. A skin-friction expression of equivalent accuracy would also be**

needed. It is therefore plausible that the presentation is inaccurate to show the expected connection of cause and effect.

The average-power speed is a velocity scale that can be derived from the energy content and duration. The impact on the surge potential strength is shown in Figure 6.5. Although not conclusive at all, this gives a little credit to the speculation that **the surge strength may still follow a one-to-one relation with a speed scale of the windstorm (as and if they have enough time to tend to a steady state)**. However three values, instead of two as in Figure 6.3, are certainly still insufficient to draw any conclusion. Also the energy content should be worked out more accurately.

Figure 6.6, Figure 6.7 and Figure 6.8 show the scatter against the initial and final direction, and the windswept compass width. The three quantities are clearly related. Northeasterly winds and winds veering to NE are irrelevant. **Winds that start to blow from SW, W and NW and end blowing from W and NW, including absence of veering, deploy the largest amount of water**. The veer from SW to N (135 deg) in particular seems to be the least dangerous.

Figure 6.9, lastly, describes the rotational behaviour in terms of rate of rotation, and complements the previous three charts by adding the temporal information (18 values ranging from 0 to 22.7 deg/h). **The most rapid rates of rotation do not enhance the surge generation, but surges of any intensity can be created with lower rates of rotation (slow rotating winds) or none (steady-direction winds)**.

Based on the above chart, it is clear that it is not possible to establish one-to-one connections between the surge potential strength and the parameters of our synthetic windstorm. The only variable subject to an opening is possibly the peak wind speed or the average-power speed, but a more refined study would be necessary to unravel this point. It is, therefore, immediate to conclude that only multivariate analyses can help single out what is (are) the combination(s) of windstorm factors that have a definite surge-enhancing power.

Table 6.1 to Table 6.3 show a two-parameter tabulation of the top-50 surges based on the (T,c), (e,c) and (e,T) pairs that define the temporal profile for speed. The percentages of each combination and of each class are given together with the corresponding excess volume, since extreme values are on focus here. It is obvious that a similar exercise is purely illustrative, since a 50 sample strong population is too small to draw firm conclusions. This can be, for example, a guideline to draw a denser test set of windstorm creating surges of the same rank as the top-50's. This nonetheless, we can gain quantitative information for example on dominance of long trapezoidal profiles that take the lion's share in any classification; but also that the two trapezoidal shapes do not produce large widely different surges unless they are of short duration. In the same line, suitably chosen groups could be investigated such as the whole set of fully triangular profiles.

In general, the order with which certain tabulation filters are applied to group so many events is arbitrary and reflects the aim of whoever processes those data. In particular, we do not aim here at carrying out a complete database analysis, but rather at suggesting an approach to extract relevant information from those data. Based on similar procedure, indeed, our analysis could be extended on other windstorm prototypes and/or perform additional simulations to make the test set sufficiently large to draw firm conclusions.

To conclude, Figure 6.10 to Figure 6.14 show the scatter plots of the local (maximum) alert levels at the test stations against the test-set windstorms' duration, peak speed, energy content, windswept compass width and rate of rotation. The information contained in those plots is not commented here, as it would consist in rephrasing the same comments for the surge strength in the light of the surge framework chart of Figure 5.1The alert and safety threshold are clearly indicated. As expected, the scores at Delfzijl are consistently higher than those at Lauwersoog and Den Helder. Delfzijl, additionally, is the only station where storms with 25 m/s speed generate alert scores larger than the alert threshold. The features appearing in the other charts are not deemed worthy of separate comments.

Duration | shape	c=0.33	c=0.66	c=1.00	Whole row
T = 24 h	10 (23.9)	10 (19.7)	0	20
T = 48 h	18 (24.6)	16 (24.1)	8 (17.5)	42
T = 96 h	18 (24.2)	10 (23.8)	10 (20.1)	38
Whole column	46	36	18	

Table 6.1 Top-50 surges. Percentage of occurrence and maximum excess volume (in braces) of windstorms with speed profiles having given duration and triangular fraction.

Energy c. | shape	c=0.33	c=0.66	c=1.00	Whole row
e = 0-5 km^3/s^2	10 (23.9)	26 (24.1)	18 (20.1)	54
e = 5-10 km^3/s^2	18 (24.6)	10 (23.8)	0	28
e = 10-15 km^3/s^2	18 (24.2)	0	0	18
Whole column	44	26	10	

Table 6.2 Top-50 surges. Percentage of occurrence and maximum excess volume (in braces) of windstorms with speed profiles having given duration and energy content fraction.

Energy c. | Duration	T = 24 h	T= 48 h	T = 96 h	Whole row
e = 0-5 km^3/s^2	10 (23.9)	24 (20.6)	10 (20.1)	54
e = 5-10 km^3/s^2	0	18 (20.4)	10 (23.8)	28
e = 10-15 km^3/s^2	0	0	18 (24.2)	18
Whole column	20	42	48	

Table 6.3 Top-50 surges. Percentage of occurrence and maximum excess volume (in braces) of windstorms with speed profiles having given duration and energy content fraction.

7 Summary and conclusions

7.1 Summary of methodology

This section summarises the methodology followed in the present study. Text in **boldface** highlights keywords or important concepts.

'Prototype storm' is the name used for the behaviour with which the wind measurements appeared to create the most severe year-record surges in the (eastern) Wadden Sea (WS) in the period 1981-2006 – including, for example, the top-rank surge of 1 Nov 2006. This behaviour is consistent with the transit of pressure lows north of the Dutch coast and moving eastwards across the North Sea. Cyclonic circulation brought wind acceleration and rotation overhead. To this extent, in this study prototype storm was synonymous with atmospheric cyclonic circulation.

In this work we have investigated one possible **prototype-storm model** to simulate artificial surges in the entire WS. This has been done by directly setting a **uniform, time-varying wind field**, decoupled from a pressure system and blowing over a limited area encompassing the Dutch coast. The wind field is thus entirely defined through the **temporal profiles** for the speed and direction that, additionally, are chosen independently. Such temporal profiles were **parameterised**: this was done by setting six **profile parameters** such as duration, initial and peak values, and a **shape function** that expresses the change from initial to final conditions.

The values of the profile parameters were chosen as to represent a few plausible as well as extreme ranges of variation. The shape functions were chosen as to mimic the rising and veering winds suggested by the prototype storm: we thus adopted **triangular and trapezoidal** shape functions. We have also considered steady-direction winds. A test set of 270 synthetic windstorms was eventually created by combining the profile parameters and shape functions for both wind speed and direction. The same procedure has been used to construct some closely-fitting synthetic profiles for the year-record historical storms studied in Alkyon (2008a) – named '**eyecasts**' here.

A **conceptual framework** was devised to visualise and categorise those storms not just in terms of profile parameters, but also in terms of an estimated capacity of doing work on the waters (**energy content**), and of their rate of rotation.

The windstorm duration, peak speed and energy content thus act as the **framework parameters for the speed**. A physically-based equation particularised for a temporal profile establishes the connection between the framework parameters for each storm, and is called **speed framework equation**. Such an equation is here a first-order expression for the energy transfer between airflow and water flow based on scaling arguments.

Both the speed framework parameters and equation eventually lead to the description and condensation of the particular temporal speed profile as a windstorm's **speed placemark** in charts. These charts, where the framework parameters appear either on the axes or as contour lines, are naturally called **speed framework charts**. A placemark may not be unique to one windstorm only, insofar as different events may end up having the same framework parameters after different temporal profiles. Also, the evolution of a

windstorm can be represented as a track of time-progressing placemarks on those charts, making its energy-transfer history evident.

A similar reasoning applies to the wind direction. The **direction framework parameters** coincide with the profile parameters that are duration and initial and final directions. Because the dynamical effect of the time-varying wind directions on water are not clearly understood, the directional information can be connected merely kinematically. The equation for the angular speed, or rate of rotation, is the **direction framework equation**, which is sensitive to modelling choices in the direction shape function inasmuch as the wind may turn for only a period of the storm (as we assumed). Similarly to the speed, **direction placemarks** position a windstorm in the **direction framework chart**, and time tracks could also be drawn to visualise and read the directional history.

The surge classification and interpretation contains global as well as local indicators. A surge's **potential strength** on a basin-wide scale is indicated by the maximum **wind-driven excess volume** (surge volume, surge water) built up by the windstorm while it develops. It occurs at the time when the WS contains the largest amount of water. The local intensity of the surge is indicated by the maximum high water and normalised by the regulatory safety levels in order to give a local **alert score**. The **test stations** of Den Helder, Lauwersoog and Delfzijl cover the western, central and eastern WS. The alert score provides a hazard-normalisation across the WS and represents a nominal degree of hazard that the windstorm has placed against the test station. Maximum alert scores and maximum wind-driven excess volumes allow the display of the surges as placemarks on a **surge framework chart**, which is used to single out **alerting events** based on a chosen **alert threshold**. Alerting events are connected to the windstorms' parameters by one-to-one correlation and selected one-to-two correlations, either in graphical or tabular form.

The criterion to assess the viability of the schematisation of a prototype windstorm was based on simply comparing the predicted surges with the observed ones for the selected historical storms. Applying more sophisticated criteria is needed after the present concept of a prototype windstorm has improved.

7.2 Conclusions

The primary objective was to verify whether the duration, initial and final conditions, and rates of change of a windstorm are "a necessary and sufficiently complete set of parameters to describe a prototype storm". We conclude that the present schematisation of a 6-parameter prototype windstorm is still not ready as an operational tool for WTI-2011.

Firstly, based on this study, we conclude that **those parameters are necessary to describe a prototype windstorm**. This is because they are a first step to account for the windstorm's unsteadiness. What has been previously identified as the prototype windstorm is the track of cyclones travelling overhead the measurement point. Such cyclones are acknowledged to be the main cause of the stormy weather in the North Sea and, therefore, are very relevant to the aim of modelling surges in the Wadden Sea. Those processes are unsteady in nature, and need to be modelled as such when used as forcing terms on the waters.

Secondly, we conclude that the aforementioned parameters **are not sufficiently complete to reproduce historical storms, because other forcing features (like, arguably, wind non-uniformity) are not accounted for in the schematisation**. They could be

realistic for very uniform and long-lasting windstorm, where the hydrodynamics can effectively approach a steady state, but the probability of occurrence of such storms should be assessed separately. We also have fitted synthetic windstorms of the chosen number of parameters and shape to historical wind histories and have computed the related free surface and flow fields. The inspection of the surges at onshore locations supports the conclusion that the present wind schematisation is insufficient to deliver accurate realistic enough simulations.

Fourthly, from the numerical experiments of the test-set synthetic storms, we found that groups of windstorms exist that give alert scores just over a value of one (see Figures 5.13 and 5.17). Clearly, these storms are not the most severe in our population of wind storms, but those could be dangerous enough as and if they occur in reality. Those might be a subset of storms worthy of being included, in perspective, in the determination of the HBC.

Fifthly, the peak surges for the six historical severe storms considered in Alkyon (2008a) could not have occurred with a uniform unsteady wind. Further, because the surge peaks occurred much earlier than the timescale needed to reach the steady state, this suggests that own timescales of the water motion develop in the Wadden Sea, which are not directly associable to the windstorm time scales. Uniformity is the unrealistic feature of the imposed wind field that can have prevented a close match between the simulated and realistic surge histories at the shore. If this diagnosis is confirmed by aimed investigations, this means that such hydraulic timescales are peculiarly generated by non-uniform unsteady wind fields over a semi-enclosed shallow basin.

Sixthly, currents occurring at the moments of high water are rather important for the wave climate prediction (Alkyon, 2007). The same surge level at any given location can, in fact, occur in association with diverse velocity fields. This additional circumstance has not yet received much attention and is not guaranteed by the current schematisation of the prototype storm. Said again, the present method of determining the Hydraulic Boundary Conditions still ignores current effects on the wave conditions

Seventhly, applying the concept of prototype storms to the determination of the HBC requires assigning probabilities of occurrence to the individual storms that are parameterised. As follows naturally from the above discussion, the present six-parameter windstorm model is not yet capable to produce realistic surges and associated currents. Clearly, the number of parameters should be extended, but the general methodology for the prototype windstorm indicated in Section 7.1 should be reviewed, modified or extended, especially allowing for the non-uniformity of wind fields.

Lastly, we point out that, for our purpose, the prototype windstorm is not just a mathematical formalism, but a preferred arrangement of the weather systems that produces critical surges on the Dutch coast of the Wadden Sea. The schematisation that we have used so far was inspired by reading the records of wind speed and direction locally at Huibertgat and Texelhors occurring during the year-record surges studied in Alkyon (2008a). This study acknowledges that such a preferred arrangement is not unique (so the number of prototypes increases) and concludes that the uniform/unsteady schematisation is still too restrictive to represent the real effect of such weather systems (so the modelling effort for such prototypes needs to be upgraded).

8 Recommendations for future studies

This study unveiled much insight in the mechanisms responsible for the generation of surges in the Wadden Sea. It also revealed knowledge gaps that need further attention to improve the concept of hypothetical windstorms for use in deriving Hydraulic Boundary Conditions. In addition, some working assumptions need to be improved for the same purpose. Below recommendations for further studies are summarized.

- The **interaction between the tide and wind-driven surge** is not linear, and superimposition of the respective water levels is only acceptable for sake of expediency. Offsets in peak time and peak water height do occur, and it is not well known whether and when the interaction enhances or reduces the hazard. The same applies to both forecasts and hindcasts. Historical records are given in terms of total water levels. **A review of the relevant scientific literature to define the state of the art is highly recommended**.

- Synthetic windstorms seem to be a valuable tool to gain insight on the hydrodynamic behaviour of the Wadden Sea in stormy condition because they are based on mechanical models and because a definite dynamics is at play in the Wadden Sea. When synthetic scenarios are used to 'explore' the features of the surges generated by a range of windstorm parameters, it should be borne in mind that those parameters need to be eventually linked to their probability of occurrence. **The probabilities of occurrence of windstorms and surges, and the physical and numerical modelling of windstorms, surges, currents and waves, should lead to a consistent description of the flow and cross-validate each other**. Whether and to which extent this is the case in the current state-of-the-play should be clearly defined. **A review of the scientific literature and of other efforts already undertaken in this connection is recommended**.

- Modelling historical surges with time-varying and **uniform** synthetic winds is not accurate enough to reproduce the behaviour of the water level history and currents realistically. **Therefore, it is recommended that future synthetic windstorms allow for space non-uniformity. It is also recommended that such space-uniformity is obtained by modelling synthetic pressure fields that reproduce the atmospheric systems and produce wind speeds and directions as a result.**

  The parameters defining the prototype windstorm will then regard the pressure fields and, for the present storm prototype, synthetic pressure lows in the North Sea. Because those parameters are many (see, for instance, Bijl (1995)), accuracy and realism in the improved modelling can be tuned to purpose by focussing on a selection of those (for example, non-travelling pressure lows with different sizes to test wind non-uniformity alone). The wind field can be worked out from the pressure patterns by so-called 'balanced-flow' estimates such as the geostrophic speed (restrictively, Bijl (1995)) or the gradient speed (accounting for centripetal acceleration). The effect of atmospheric pressure on water levels will be accounted for automatically.

- Wind-generated surges result from the application of **simplified models for the wind drag** that translate the speed at a certain height into a mechanical action on the surface. It is not well known how well these models perform for higher wind speeds that are relevant to storms. **A review of the relevant scientific literature** to define the state of the art is highly recommended, as it may have an effect on the predicted surge levels. New acquisitions should be implemented and tested thereafter.

- The numerical solver works under the assumption of infinitely high dykes, so the predicted growth of the surge for water levels above the dykes' crests is somewhat academic. Extremely severe synthetic windstorms will obviously produce extremely severe surges, the effects of which are not currently modelled, but which are arguably conducive to catastrophic effects (over-washing of the barrier islands and overflowing of the dykes). **It is recommended that future studies using synthetic windstorms focus on storm parameters that can raise the waters up to the levels of those crests** (with adequate engineering margins of a few meters). Also, those are the conditions that would cause manageable hazard. **Those forcing conditions might be not statistically extreme when taken individually, but produce extreme surges if realistically combined**.

- **A review of the available meteorological and hydrological records that connects the occurrence of nearshore surges in the Wadden Sea with typical atmospheric patterns of the North Sea will provide important insight from the past events**. The surges should pertain to stations spread over the Wadden Sea coast and covering the western, middle and eastern basin (say Den Helder, Lauwersoog and Delfzijl). This analysis could increase the number of prototype windstorms. This is also important to become aware of which forcing conditions should be considered as 'ordinary' and which one should be regarded as 'exceptional'. To the authors' best knowledge there's already been effort to connect typical weather systems in the North Sea (identified for example by Kruizinga (1978), among which the pressure patterns generating the prototype storm) and surges on the 'closed' Dutch coast (see for example at Hoek van Holland, see Dillingh et al. 1993). **A similar work concerning the Wadden Sea area is recommended, and challenges added by the complexity of the Wadden Sea system can be expected.**

- **Future flow simulations should be run on the complete Model Train up to the resolution available from the Kuststrook domain**. This gives the solver additional resolution for the hydraulic processes that have smaller time- and length scales and that occur when the wind forcing varies rapidly enough within natural rates of change.

- **The system of barrier islands and tidal inlets could have a filtering effect on the large-scale wind-driven currents in the North Sea, whereby only the flow driven by the atmospheric forcing of the southernmost North Sea may determine the surge levels inside the Wadden Sea**. Such a speculation, which is suggested by an incomplete set of simulations, merits further investigation. But it is likely to become outdated as soon as the atmospheric forcing is modelled by synthetic parent pressure fields and the wind field becomes not uniform. This is because the delimitation of the active wind field follows directly from the given size of the pressure system.

- **The avenue of classifying the potential of windstorms to generate surges based on its ability to do work on the waters needs further attention**. In particular, using a scale (rather than a complete expression) for the energy transfer from air- to water-flow may be crude in the light of the drag and skin-friction coefficient being dependent on the speed velocity. On the other hand, the related concept of average-power speed seems to have some merit. Also, once that the surge reaches a steady state, the windstorm duration ceases to be a significant timescale. The handling developed in Alkyon (2008a) and here needs refinement. **Further developments of this concept should consider those enhancements, especially if semi-empirical connections between windstorm and surges as 'whole events' for the Wadden Sea are sought**.

- **The avenue of classifying the potential of surges through wind-driven excess volumes and alert scores appears insightful**, but it is not tested yet on many enough types of windstorms to be guaranteed. Therefore, **it is recommended that the application and interpretation of these quantities is carried out with reserve and with due attention paid to the applicability of the assumptions used in its determination**.

References

Admiralty Sailing Directions, 1999. *North Sea (East) Pilot (NP55)*. UK Hydrographic Office (3rd edition).

Admiralty Sailing Directions, 1959. *Baltic Pilot, vol. I (SD18)*. UK Hydrographic Office (8th edition).

Alkyon, 2007. Hydro-dynamics in the Wadden Sea during storm conditions. Current and wave conditions during the storms of 1 Nov. 2006 and 18 Jan. 2007. Report A1848. (J. Adema and G.Ph. van Vledder).

Alkyon, 2008a. Simulation studies for storm winds, flow fields and wave climate in the Wadden Sea. Report A2108. (G Lipari, G. Ph. van Vledder, J. Cleveringa, J. Adema)

Alkyon, 2008b. SWAN hindcast in the eastern Wadden Sea and Eems-Dollard estuary. Report A2191 (J. Adema, G.Ph. van Vledder and O.R. Koop).

Bijl, W., 1995. Impact of a wind climate change on the surge in the southern part of the North Sea. Report RIKZ-95.016. RIKZ, The Hague.

Dillingh, D., de Haan, L., Helmers, R., Können, G.P., van Malde, J., 1993. De basispeilen langs de Nederlandse kust. Statistisch onderzoek. Report DGW-93.023. Dienst Getijdewateren - RIKZ, The Hague.

Geerse, C.P.M., 2006. Hydraulische randvoorvaren 2006 Vecht- en Ijsseldelta: statistiek Ijsselmeerpeil, afvoeren en stormverlopen voor Hydra-VIJ. RWS-RIZA.

Gerritsen, H., 2008 (personal communication, comments on draft version of report; see Appendix A).

Kruizinga, S., 1978. Objective classificatie van dagelijkse 500 mbar patronen. Scientific Report 78-8. KNMI, De Bilt.

Parker, S.P. (ed.), 1988. *Meteorology Source Book*. McGraw-Hill. (Entries: Front; Cyclone)

RIKZ, Getijtafels voor Nederland 2009, SDU Uitgevers, Den Haag, 2008.

On-line resources

American Meteorological Society. Glossary of Meteorology. URL: http://amsglossary.allenpress.com/glossary. Last accessed 5 Sept 2008.

Rijkswaterstaat. Waternormalen, URL: http://www.waternormalen.nl. Last accessed: 17 Nov 2008.

Rijkswaterstaat. Waterbase, URL: http://www.waterbase.nl/. Last accessed: 7 Jan 2009.

Wikipedia. Overijssel. http://en.wikipedia.org/wiki/Overijssel. Last accessed: 21 Nov 2008.

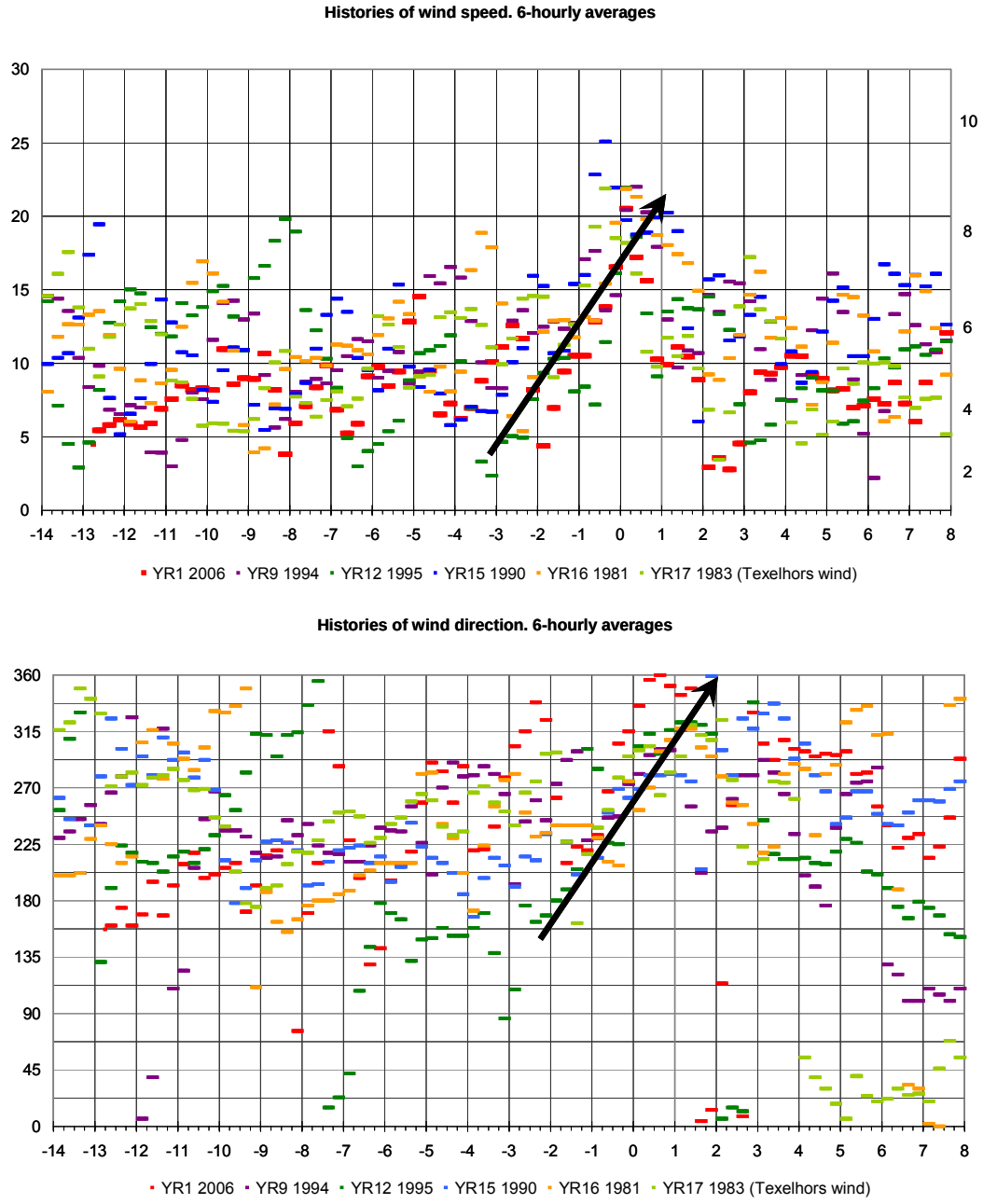

Figure 2.1 "Wallpaper charts". Histories of wind speed (above) and direction (below) for the six highest year-record (YR) surges at Delfzijl in the period 1981-2006. Time in fractional days – the interval (0, 1) is the day of the highest surge. Wind values are averaged over 6-hour intervals for clarity. The arrows are qualitative. From Alkyon (2008).

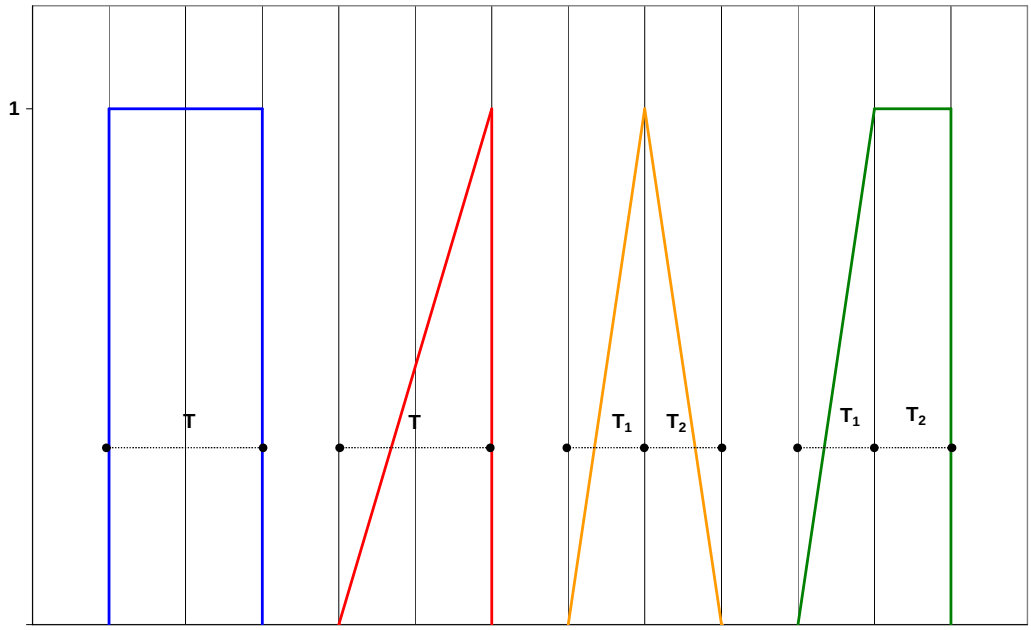

Figure 3.1 Shape functions for the synthetic speed profiles: rectangular (blue), right-angled triangle (red), acute triangle (orange) and trapezium (green). The durations T_1 and T_2 in piecewise functions are equal only for convenience of representation.

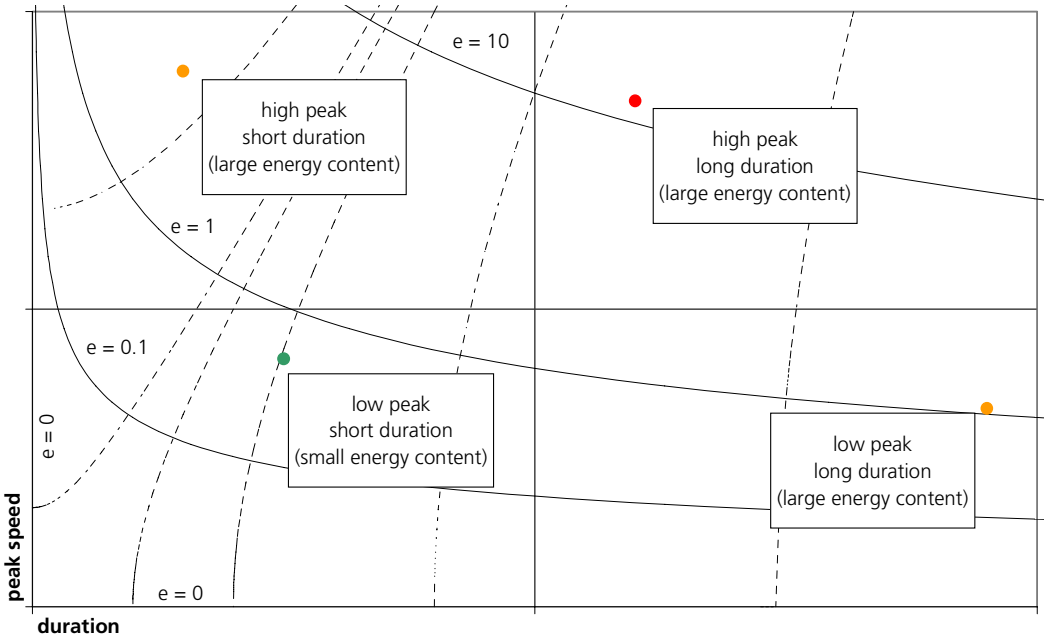

Figure 3.2 Illustration of a windstorm framework chart for speed, in the plane (duration, peak value). Contour lines of energy content for a rectangular speed profile.

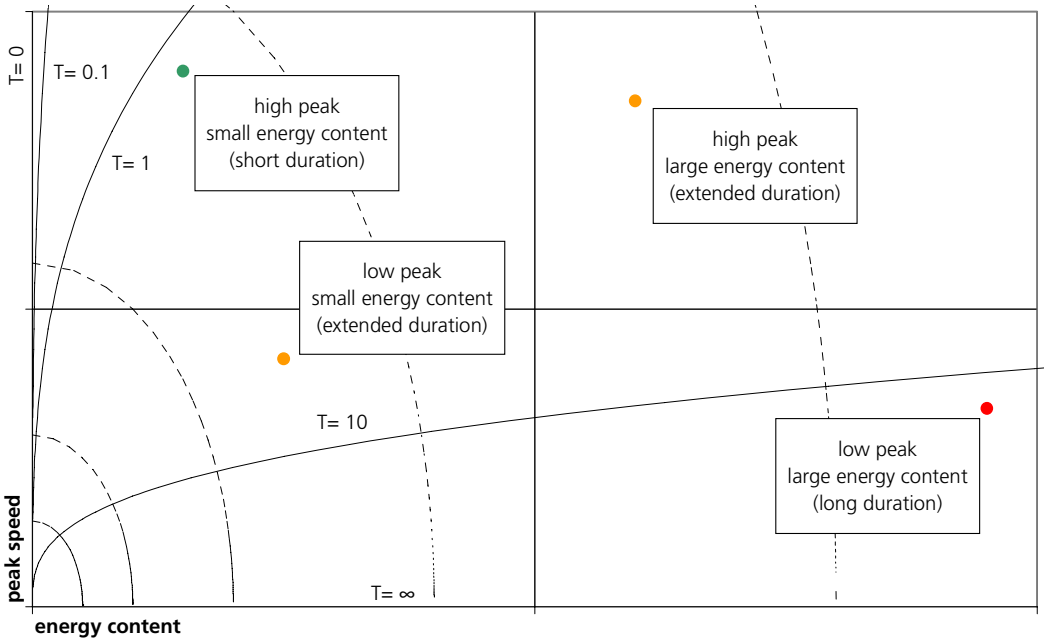

Figure 3.3 Illustration of a windstorm framework chart for speed, in the plane (energy content, peak value). Contour lines of duration for a rectangular speed profile.

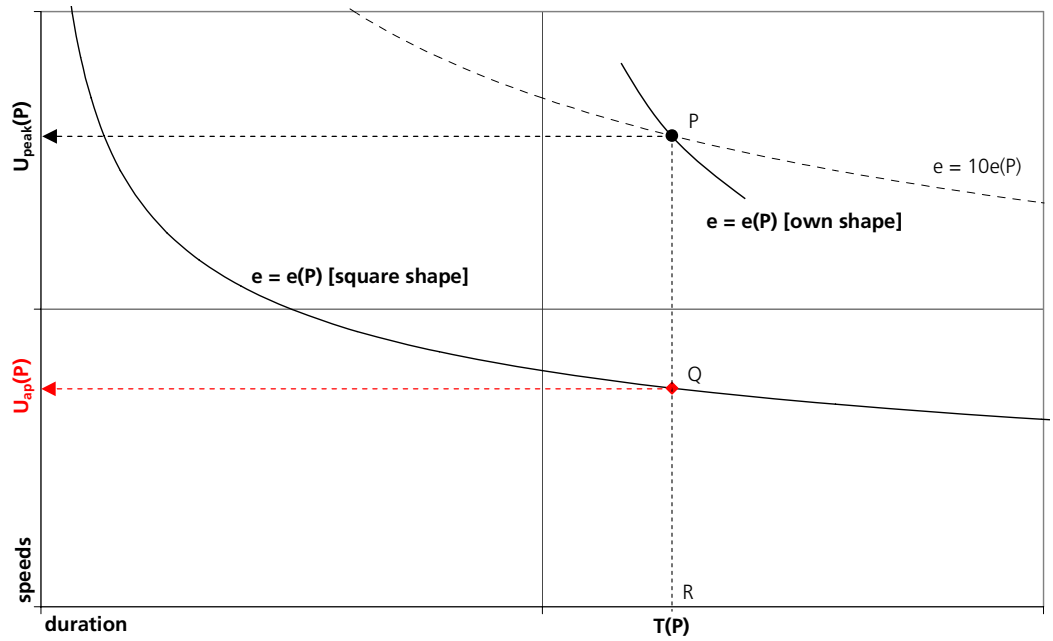

Figure 3.4 Windstorm point in a framework chart for speed: plane (duration, peak value). Determination of the average-power speed through the e-contours for rectangular shape.

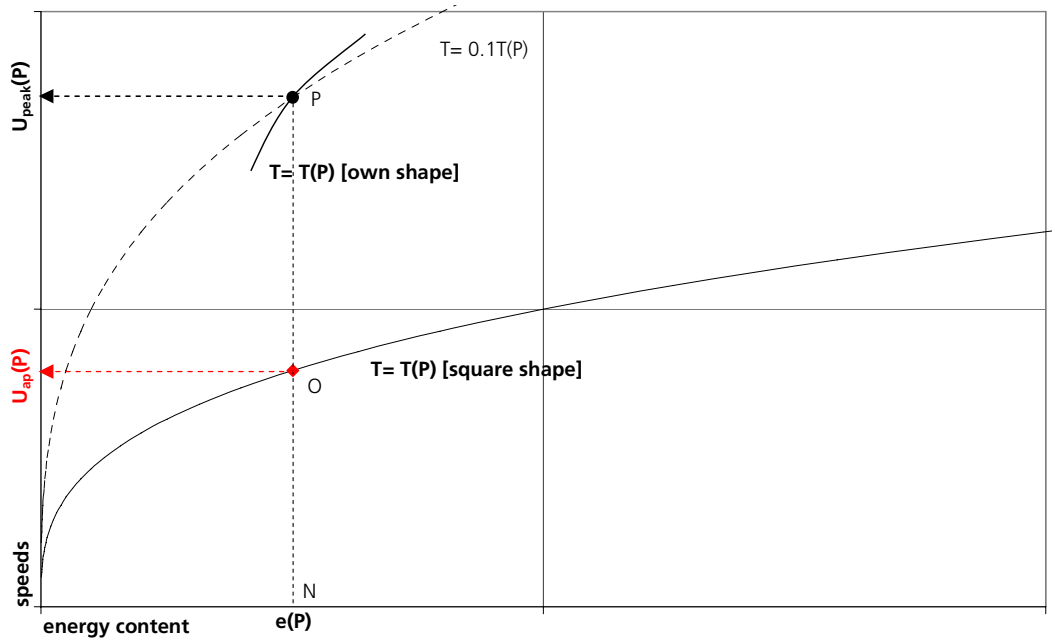

Figure 3.5 Windstorm point in a framework chart for speed: plane (energy content, peak value). Determination of the average-power speed through the T-contours for rectangular shape.

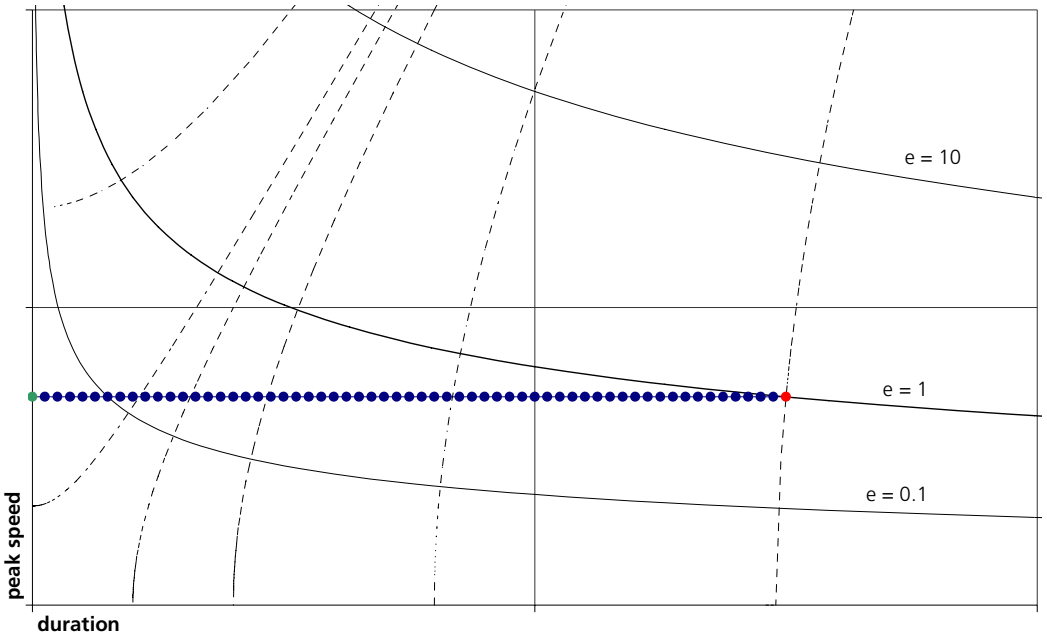

Figure 3.6 Time track of the windstorm point in a rectangular speed profile: plane (T, u_p). The dotting marks data at a regular time interval; the green and red dots correspond to the beginning and end of the storm respectively.

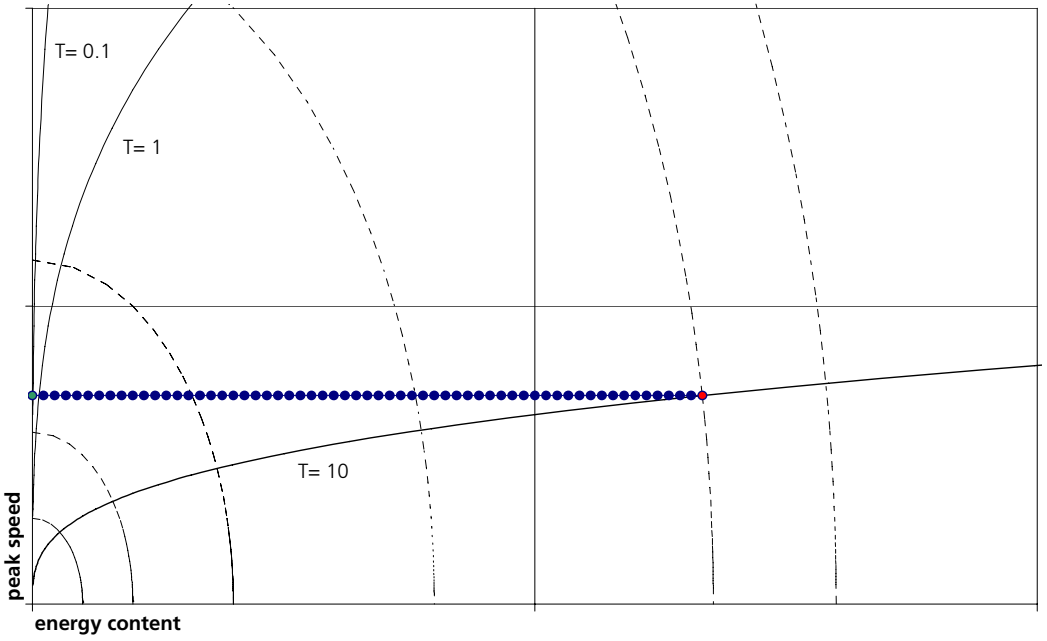

Figure 3.7 Time track of the windstorm point in a rectangular speed profile: plane (e, u_p). Same event and notation of Figure 3.6.

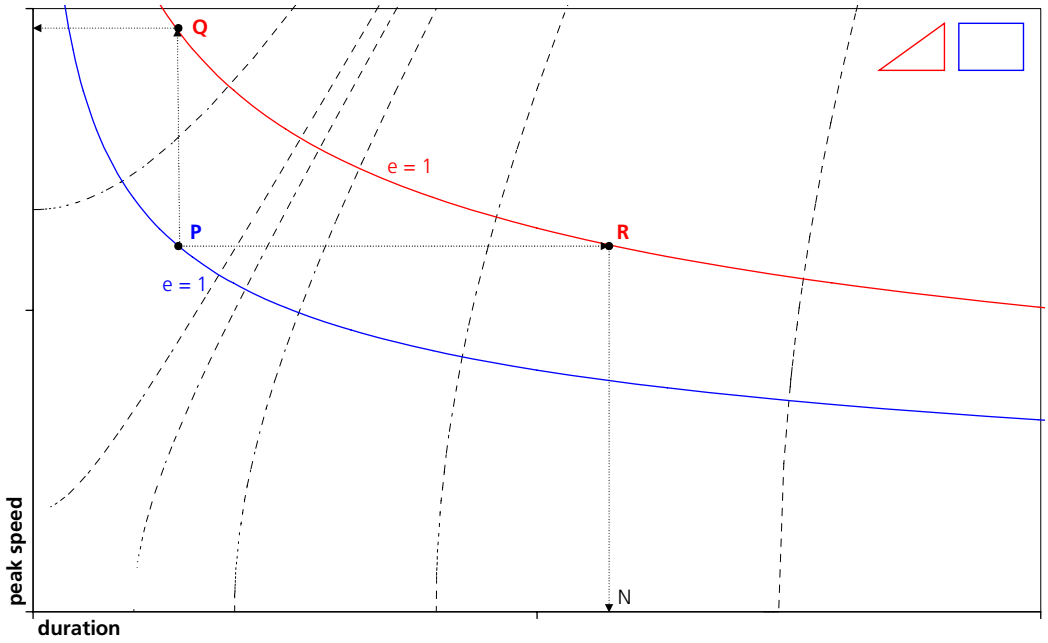

Figure 3.8 Contours of equal energy content (e) for rectangular (blue) and triangular (red) speed profiles in the (T, u_p) chart. Windstorm points: P, reference rectangular speed profile; R, triangular speed profile with same peak speed and energy content as P; Q, triangular speed profile with same duration and energy content as P.

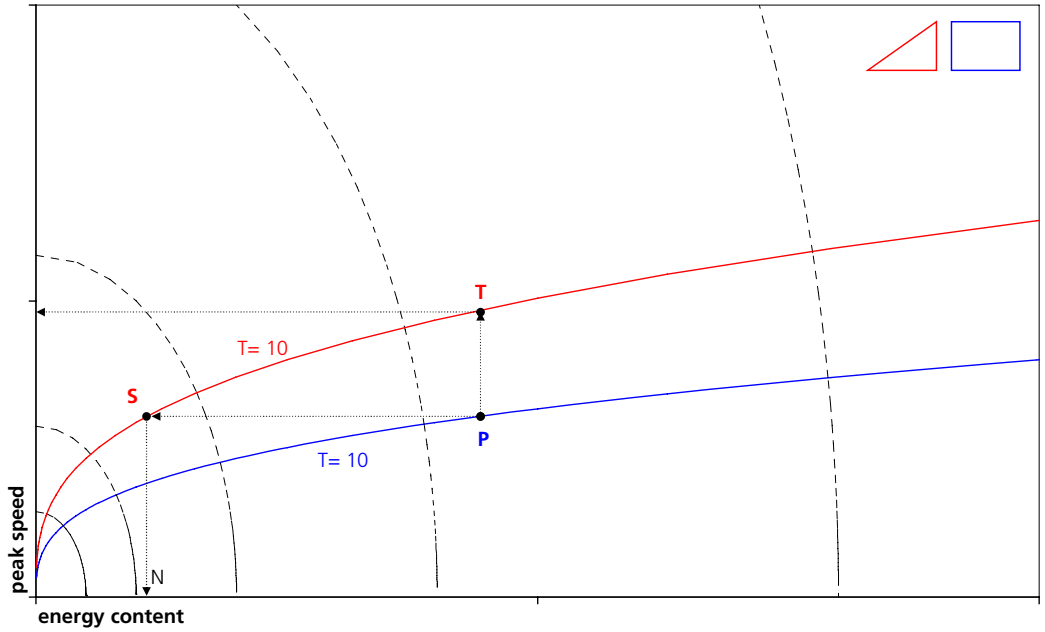

Figure 3.9 Contours of equal duration T for rectangular (blue) and triangular (red) speed profiles in the (e, u_p) chart. Windstorm points: P, reference rectangular speed profile; S, triangular speed profile with same peak speed and duration as P; T, triangular speed profile with same duration and energy content as P.

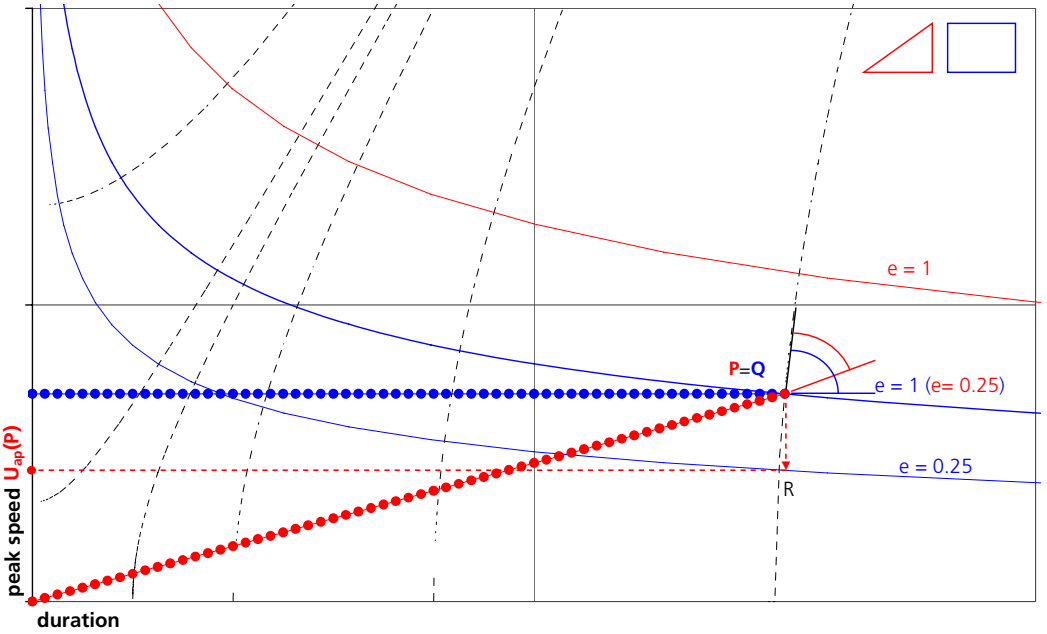

Figure 3.10 Time tracks of the windstorm points in a rectangular (blue) and triangular (red) speed profiles in the (T, u_p) chart. Dotting marks equal time intervals. Windstorm points: P, triangular speed profile; Q, rectangular speed profile; R, rectangular profile at average-power speed of windstorm.

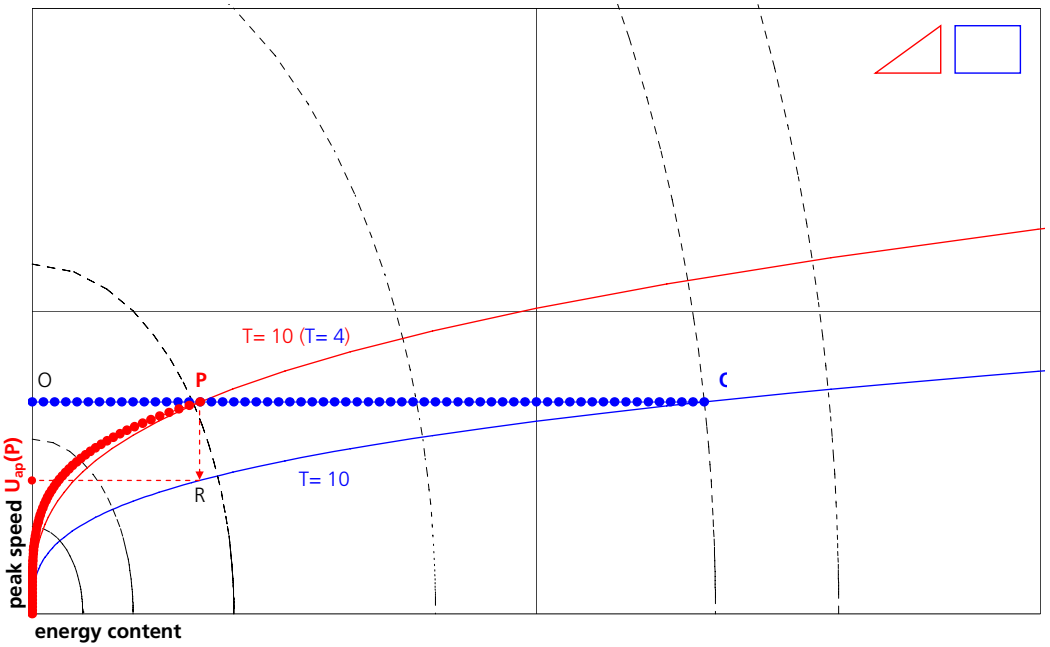

Figure 3.11 Time tracks of the windstorm points in a rectangular (blue) and triangular (red) speed profiles in the (e, u_p) chart. Same notation and speed profile as Figure 3.10.

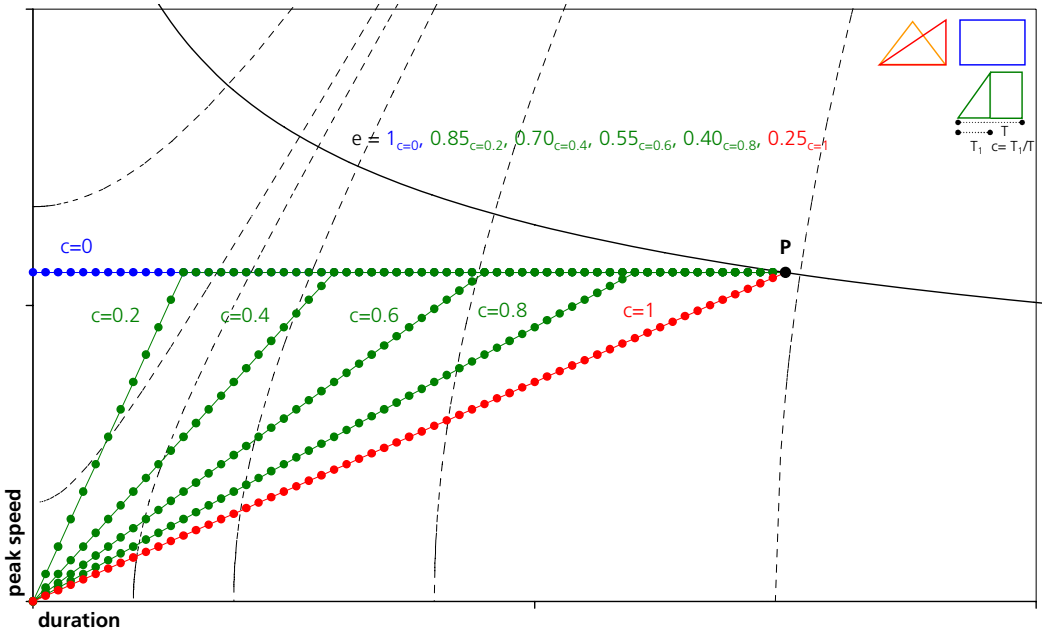

Figure 3.12 Rectangular, trapezoidal and triangular windstorms with same duration and peak speed. Time tracks and placemarks on chart (T, u_p)

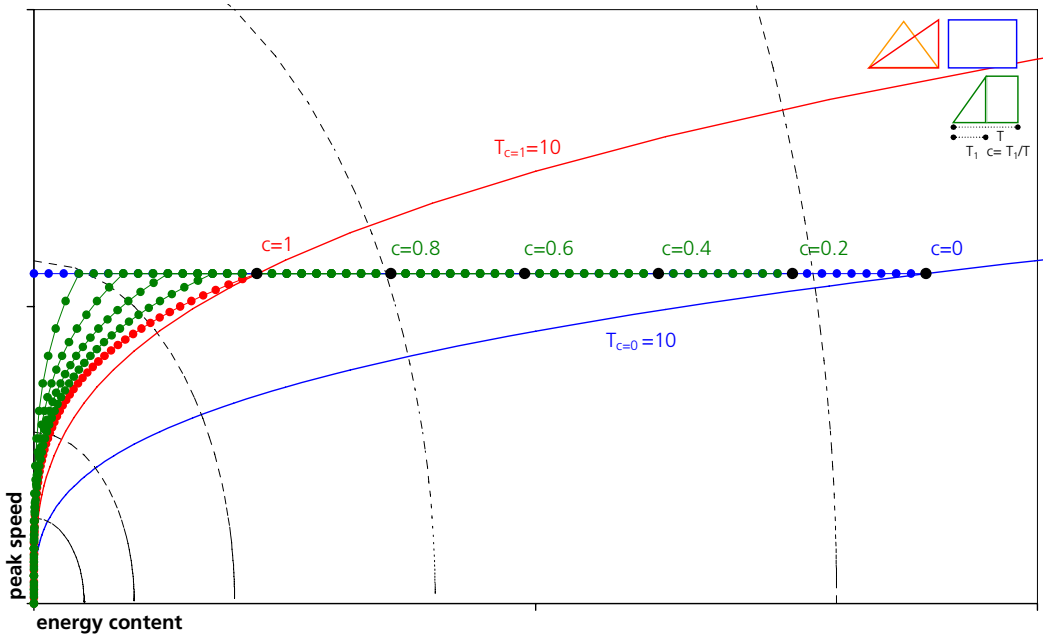

Figure 3.13 Rectangular, trapezoidal and triangular windstorms with same duration and peak speed. Time tracks and placemarks on chart (e, u_p)

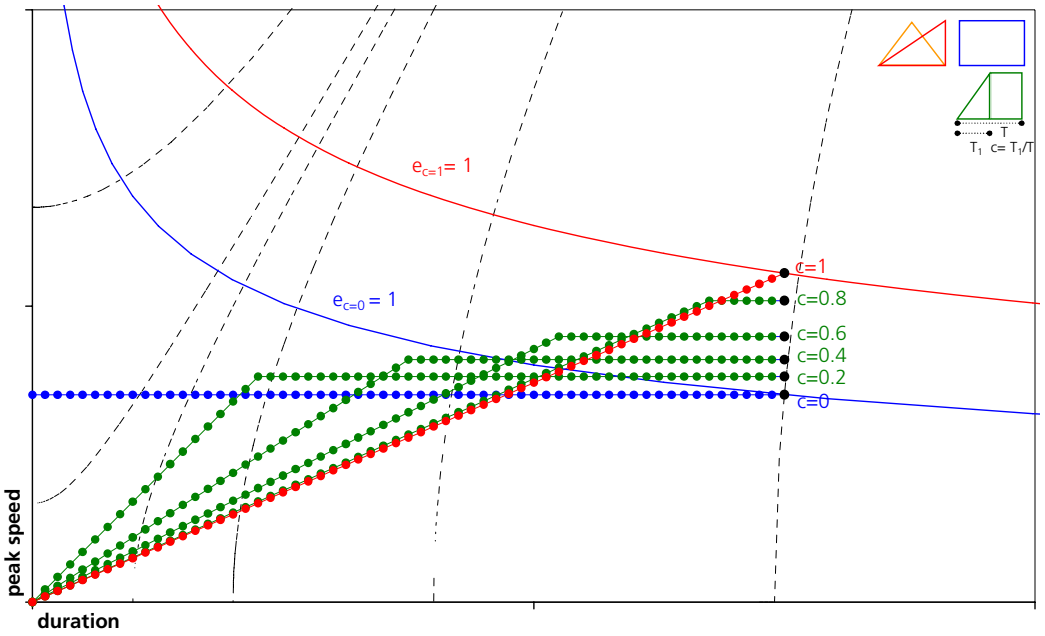

Figure 3.14 Rectangular, trapezoidal and triangular windstorms with same duration and energy content. Time tracks and placemarks on chart (T, u_p).

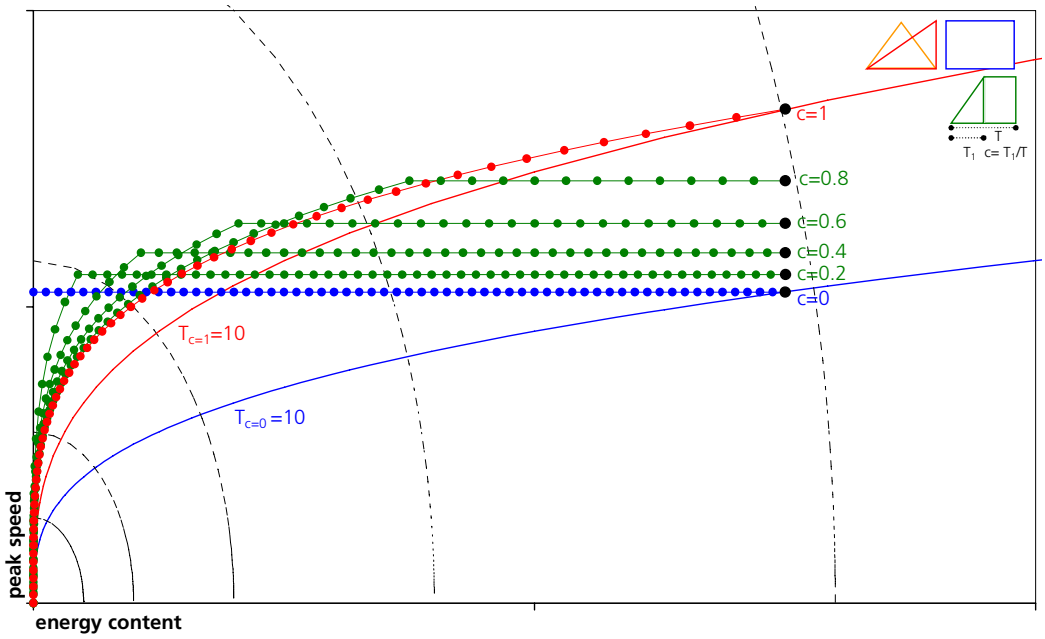

Figure 3.15 Rectangular, trapezoidal and triangular windstorms with same duration and energy content. Time tracks and placemarks on chart (e, u_p).

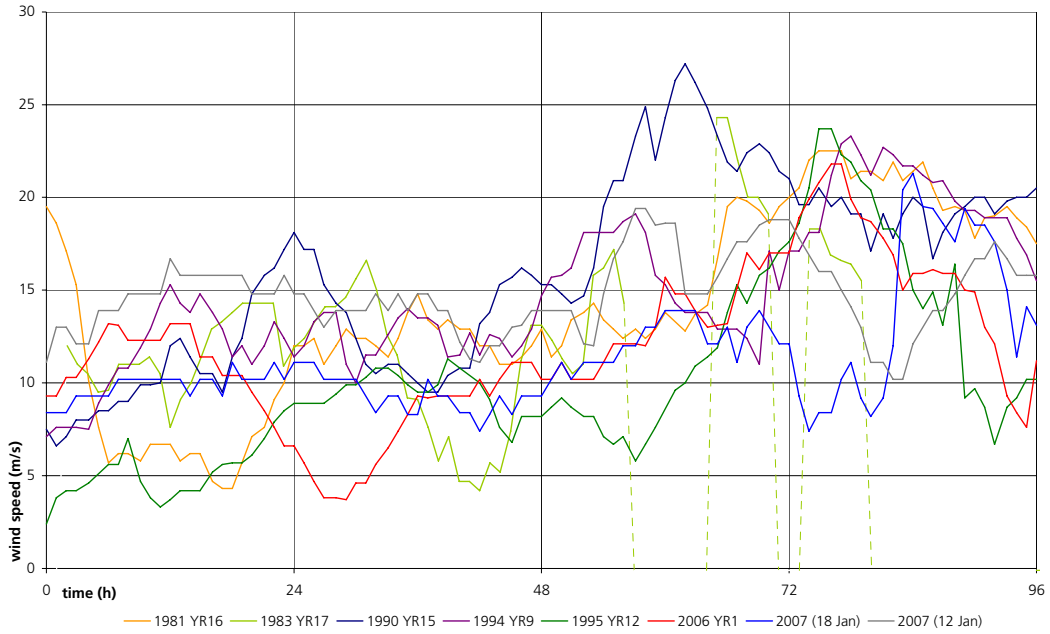

Figure 3.16 Measurements of wind speed at Huibertgat for eight surge events in the eastern Wadden Sea. Time window of 96 hours: the day of the highest surge at Delfzijl is the last interval 72-96 hours for all signals.

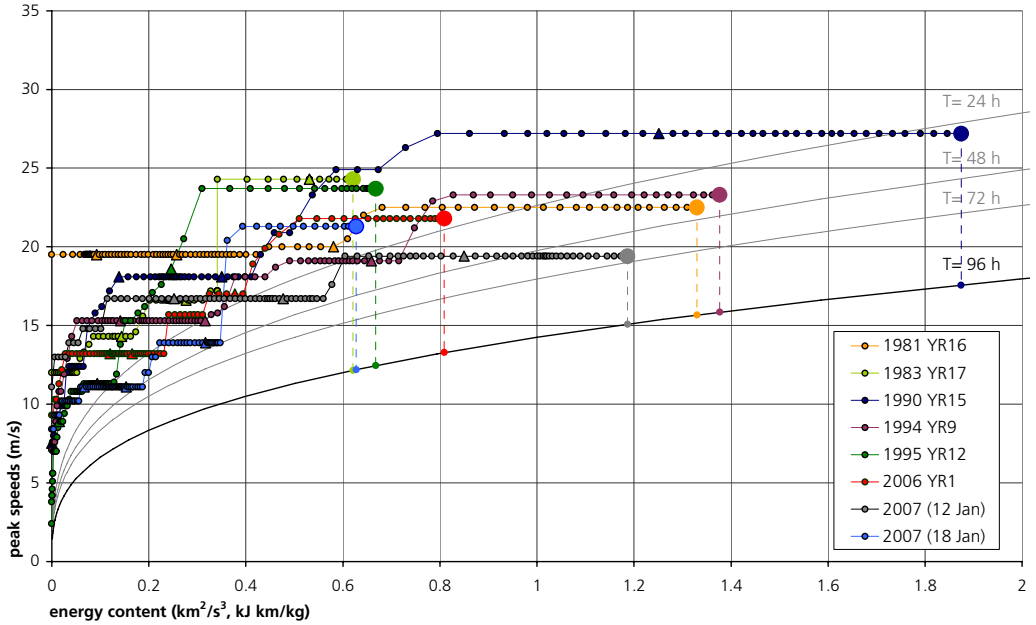

Figure 3.17 Time tracks of the measured signals of Figure 3.16 in the chart (u_p, e). Dotting represents data at equal time intervals. Large bullet points: windstorm points (at 96 h); triangles: 24-hour marks. The data points on the contour T=96 h correspond to the average-power speeds for each signal.

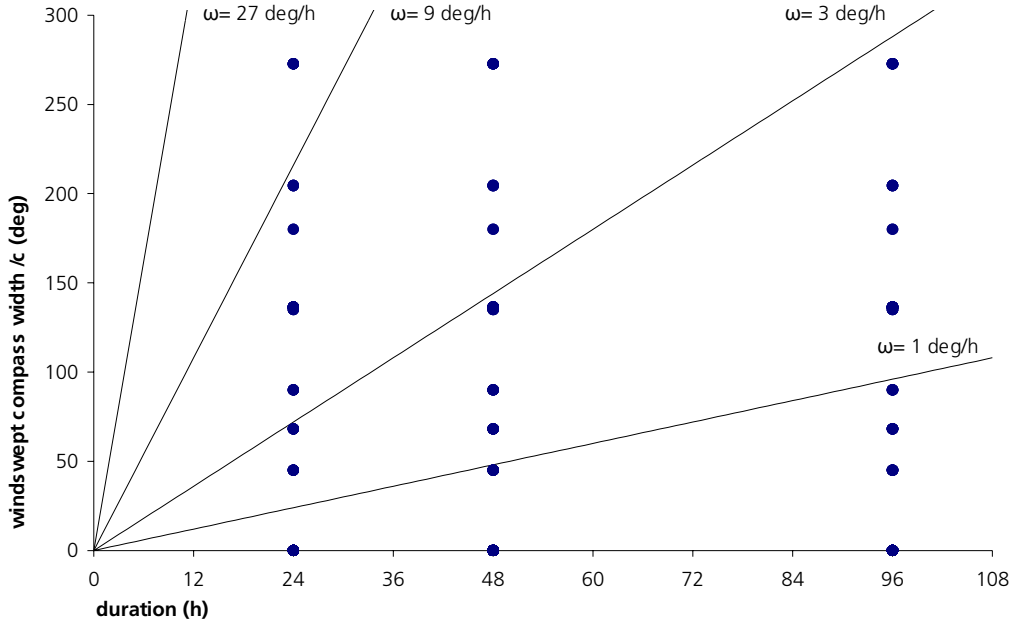

Figure 3.18 Framework direction chart: windswept compass width divided by triangularity ratio (deg) v duration. Contours are isolines for the rate of rotation. Placemarks taken from the test set of Chapter 4.

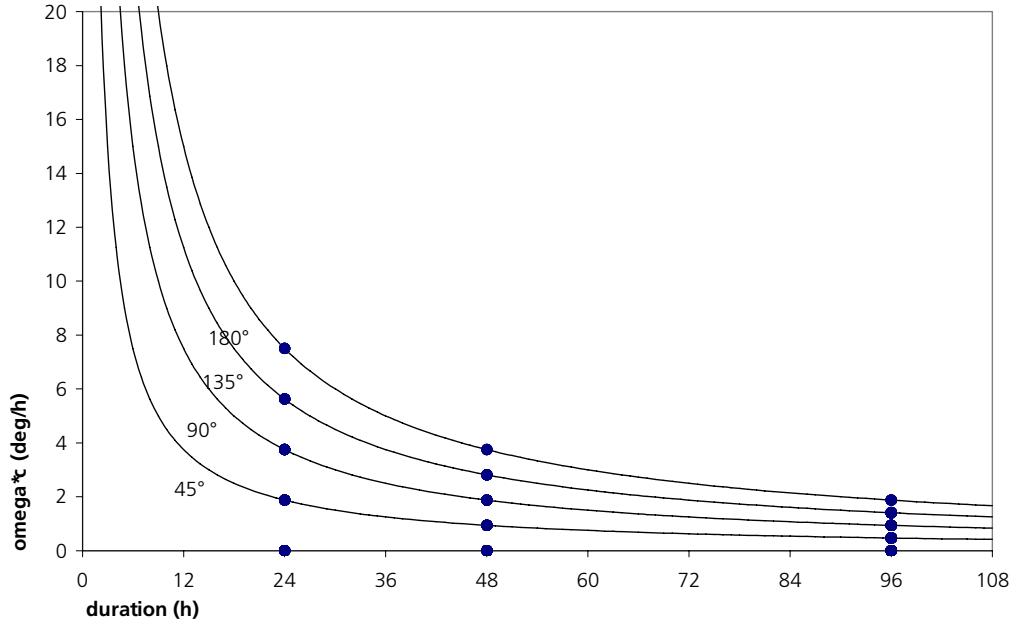

Figure 3.19 Framework direction chart: rate of rotation times triangularity ratio (deg/h) v duration. Contours are isolines for the windswept compass width. Placemarks taken from the test set of Chapter 4.

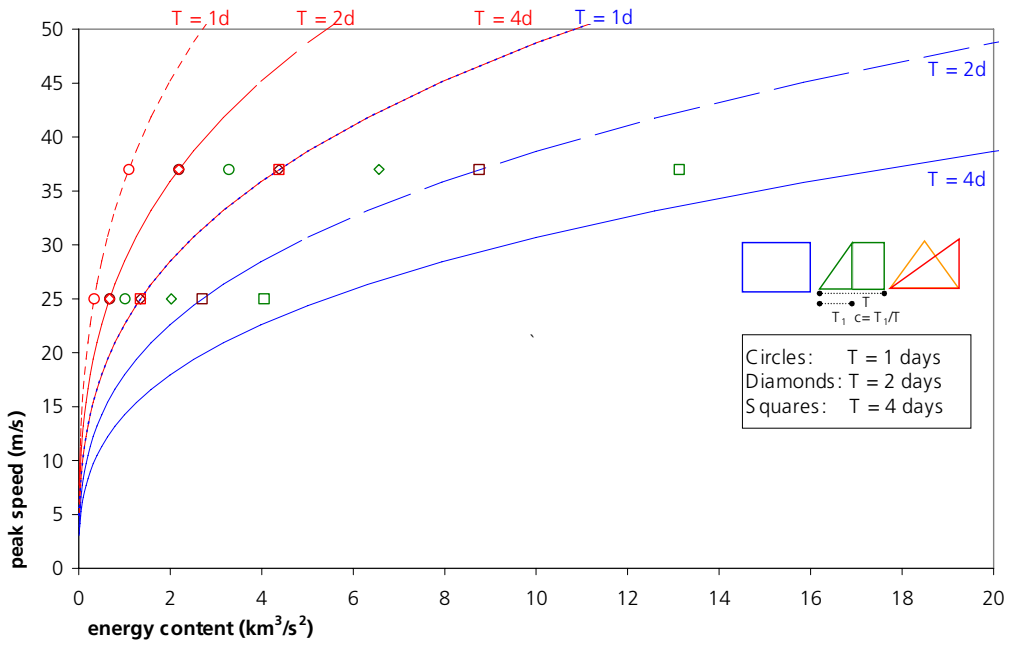

Figure 4.1 Framework speed chart in the plane (e,u_p) for the windstorms of the test set

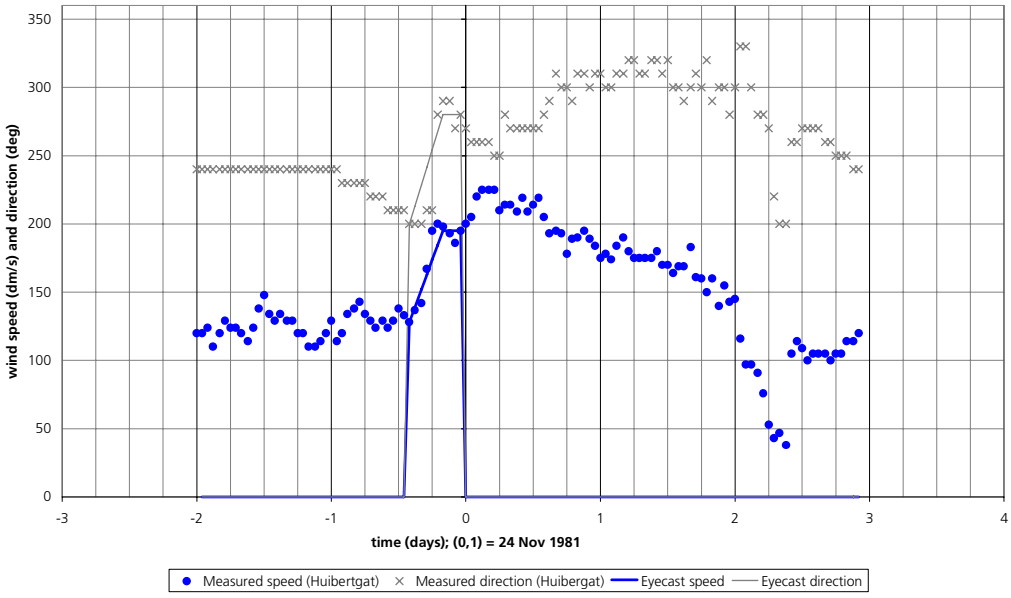

Figure 4.2 Synthetic approximate profile (eyecast) for the event of 24 Nov 1981. Symbols: measured data. Lines: eyecast.

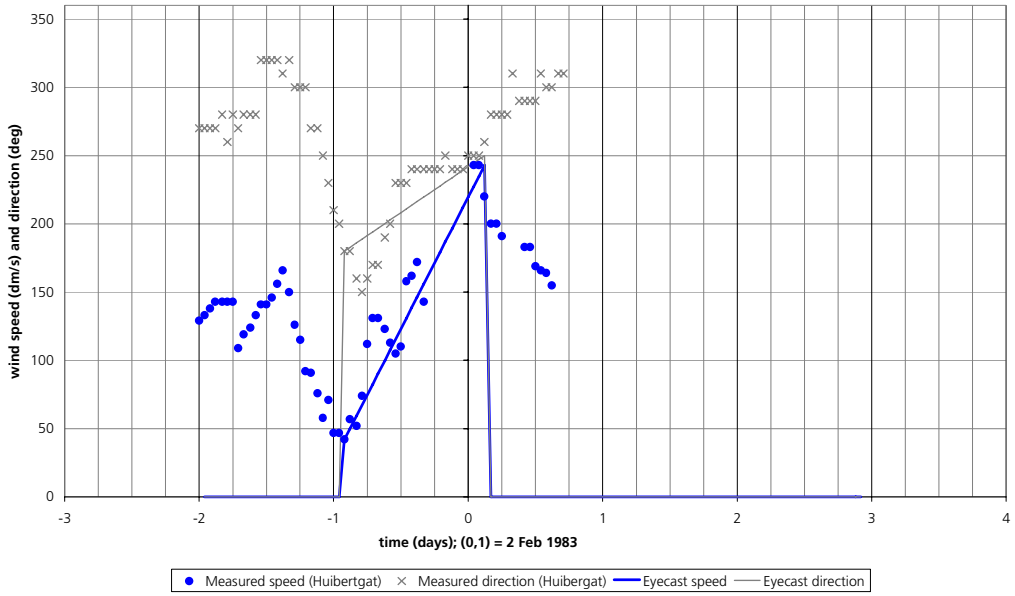

Figure 4.3 Synthetic approximate profile (eyecast) for the event of 2 Feb 1983. Symbols: measured data. Lines: eyecast.

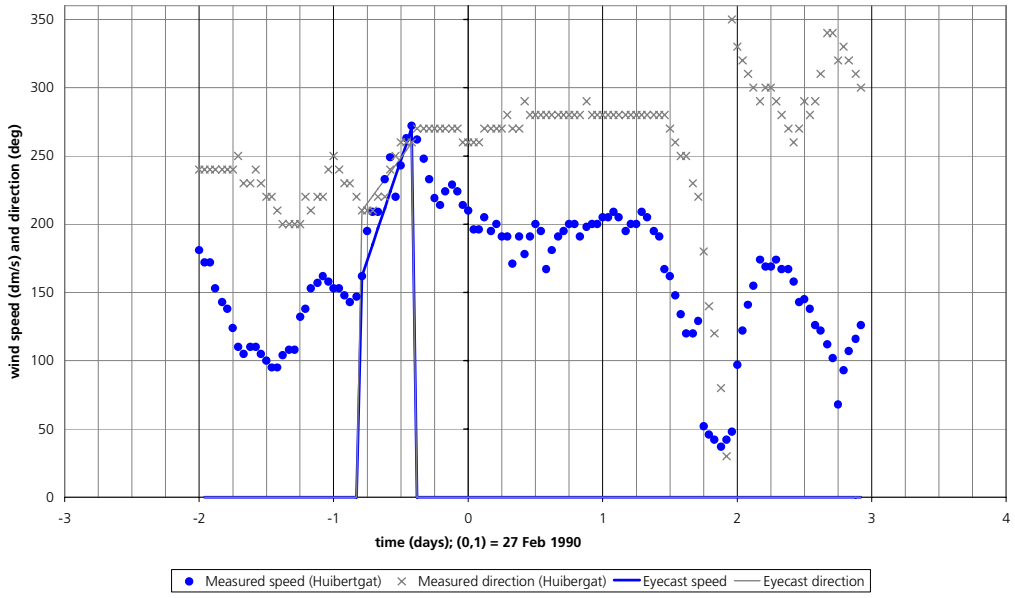

Figure 4.4 Synthetic approximate profile (eyecast) for the event of 27 Feb 1990. Symbols: measured data. Lines: eyecast.

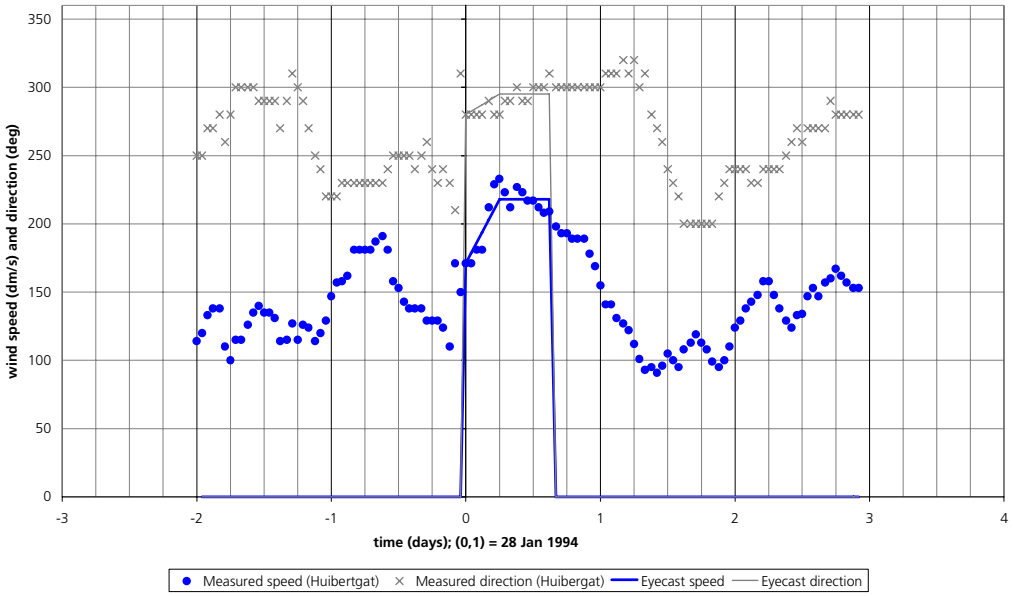

Figure 4.5 Synthetic approximate profile (eyecast) for the event of 28 Jan 1994. Symbols: measured data. Lines: eyecast.

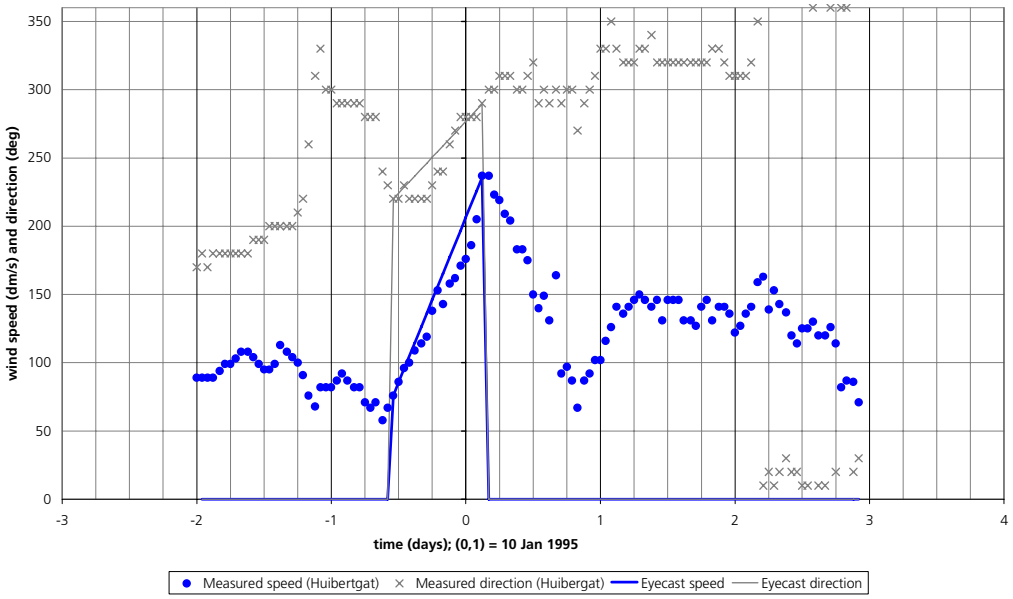

Figure 4.6 Synthetic approximate profile (eyecast) for the event of 10 Jan 1995. Symbols: measured data. Lines: eyecast.

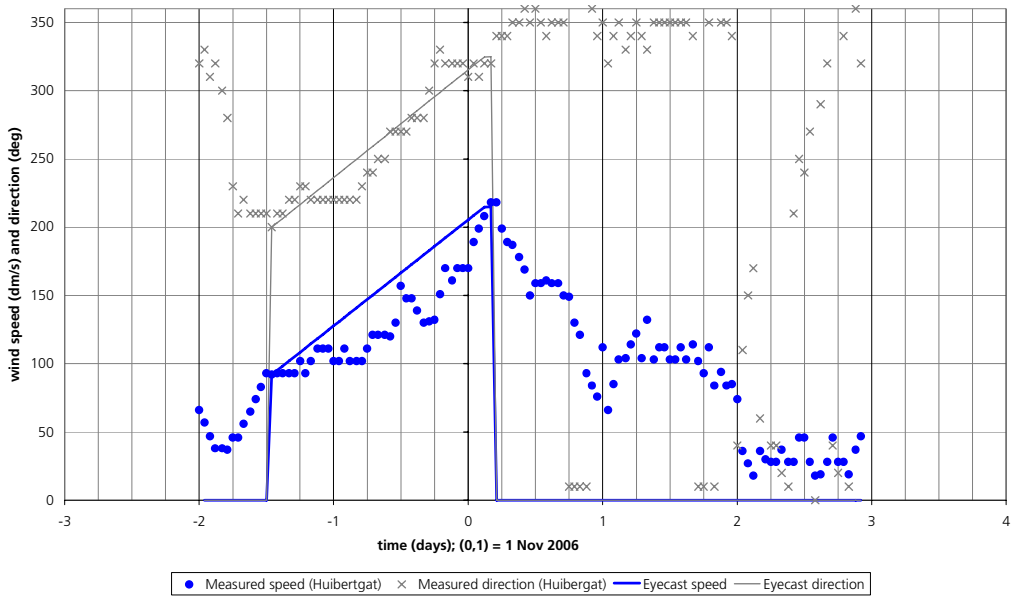

Figure 4.7 Synthetic approximate profile (eyecast) for the event of 1 Nov 2006. Symbols: measured data. Lines: eyecast.

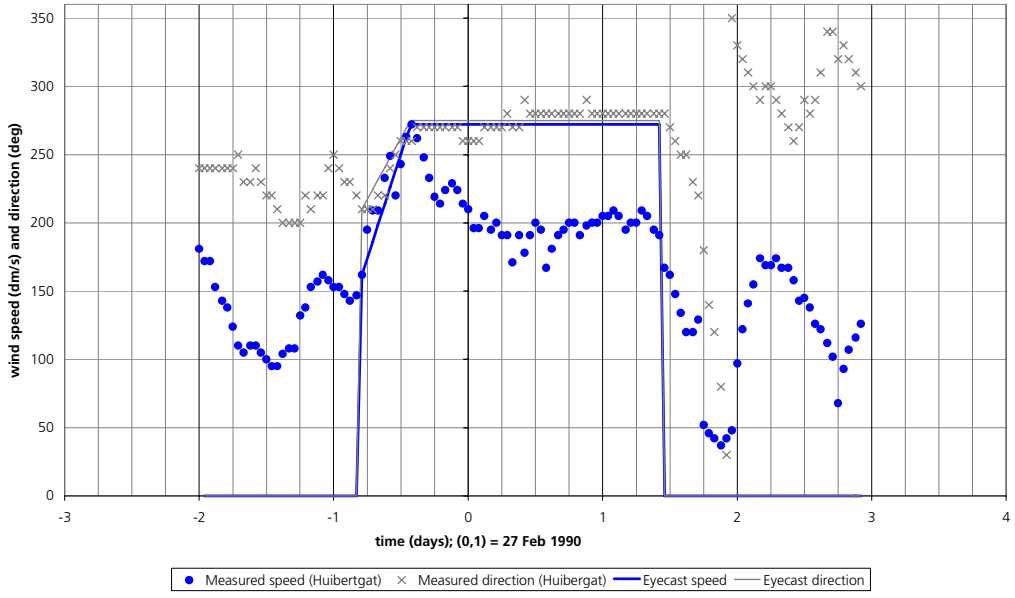

Figure 4.8 Synthetic approximate profile (eyecast) for the event of 27 Feb 1990. Variant with peak-speed tail. Symbols: measured data. Lines: eyecast.

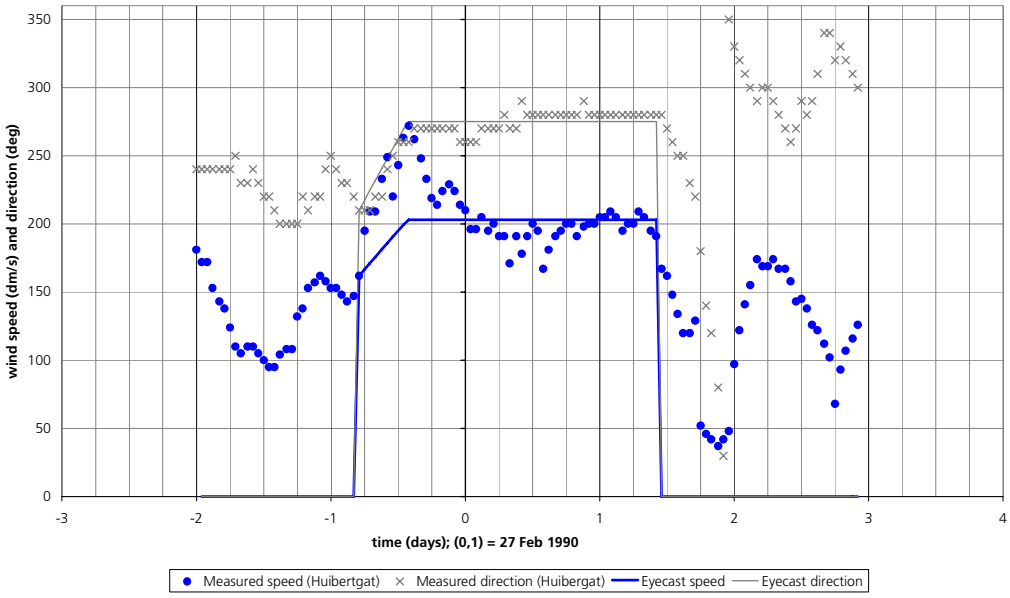

Figure 4.9 Synthetic approximate profile (eyecast) for the event of 27 Feb 1990. Variant with average-speed tail. Symbols: measured data. Lines: eyecast.

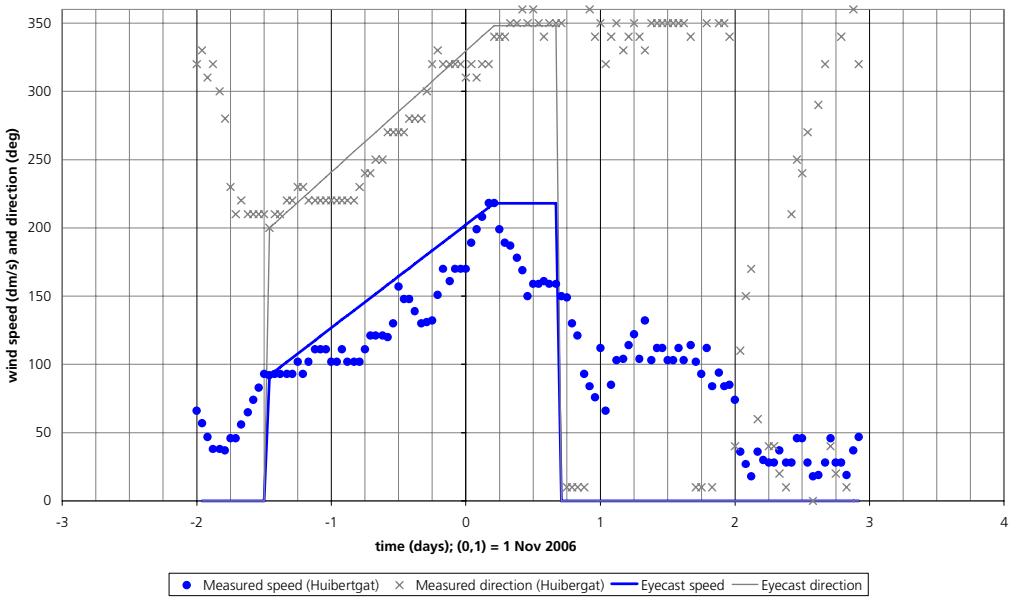

Figure 4.10 Synthetic approximate profile (eyecast) for the event of 1 Nov 2006. Variant with peak-speed tail. Symbols: measured data. Lines: eyecast.

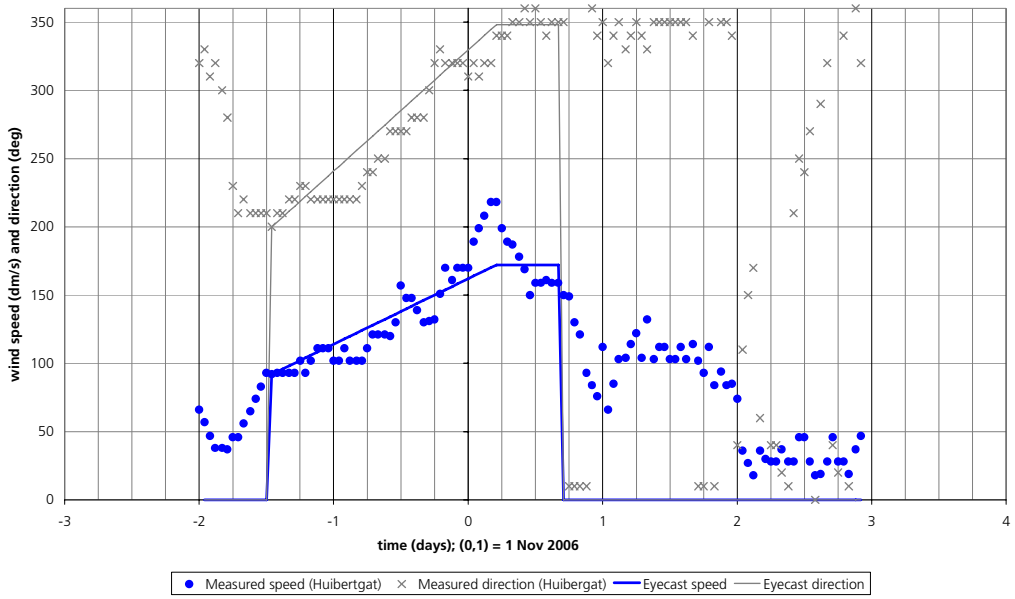

Figure 4.11 Synthetic approximate profile (eyecast) for the event of 1 Nov 2006. Variant with average-speed tail. Symbols: measured data. Lines: eyecast.

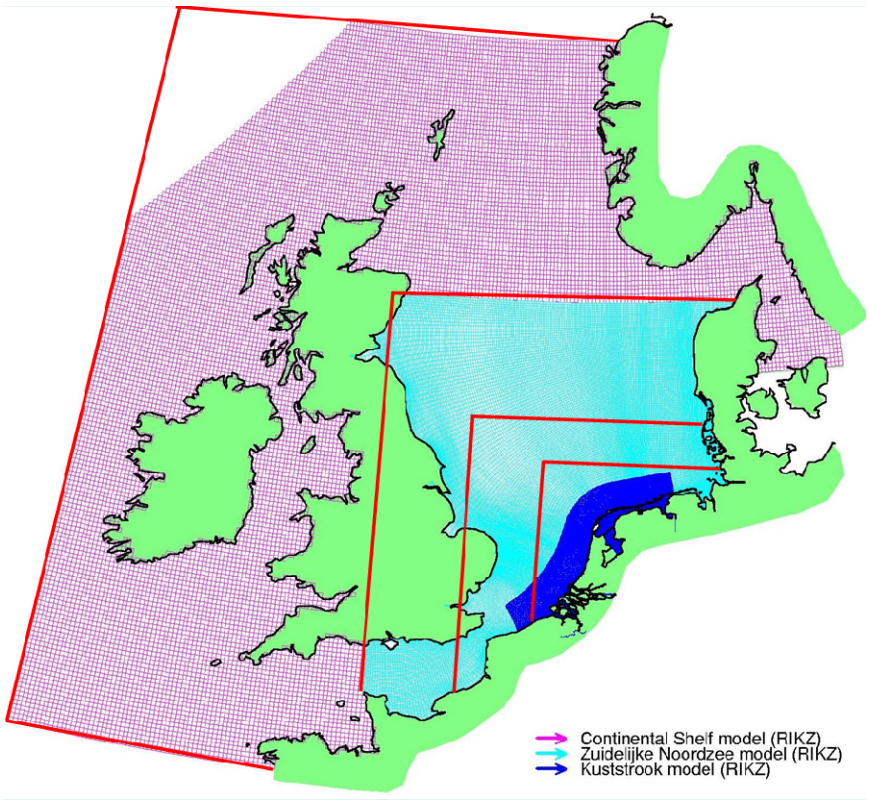

Figure 5.1 Test areas for sensitivity to wind blown domain.

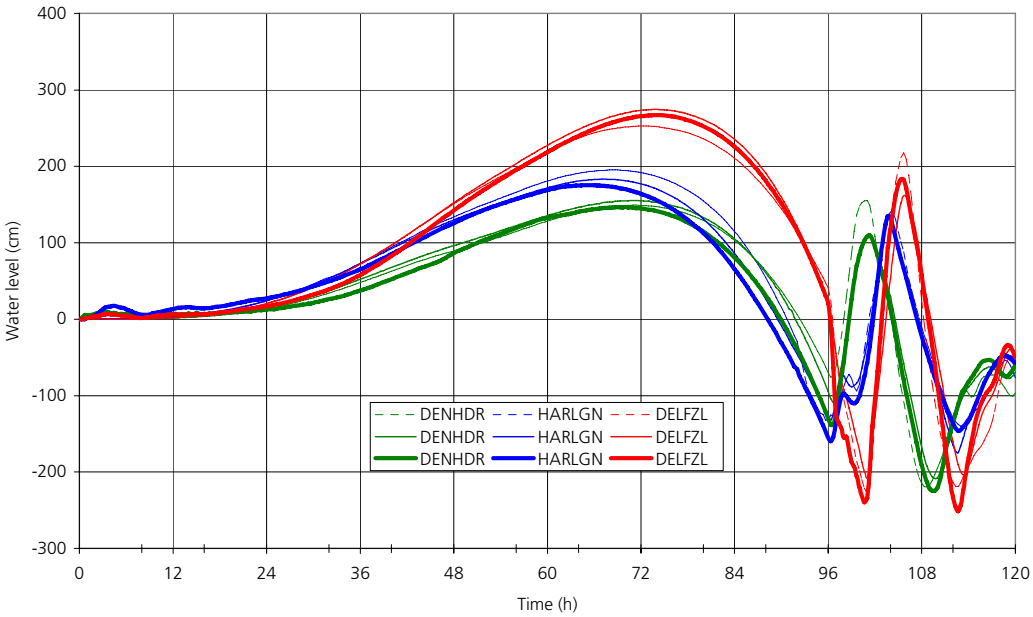

Figure 5.2 Water levels at WS stations (cm) against time (h). Slowly-varying storm, duration 96 h. Windblown area: CSM ('XL'). Thick lines: Kuststrook; thin lines: ZuNo; dashed lines: CSM. Run code: t96-c100-s370-22545.

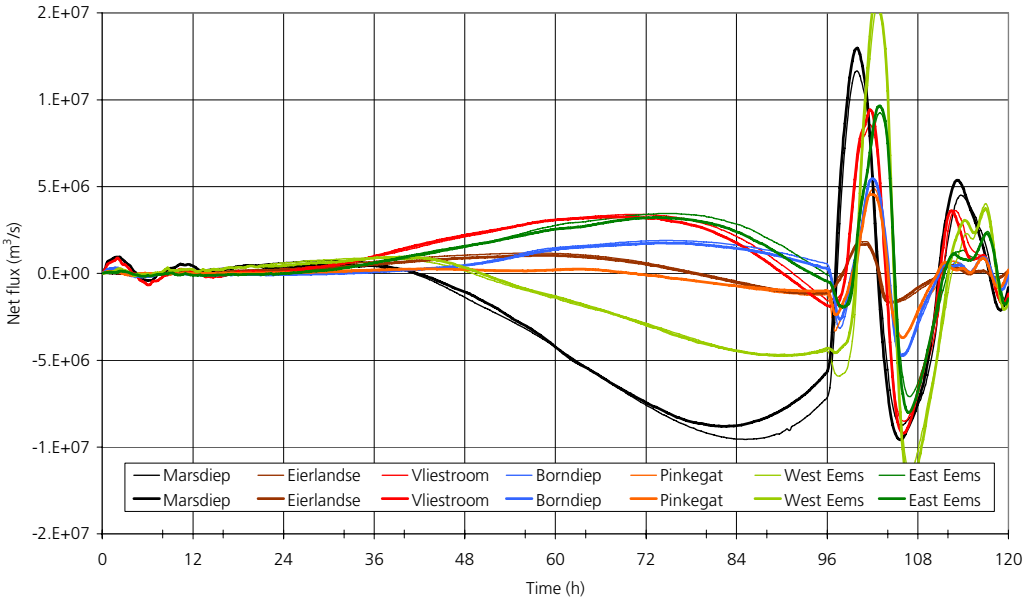

Figure 5.3 Net fluxes across the WS cross sections (m^3/s) against time (h). Slowly-varying storm, duration 96 h. Windblown area: CSM ('XL'). Thick lines: Kuststrook; thin lines: ZuNo. Positive values denote flux filling the WS. Run code: t96-c100-s370-22545.

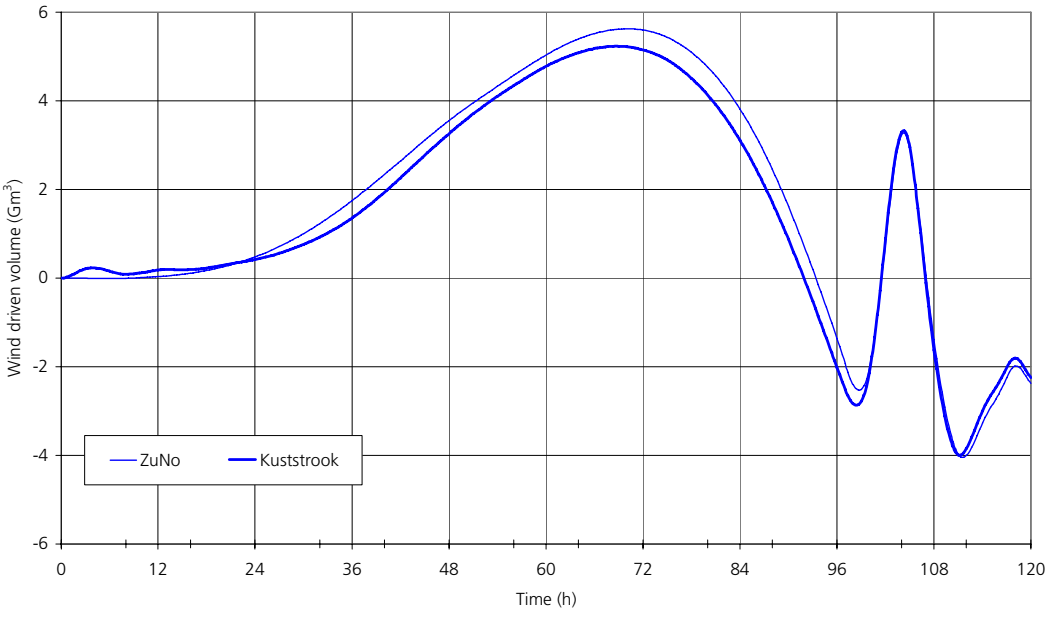

Figure 5.4 Wind-driven water volume (Gm^3) in the WS against time. Slowly-varying storm, duration 96 h. Windblown area: CSM ('XL'). Thick lines: Kuststrook; thin lines: ZuNo. Run code: t96-c100-s370-22545.

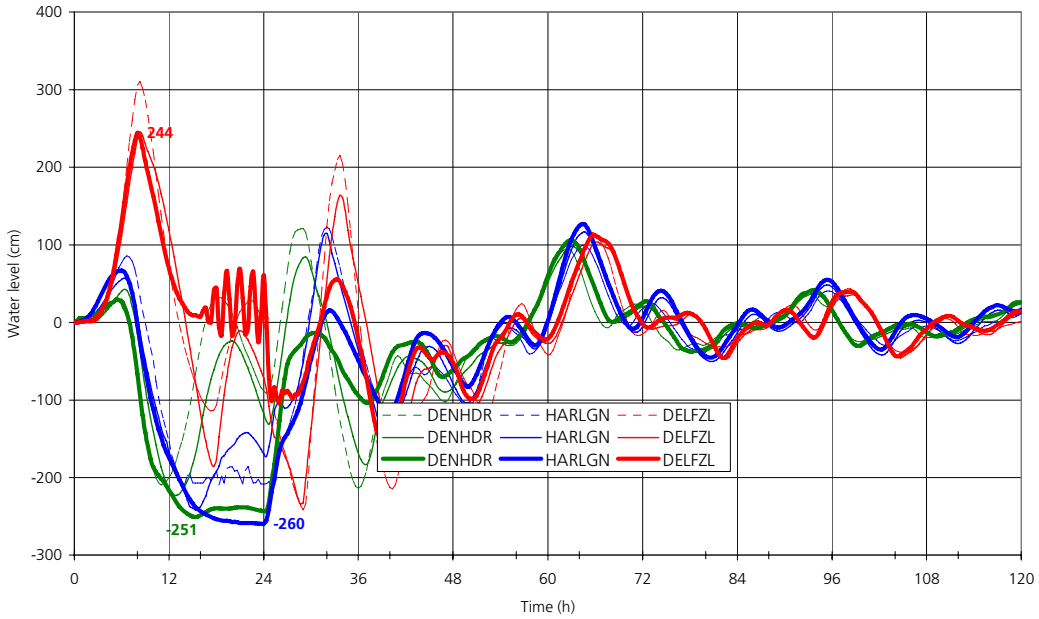

Figure 5.5 Water levels at WS stations (cm) against time (h). Fast-varying storm, duration 24 h. Windblown area: CSM ('XL'). Thick lines: Kuststrook; thin lines: ZuNo; dashed lines: CSM. Run code: t24-c33-s370-22545.

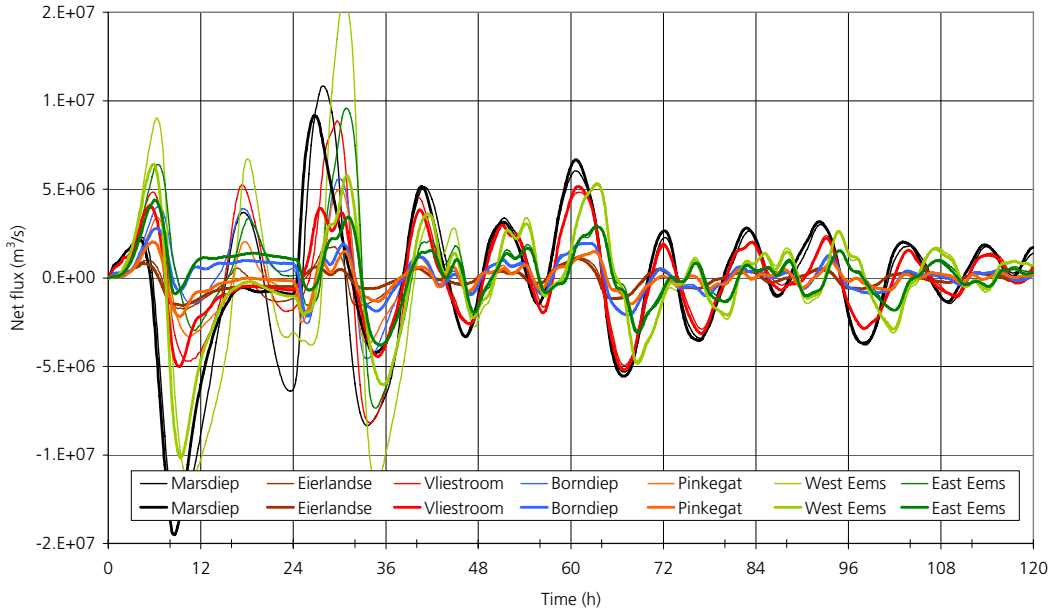

Figure 5.6 Net fluxes across the WS cross sections (m3/s) against time (h). Fast-varying storm, duration 24 h. Windblown area: CSM ('XL'). Thick lines: Kuststrook; thin lines: ZuNo. Positive values denote flux filling the WS. Run code: t24-c33-s370-22545.

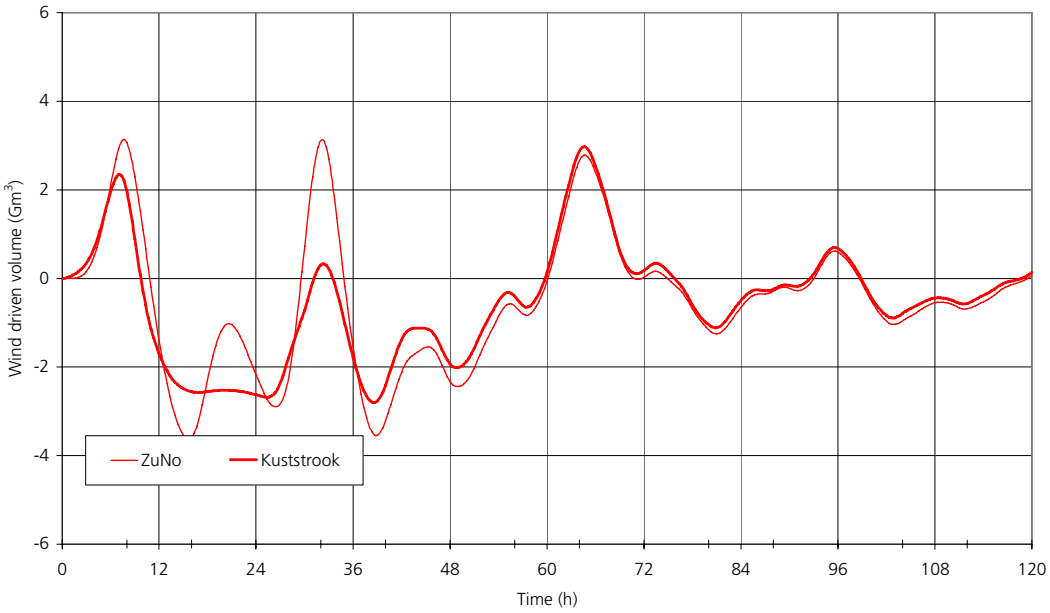

Figure 5.7 Wind-driven water volume (m^3) in the WS against time. Fast-varying storm, duration 24 h. Windblown area: CSM ('XL'). Thick lines: Kuststrook; thin lines: ZuNo. Run code: t24-c33-s370-22545.

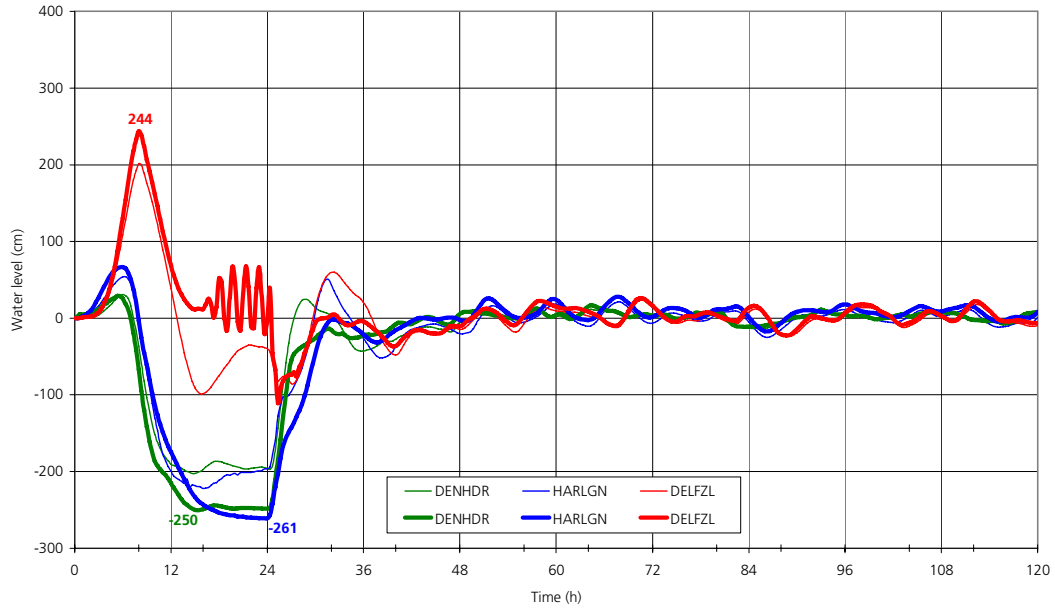

Figure 5.8 Water levels at WS stations (cm) against time (h). Fast-varying storm, duration 24 h. Windblown area: Quarter-ZuNo ('S'). Thick lines: Kuststrook; thin lines: ZuNo. Run code: t24-c33-s370-22545.

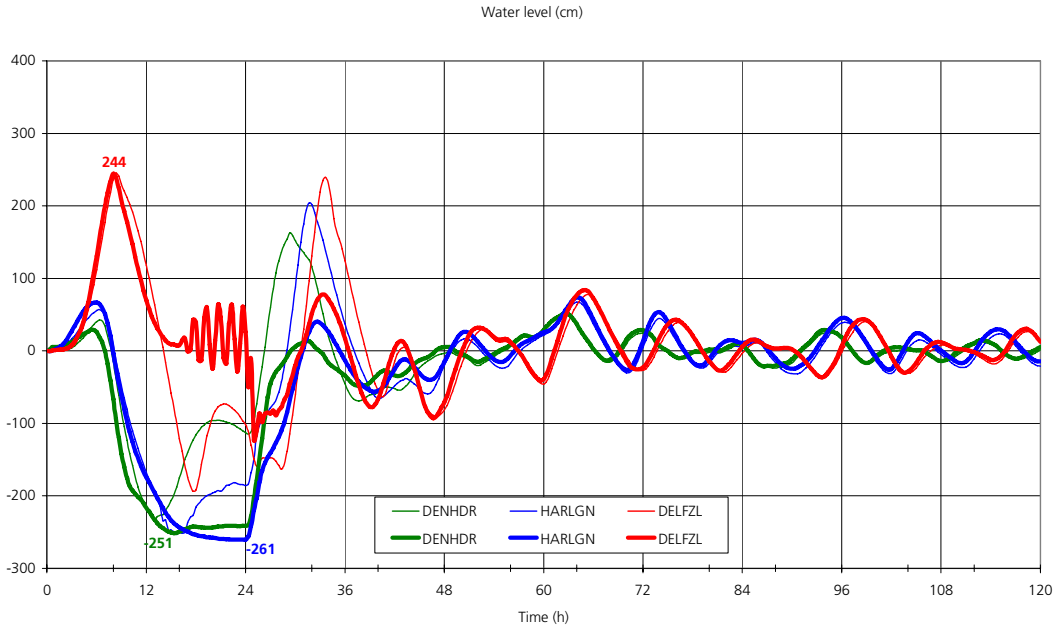

Figure 5.9 Water levels at WS stations (cm) against time (h). Fast-varying storm, duration 24 h. Windblown area: ZuNo ('L'). Thick lines: Kuststrook; thin lines: ZuNo. Run code: t24-c33-s370-22545.

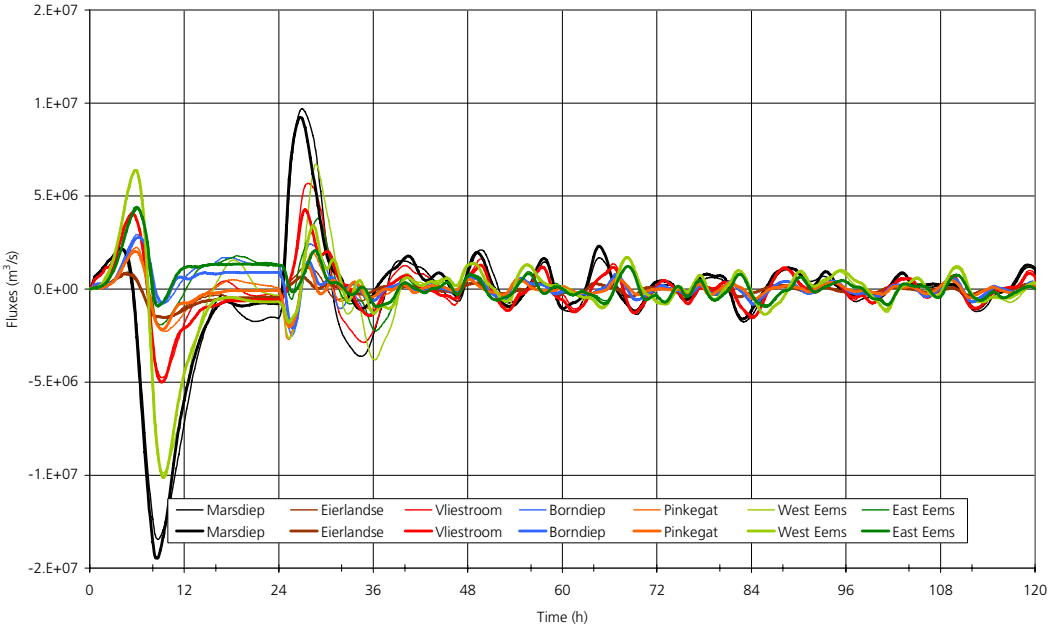

Figure 5.10 Fluxes across the WS cross sections (m^3/s) against time (h). Fast-varying storm, duration 24 h. Windblown area: Quarter-ZuNo ('S'). Thick lines: Kuststrook; thin lines: ZuNo. Positive values denote flux filling the WS. Run code: t24-c33-s370-22545.

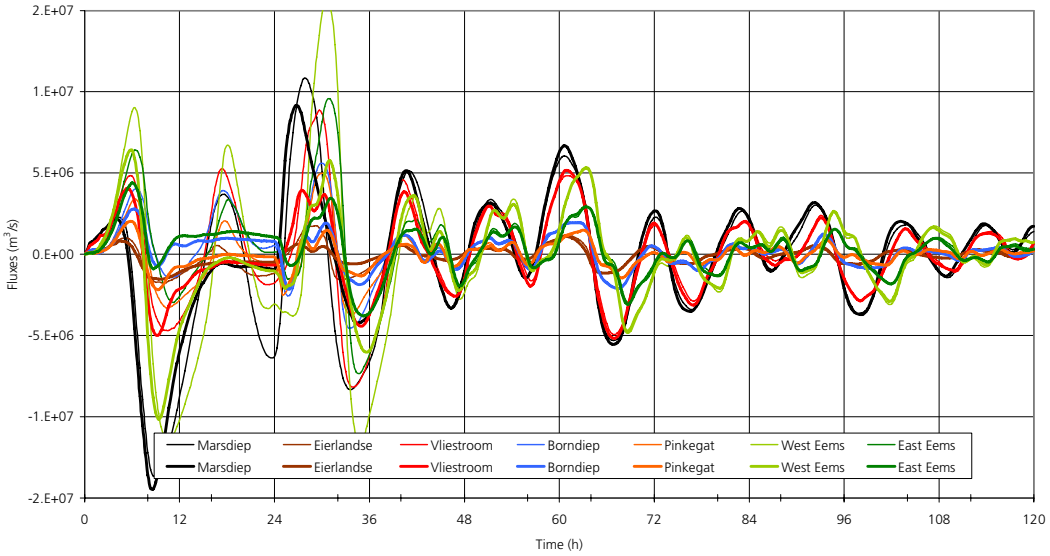

Figure 5.11 Fluxes across the WS cross sections (m^3/s) against time (h). Fast-varying storm, duration 24 h. Windblown area: ZuNo ('L'). Thick lines: Kuststrook; thin lines: ZuNo. Positive values denote flux filling the WS. Run code: t24-c33-s370-22545.

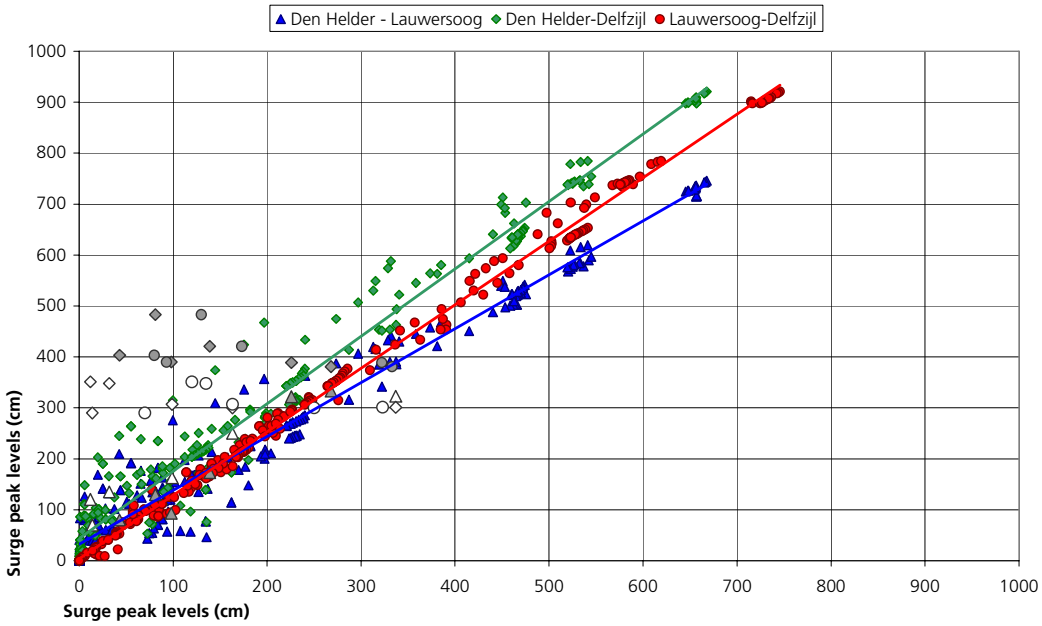

Figure 5.12 Scatter plot of peak surge levels at pairs of stations from Den Helder, Lauwersoog and Delfzijl. Grey-filled symbols: year-record events of Alkyon (2008a) as total water levels (grouped, Figure 2.1). Open symbols: year-record events of Alkyon (2008a) as tide-free water levels (grouped, Figure 2.1). Colour-filled symbols: complete windstorm test-set; windblown area: ZuNo; nested-ZuNo flow results. Symbol shapes: see legend.

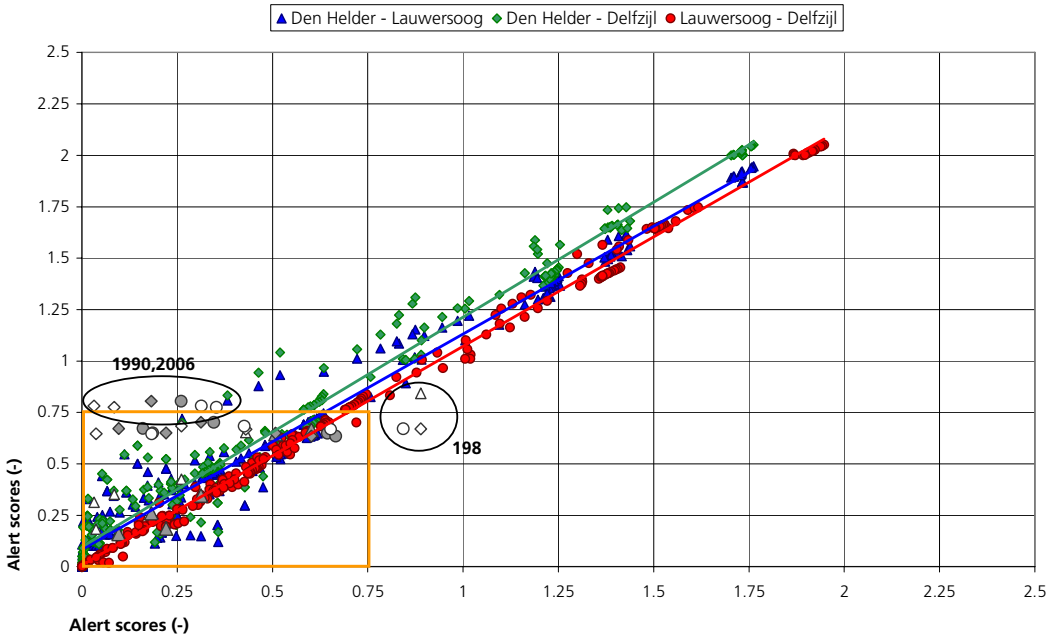

Figure 5.13 Scatter plot of alert scores at pairs of stations from Den Helder, Lauwersoog and Delfzijl. The amber square frames out the non-alerting events. Same notation as Figure 5.12.

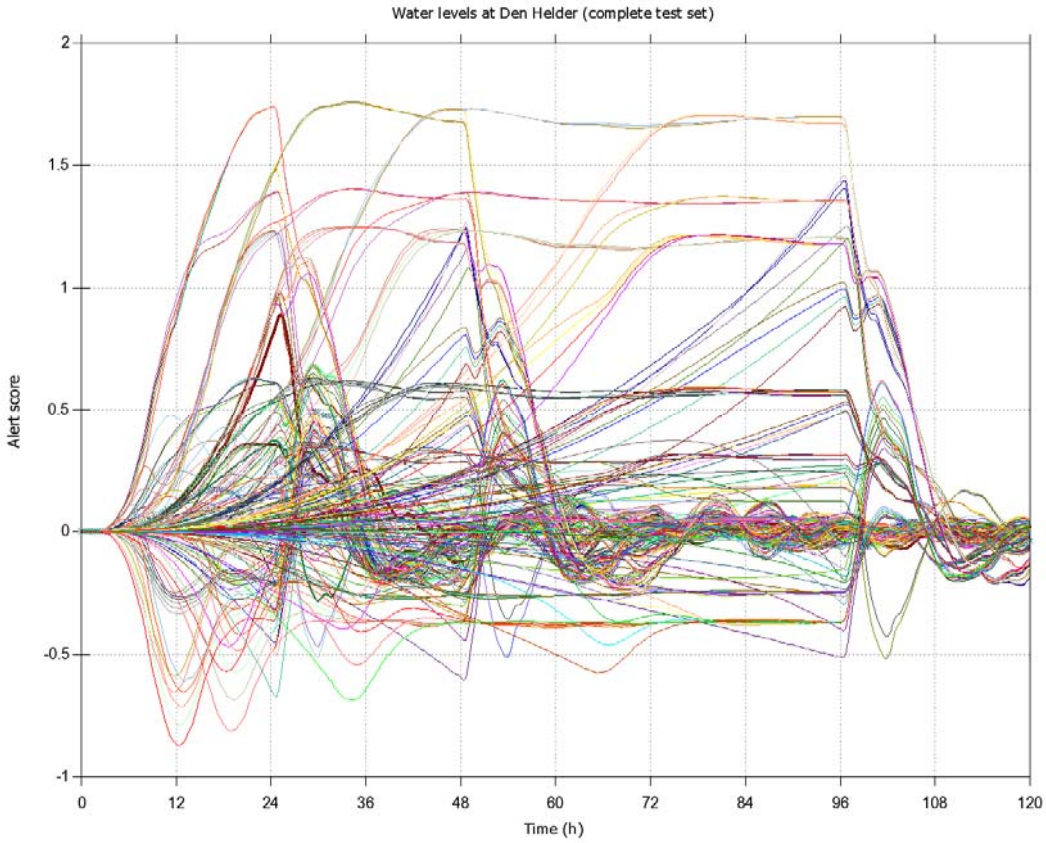

Figure 5.14 Alert scores at Den Helder (safety level 379 cm) for the complete windstorm test set. Windblown area: ZuNo. Nested-ZuNo flow results.

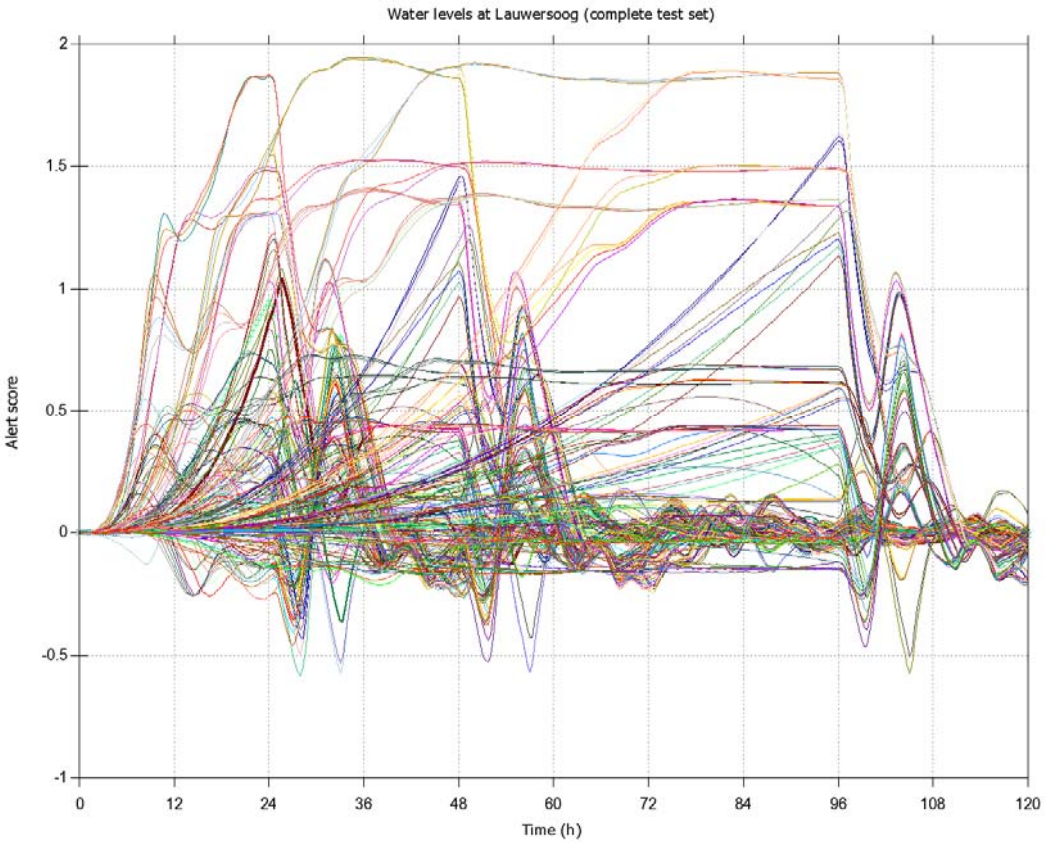

Figure 5.15 Alert scores at Lauwersoog (safety level 383 cm) for the complete windstorm test set. Windblown area: ZuNo. Nested-ZuNo flow results.

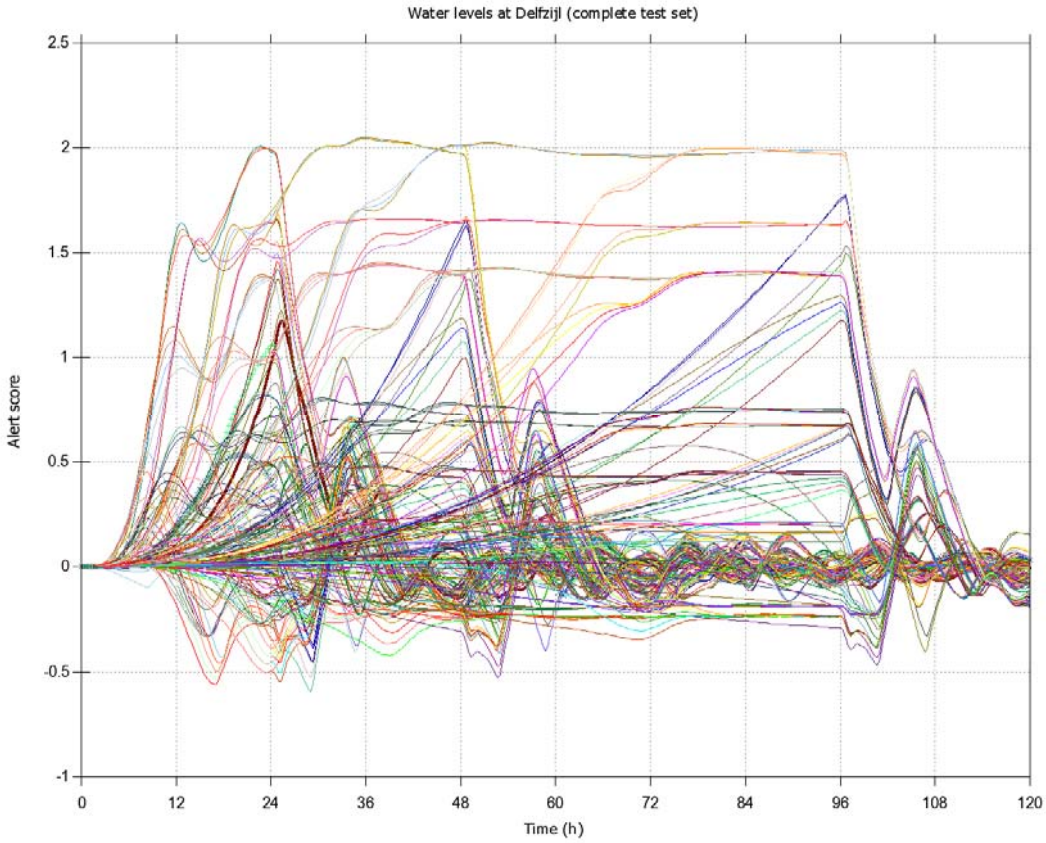

Figure 5.16 Alert scores at Delfzijl (safety level 449 cm) for the complete windstorm test set. Windblown area: ZuNo. Nested-ZuNo flow results.

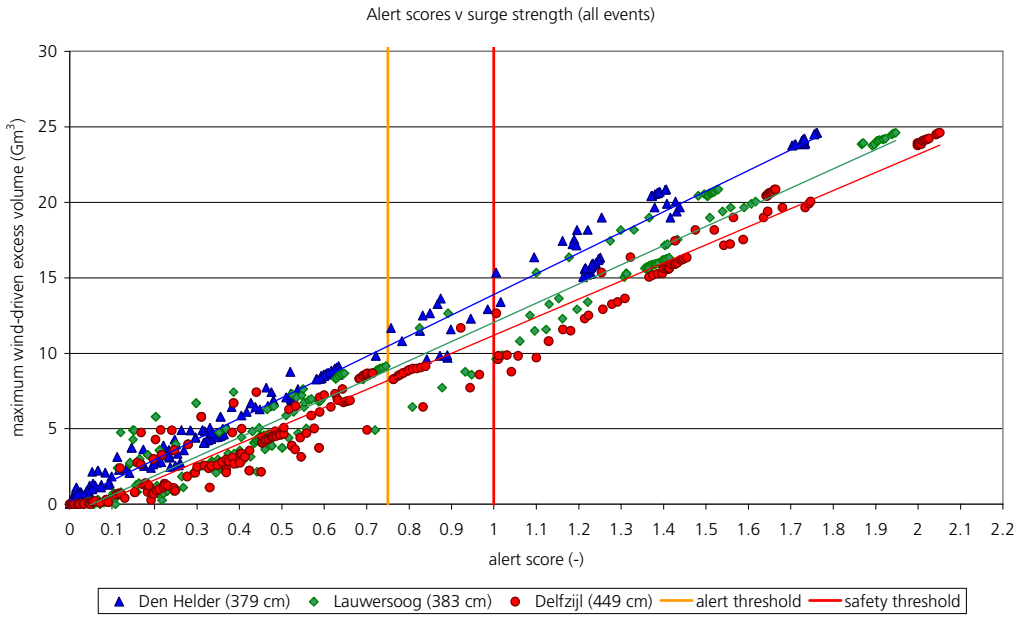

Figure 5.17 Framework chart for surges. Alert scores at the test station against the maximum wind-driven volume (surge strength). The water levels corresponding to the safety level (unity alert score) is given in the legend. Complete windstorm test-set. Windblown area: ZuNo. Nested-ZuNo flow results.

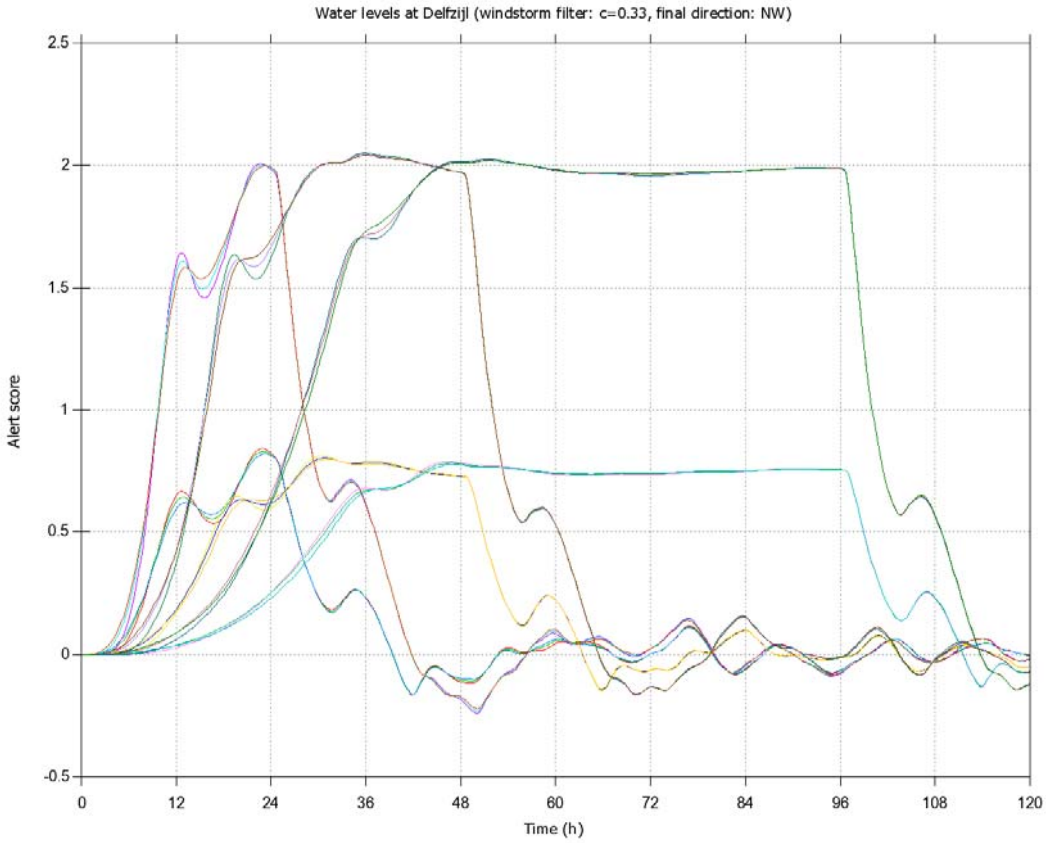

Figure 5.18 Alerting events at Delfzijl (safety level 449 cm) with 0.33 triangular fraction 0.33 and north-westerly final wind. Windblown area: ZuNo. Nested-ZuNo flow results.

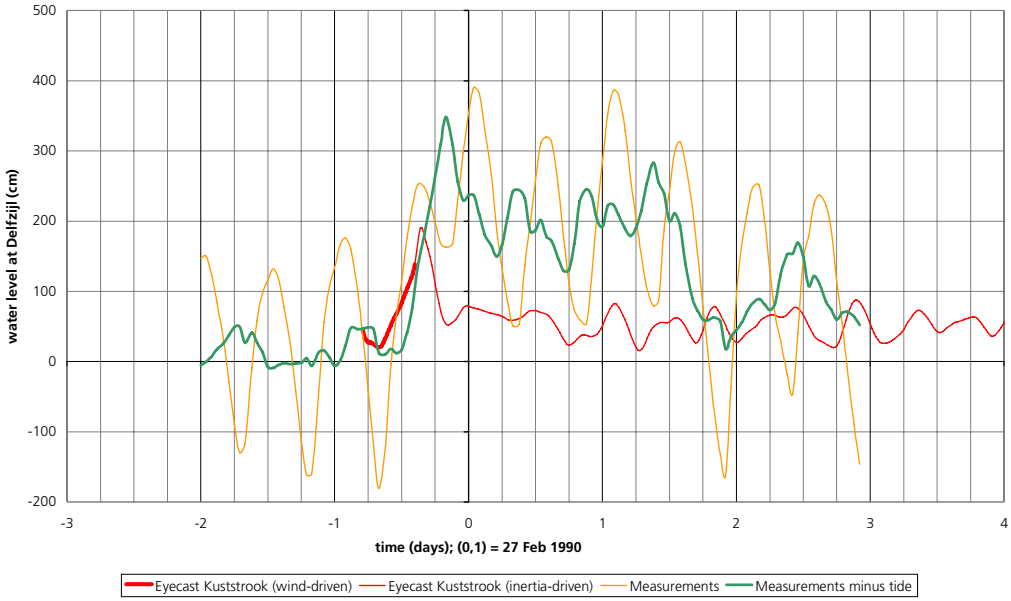

Figure 5.19 Eyecast and measured surge of 27 Feb 1990 at Delfzijl. Baseline case.

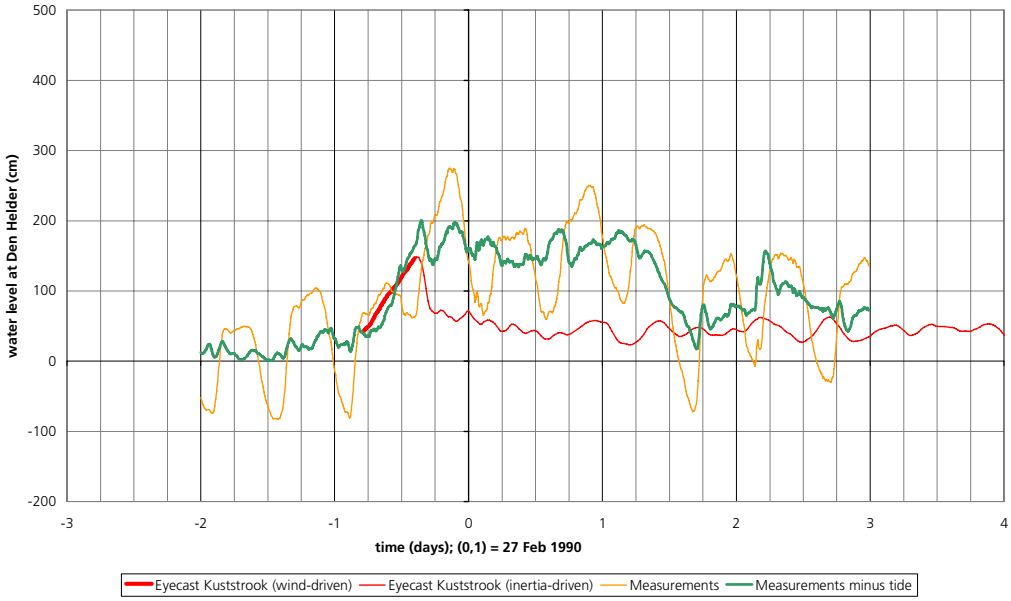

Figure 5.20 Eyecast and measured surge of 27 Feb 1990 at Den Helder. Baseline case.

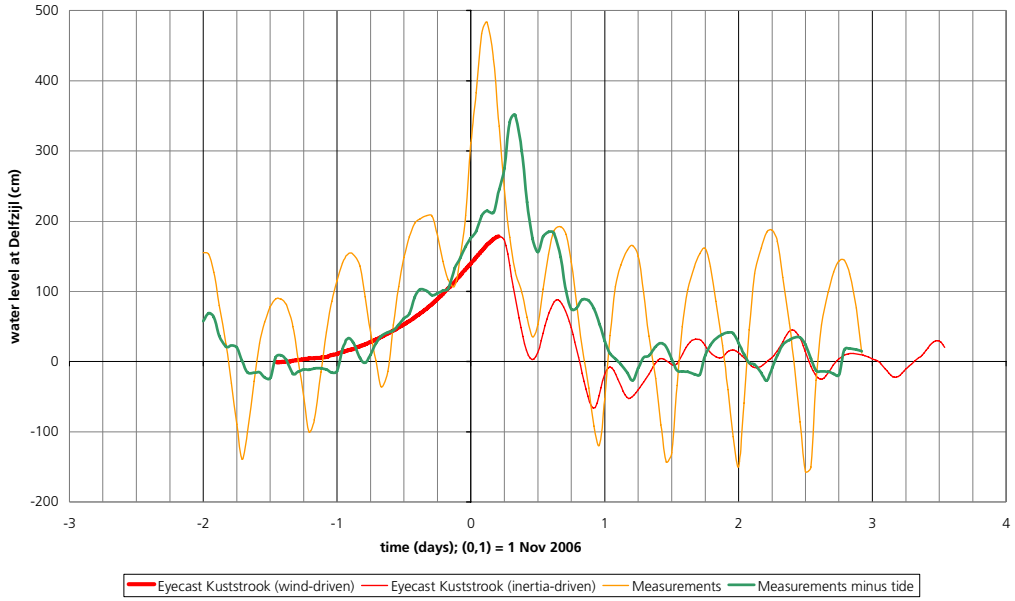

Figure 5.21 Eyecast and measured surge of 1 Nov 2006 at Delfzijl. Baseline case.

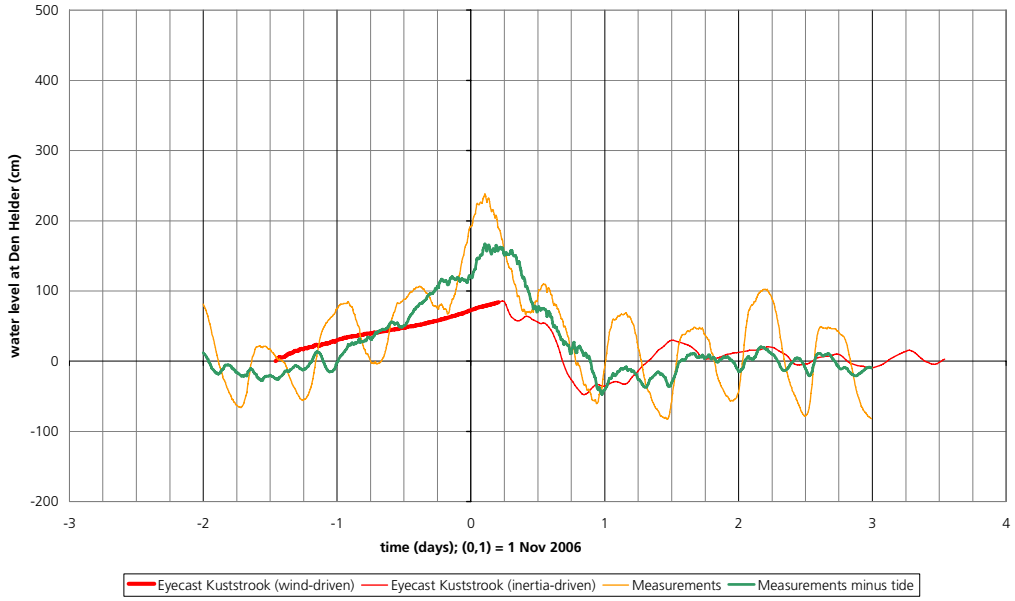

Figure 5.22 Eyecast and measured surge of 1 Nov 2006 at Den Helder. Baseline case.

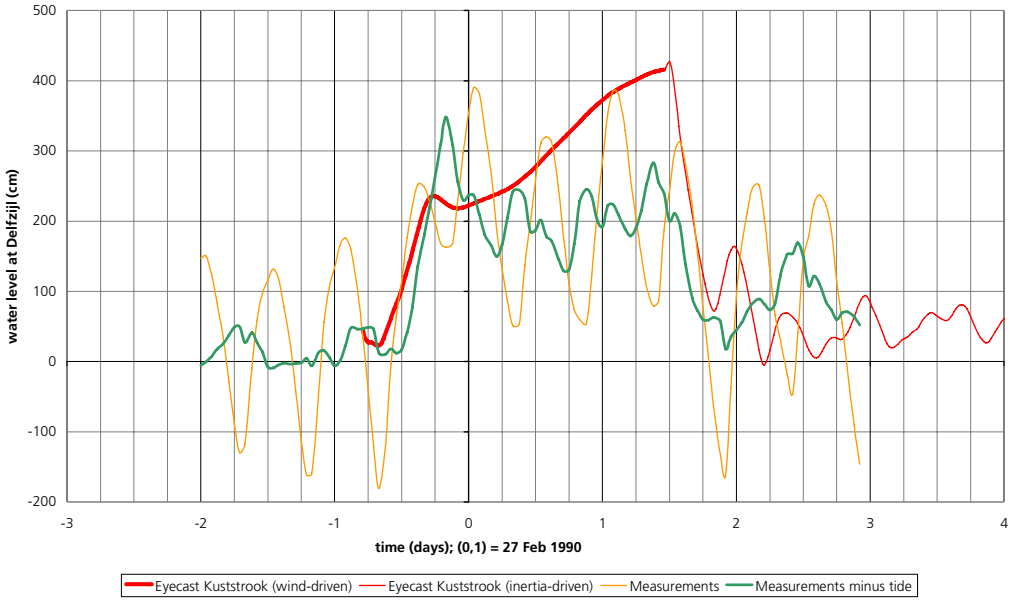

Figure 5.23 Eyecast and measured surge of 27 Feb 1990 at Delfzijl. Peak-speed variant.

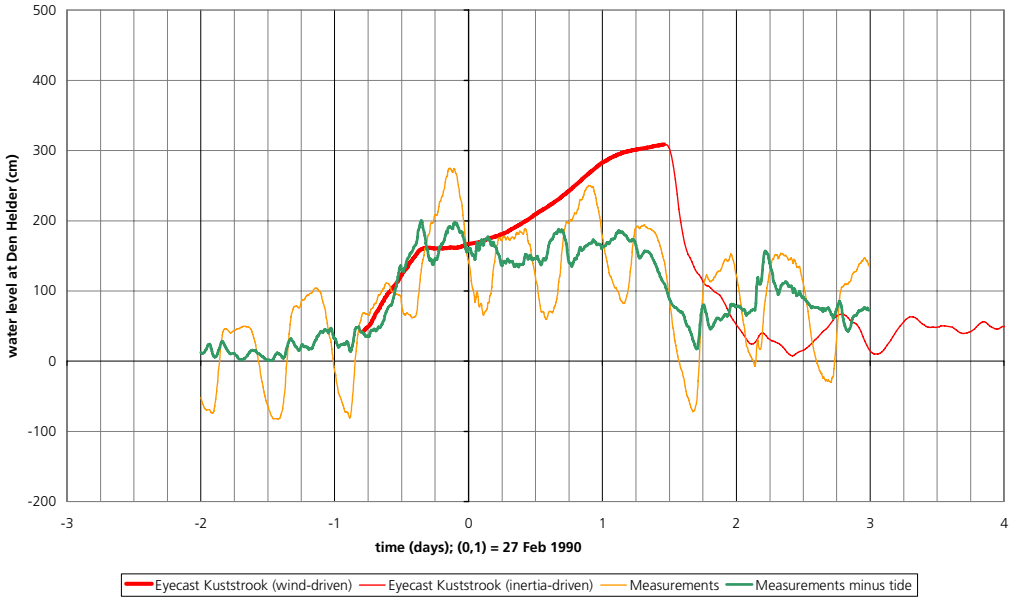

Figure 5.24 Eyecast and measured surge of 27 Feb 1990 at Den Helder. Peak-speed variant.

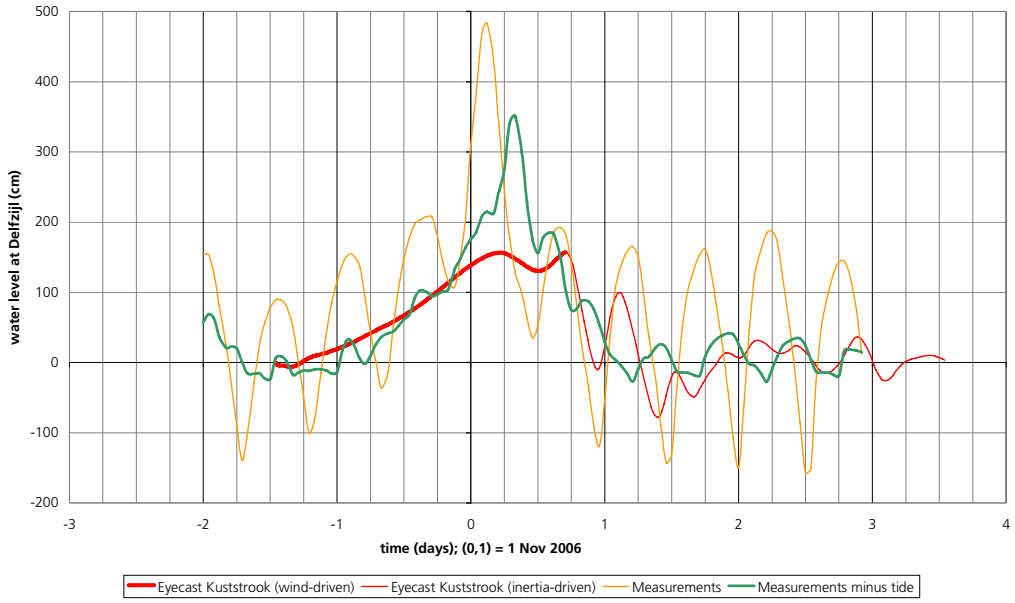

Figure 5.25 Eyecast and measured surge of 1 Nov 2006 at Delfzijl. Peak-speed variant.

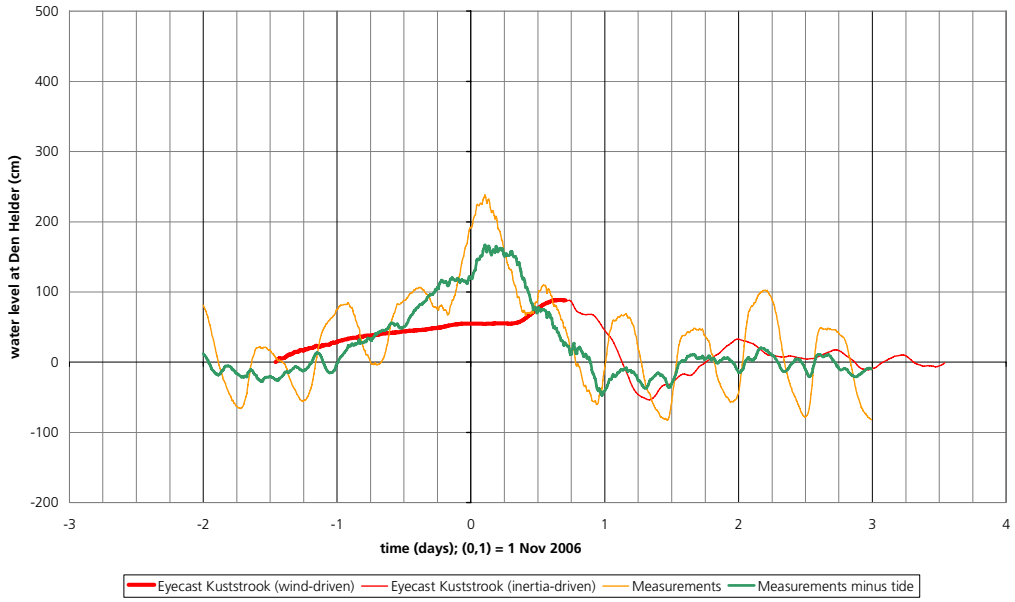

Figure 5.26 Eyecast and measured surge of 1 Nov 2006 at Den Helder. Peak-speed variant.

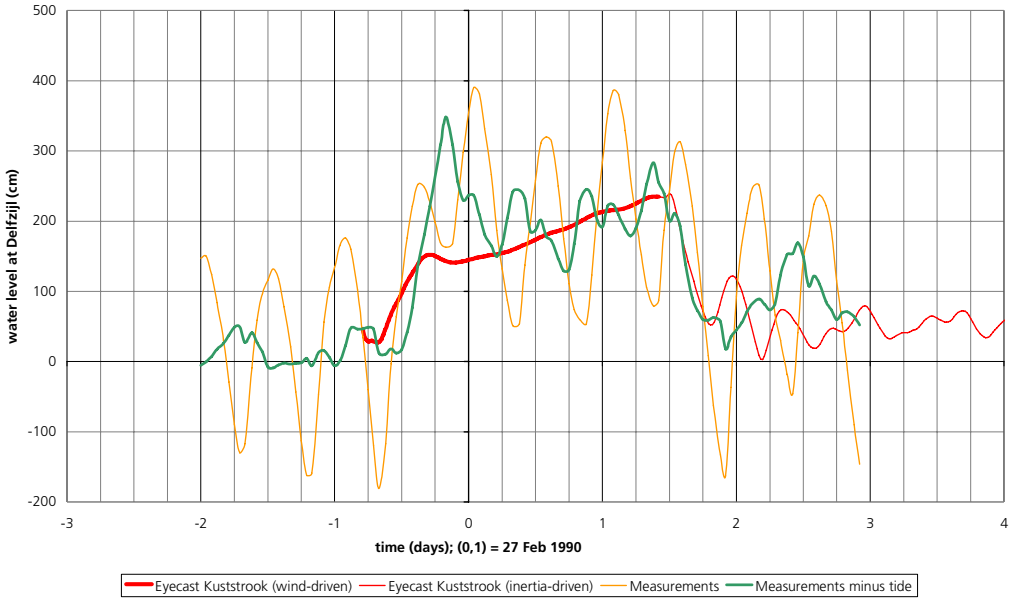

Figure 5.27 Eyecast and measured surge of 27 Feb 1990 at Delfzijl. Average-speed variant.

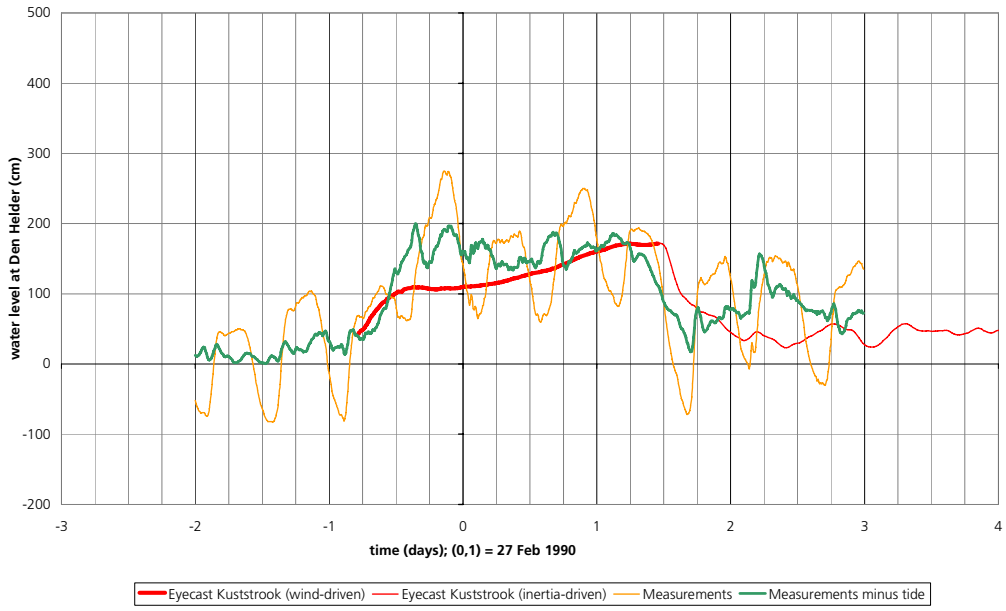

Figure 5.28 Eyecast and measured surge of 27 Feb 1990 at Den Helder. Average-speed variant.

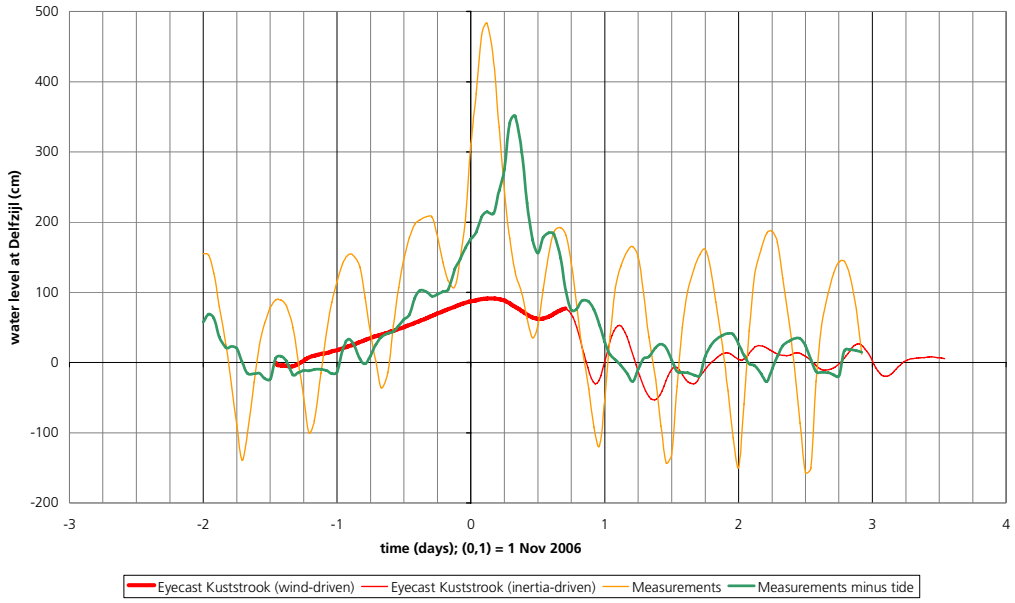

Figure 5.29 Eyecast and measured surge of 1 Nov 2006 at Delfzijl. Average-speed variant.

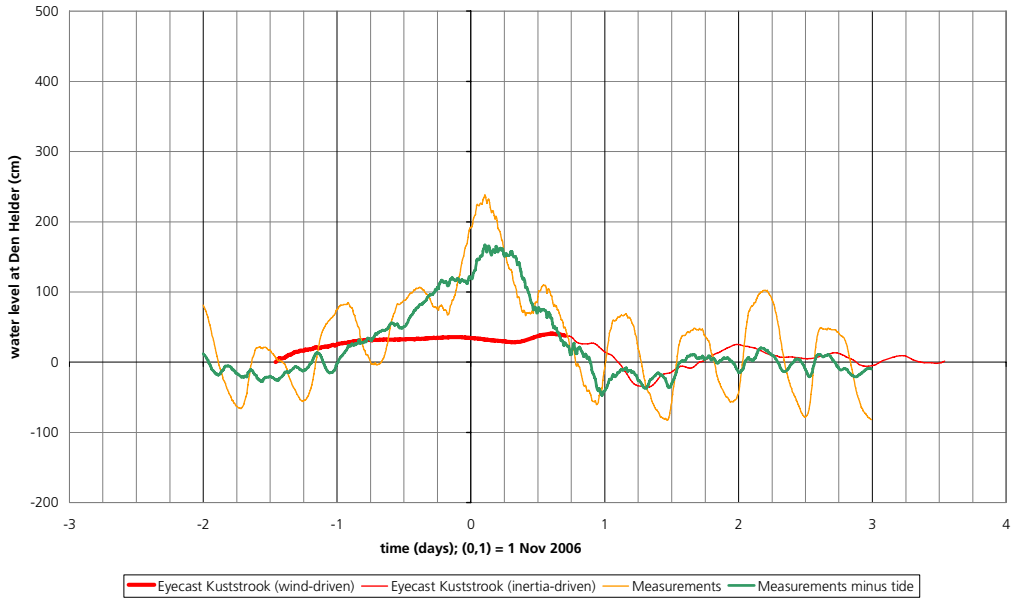

Figure 5.30 Eyecast and measured surge of 1 Nov 2006 at Den Helder. Average-speed variant.

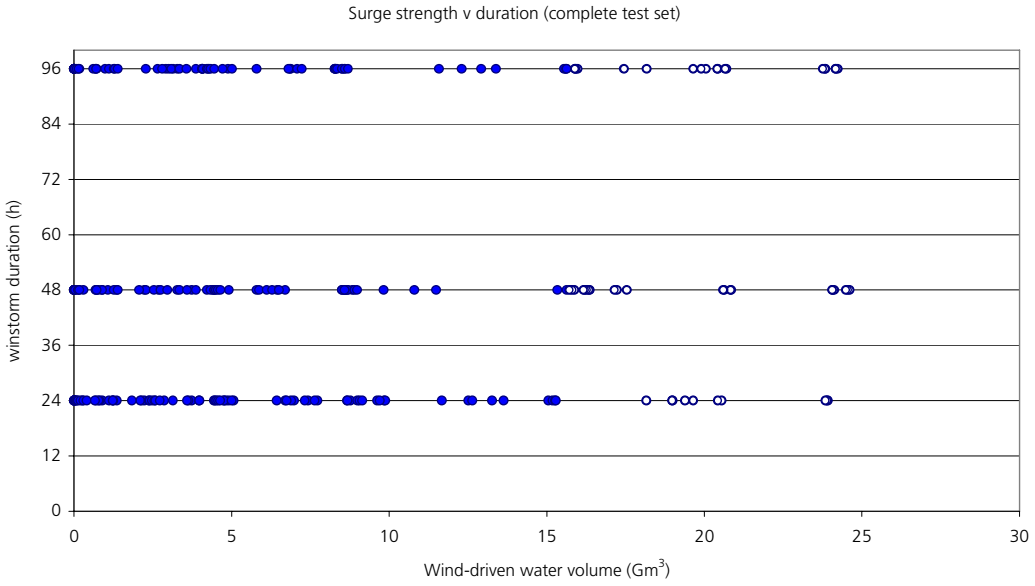

Figure 6.1 Surge strength and windstorm duration. Complete test set. Windblown area: ZuNo. Nested-ZuNo flow results. Open symbols: top-50 events.

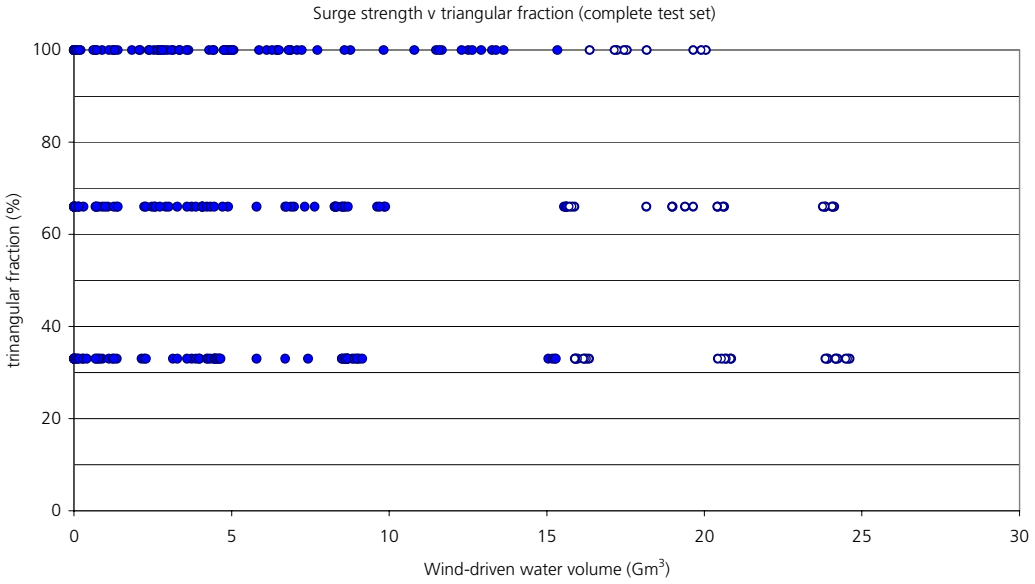

Figure 6.2 Surge strength and triangular fraction. Complete test set. Windblown area: ZuNo. Nested-ZuNo flow results. Open symbols: top-50 events.

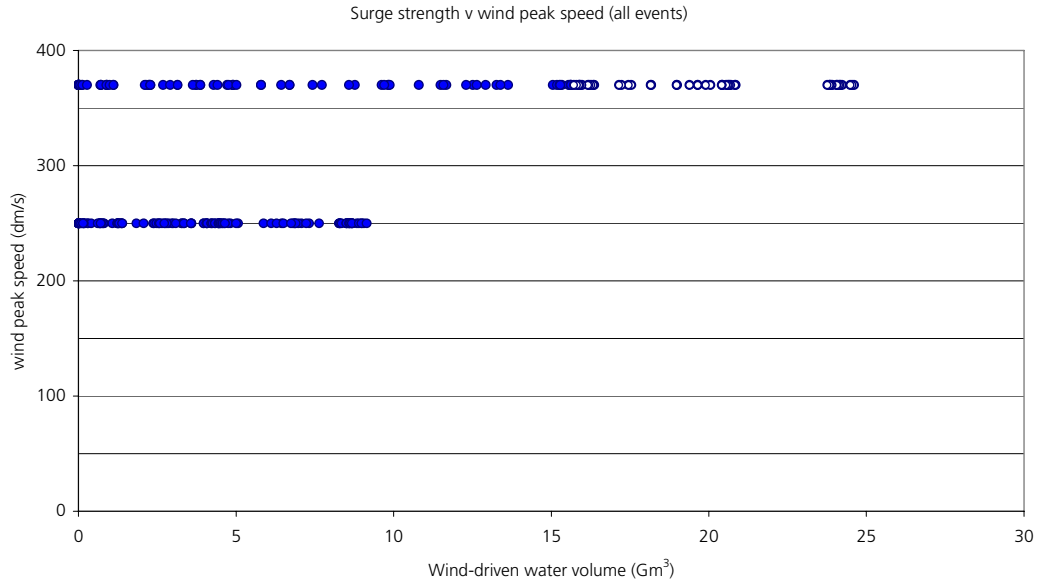

Figure 6.3 Surge strength and wind peak speed. Complete test set. Windblown area: ZuNo. Nested-ZuNo flow results. Open symbols: top-50 events.

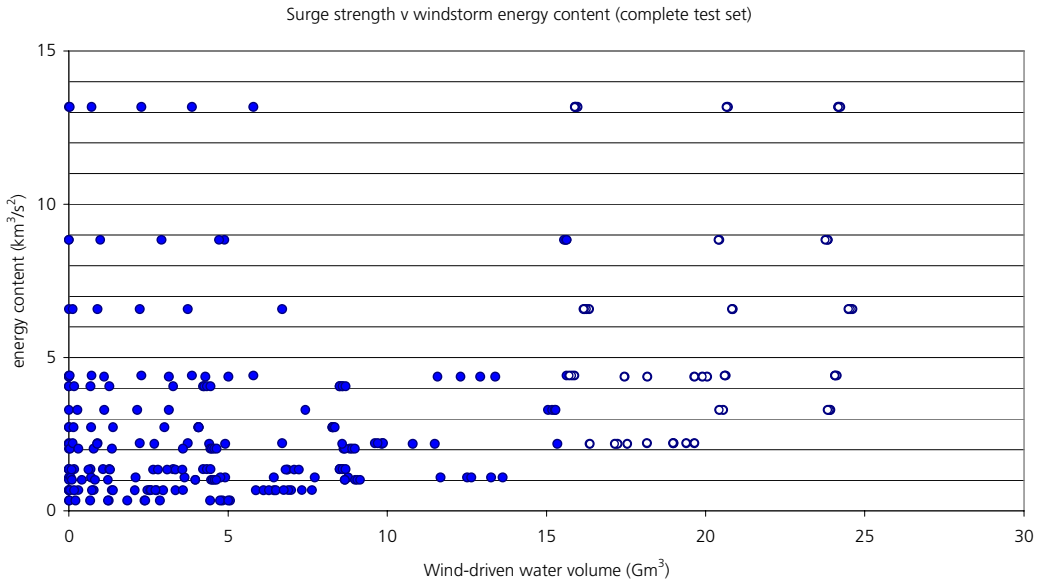

Figure 6.4 Surge strength and windstorm energy content. Complete test set. Windblown area: ZuNo. Nested-ZuNo flow results. Open symbols: top-50 events.

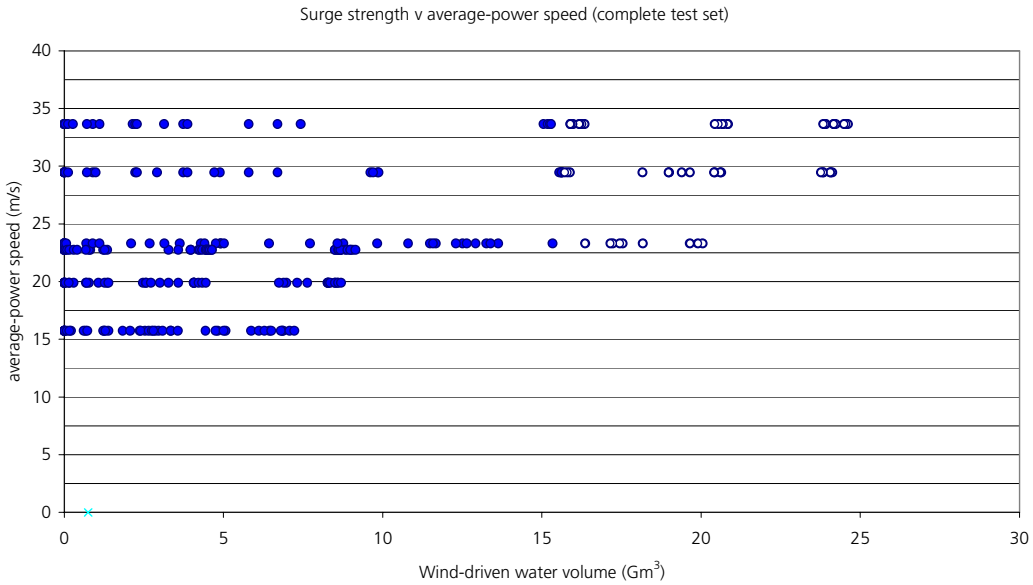

Figure 6.5 Surge strength and windstorm average-power speed. Complete test set. Windblown area: ZuNo. Nested-ZuNo flow results. Open symbols: top-50 events.

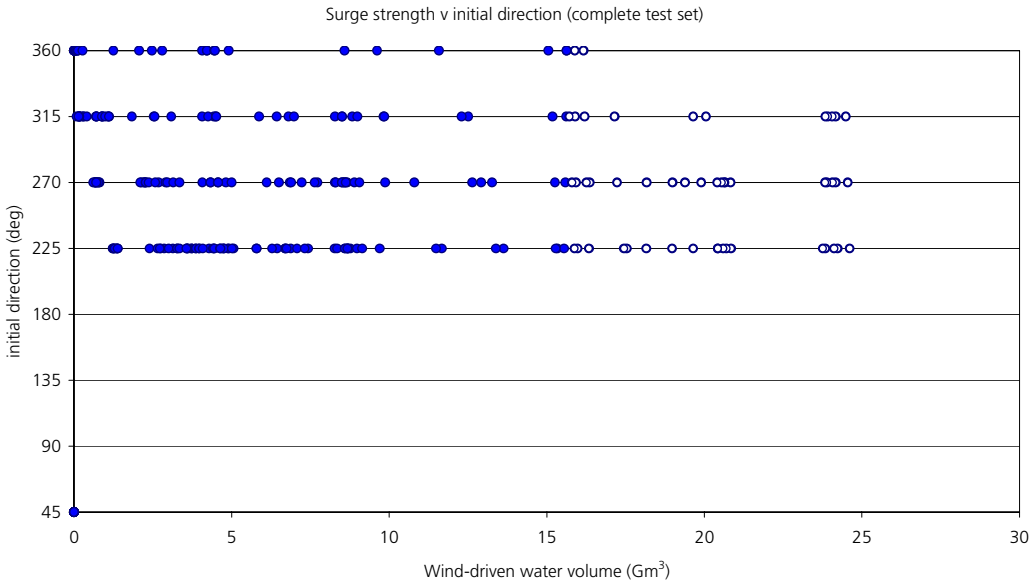

Figure 6.6 Surge strength and initial wind direction. Complete test set. Windblown area: ZuNo. Nested-ZuNo flow results. Open symbols: top-50 events.

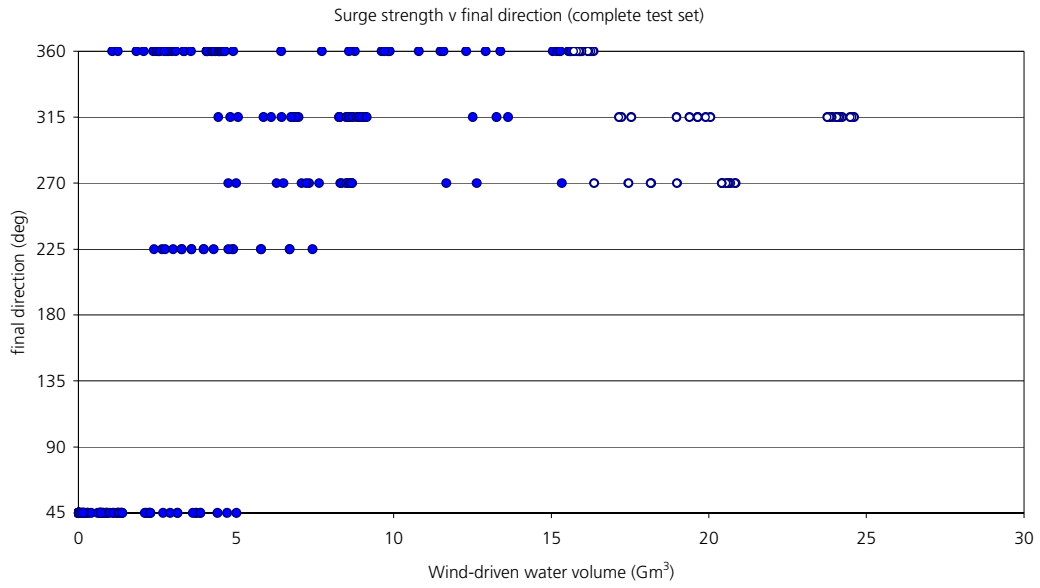

Figure 6.7 Surge strength and final wind direction. Complete test set. Windblown area: ZuNo. Nested-ZuNo flow results. Open symbols: top-50 events.

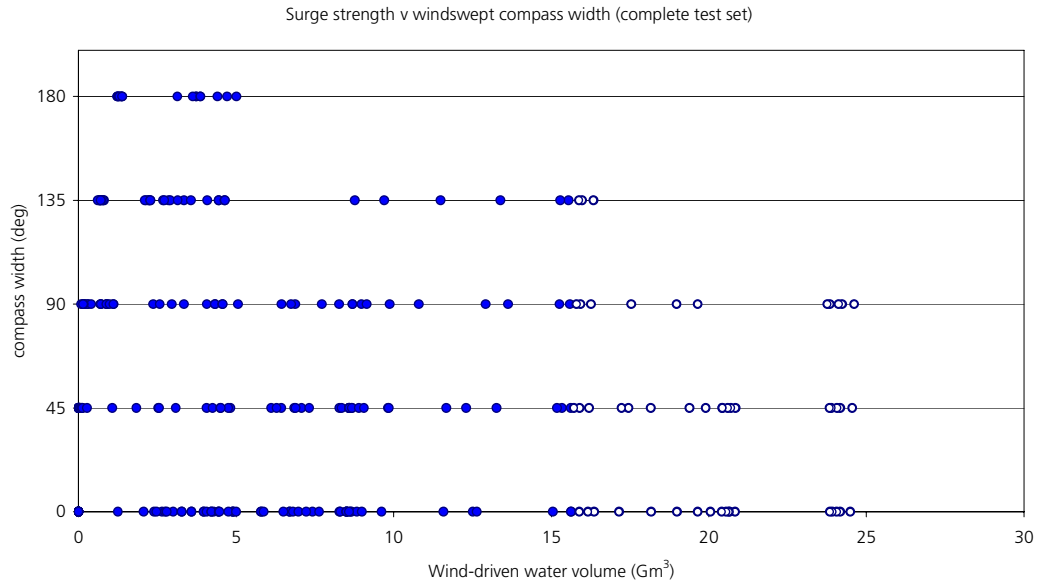

Figure 6.8 Surge strength and windswept compass width. Complete test set. Windblown area: ZuNo. Nested-ZuNo flow results. Open symbols: top-50 events.

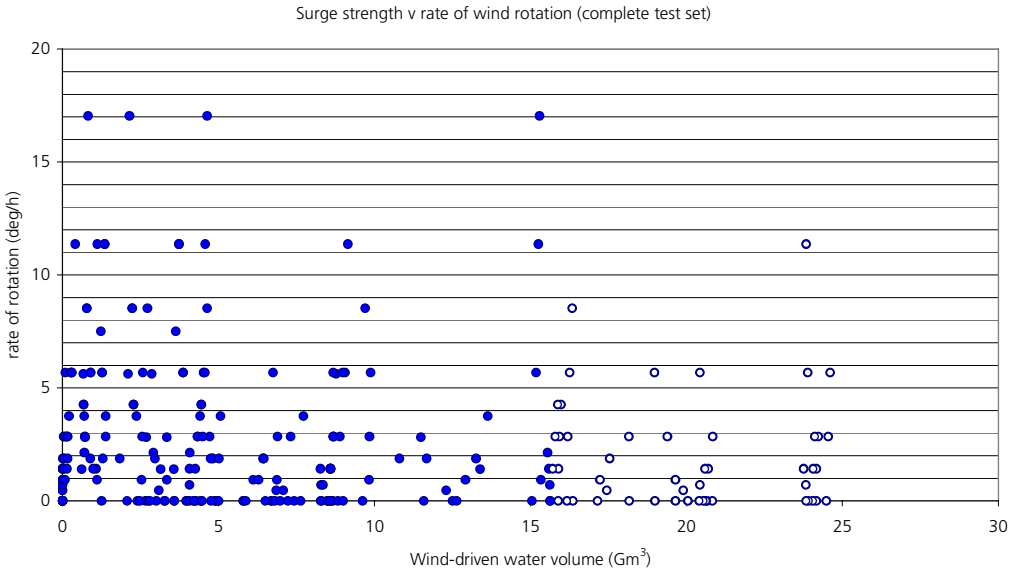

Figure 6.9 Surge strength and wind direction rate of rotation. Complete test set. Windblown area: ZuNo. Nested-ZuNo flow results. Open symbols: top-50 events.

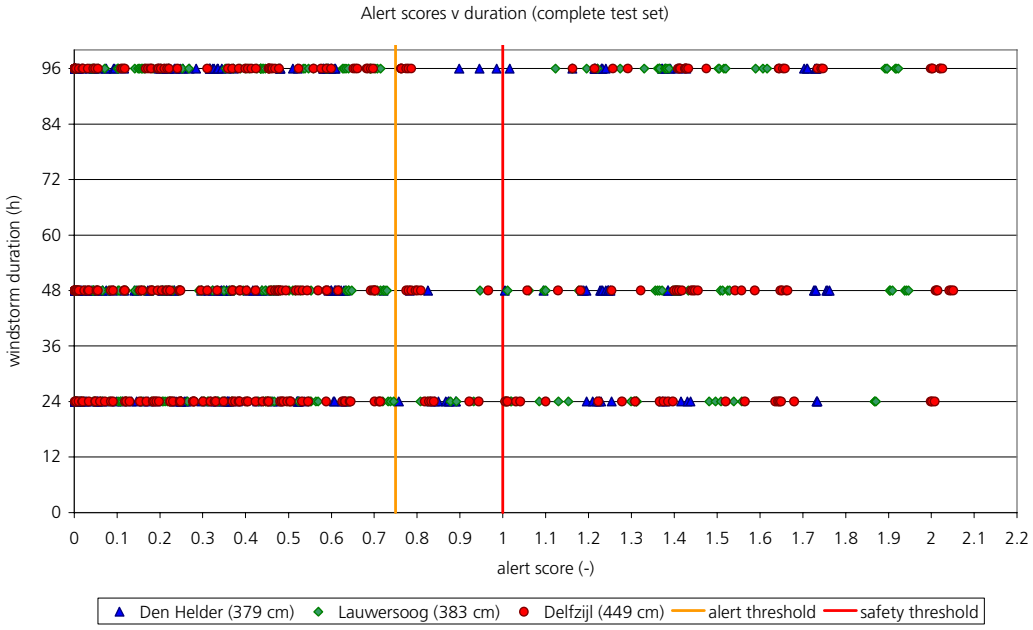

Figure 6.10 Alert scores at test stations and windstorm duration. Complete test set. Windblown area: ZuNo. Nested-ZuNo flow results.

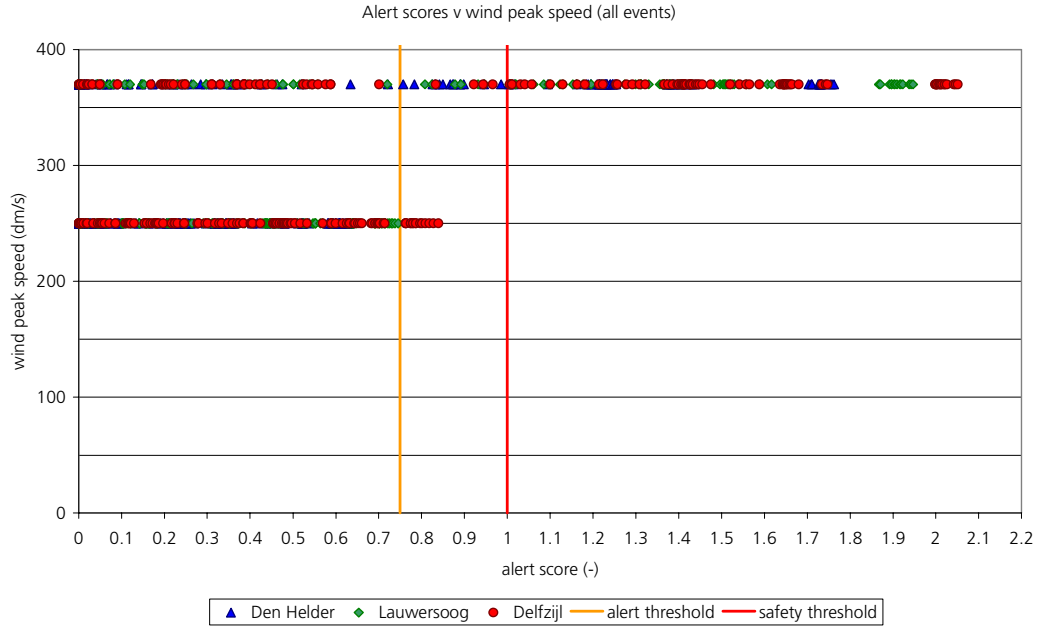

Figure 6.11 Alert scores at test stations and wind peak speed. Complete test set. Windblown area: ZuNo. Nested-ZuNo flow results.

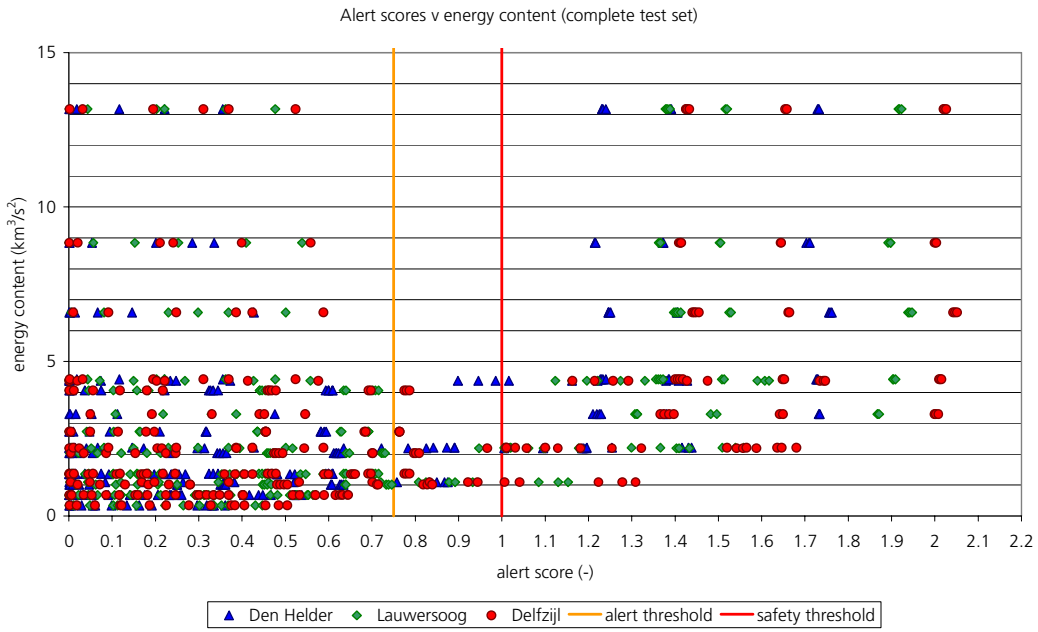

Figure 6.12 Alert scores at test stations and windstorm energy content. Complete test set. Windblown area: ZuNo. Nested-ZuNo flow results.

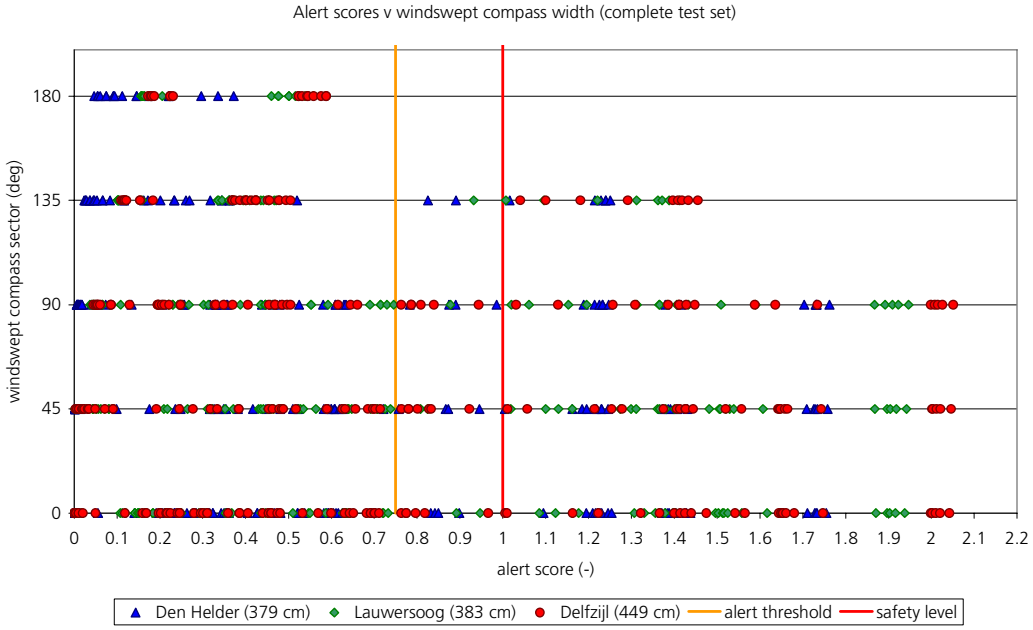

Figure 6.13 Alert scores at test stations and windswept compass width. Complete test set. Windblown area: ZuNo. Nested-ZuNo flow results.

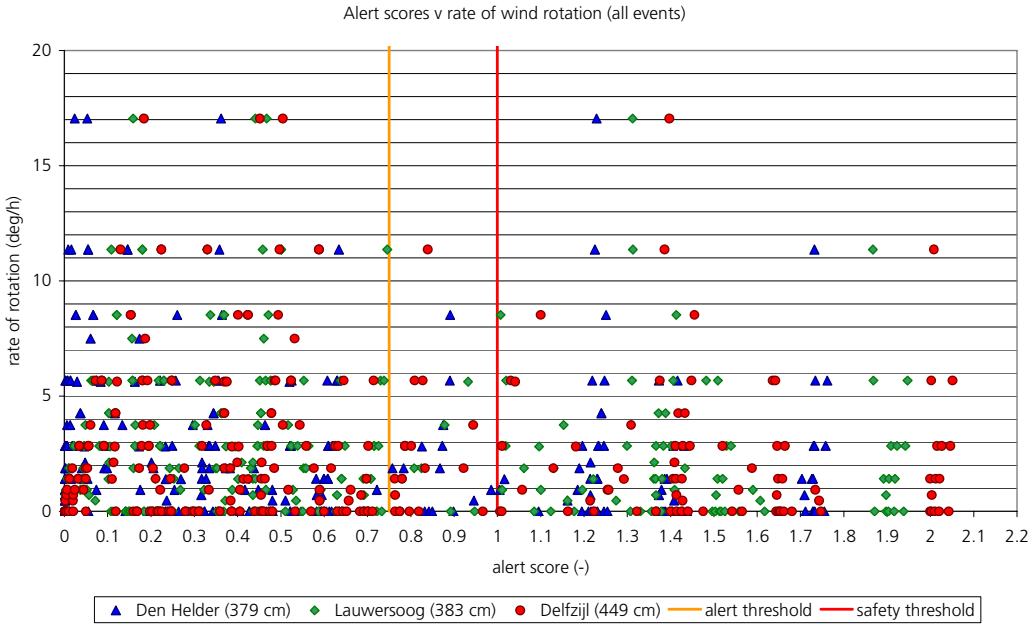

Figure 6.14 Alert scores at test stations and wind direction rate of rotation. Complete test set. Windblown area: ZuNo. Nested-ZuNo flow results.

Appendix A

H. Gerritsen's memo 'Opmerkingen bij Alkyon rapport A2239' 10 December 2008

H5100_20ReviewHG10Dec2008

memo

Aan : Jacco Groeneweg, Joost Beckers
Van : Herman Gerritsen
Betreft : Opmerkingen bij Alkyon rapport A2239
Datum : 10 december 2008
Kopie :
Afhandeling: t.u.b.

Deze notitie geeft de review van, c.q. commentaar op het concept rapport A2239: "Viability study of a prototype windstorm for the Wadden Sea surges".
Een eerste indruk van het rapport is op 5 december besproken met Joost Beckers, waarna het materiaal meer in detail is doorgenomen.

Beschikbaar materiaal:

- Bovengenoemd concept rapport A2239
- Offerteaanvraag Deltares, dd. 15 augustus 2008
- Alkyon proposal (uiteindelijk niet bekeken)

Perceptie van de klantvraag:
Op basis van de titel, samenvatting en hoofdstukken 1 en 2 van het rapport had ik behoefte aan een verduidelijking van de klantvraag.
Ik heb de klantvraag geïnterpreteerd als:

"Verifieer of de set van zes (in de aanvraag genoemde) parameters $\{\Theta_i; i=1,..6\}$ een nodige en voldoende set is om een prototype storm (="geparameteriseerde storm") te beschrijven, **in die zin dat daarmee alle relevante historische surge situaties in de Waddenzee "redelijk" gesimuleerd kunnen worden**"

Ik zou daarbij een aanpak verwachten in de trant van:

- Identificeer een reeks van (N) bekende historische karakteristieke stormvelden die tot gegeven relevante surge waardes is (M) representatieve stations in de Waddenzee hebben geleid. M is bijvoorbeeld 3: Den helder, Lauwersoog en Delfzijl.
- Probeer met een beperkt aantal voorwaartse berekeningen met een model voor Noordzee en Waddenzee, gedreven door de zes-parameterstorm, de parameterwaaarden $\{\Theta_i; i=1,..6\}$ te optimaliseren, waarbij de GoF gedefinieerd is als $GoF = 0.5\{\sum_{j=1}^{M} \frac{1}{M}\left(H_{j,sim} - H_{j,obs}\right)^2\}$
- Dit levert je N geoptimaliseerde sets, een overall geoptimaliseerde set, ranges voor alle parameters, plus het materiaal om te beoordelen of alle N gevallen (en daarmee in onze aanname alle relevante surges) in voldoende mate door dit geparameteriseerde uniforme stormveld kunnen worden gegenereerd
- Deze uitspraak bepaalt of het werken met een geparameteriseerde uniforme storm verantwoord ("viable") is of niet, en of die zes parameters inderdaad nodig en voldoende zijn
- Ter aanvulling: naar mijn mening is een zevende parameter nodig: het tijdstip dat de windrichting gaat draaien; dit is niet per definitie het moment dat de wind een vast percentage van zijn maximum heeft bereikt (denk aan 1953)

Dit is niet de aanpak van het rapport, zoals o.a. expliciet in het tweede bolletje in 2.3.1 is verwoord: dat zo'n schematische stormaanpak toepasbaar is, wordt bij voorbaat **aangenomen**. Dit komt ook terug in de laatste alinea van 2.3.2

Wellicht is mijn perceptie /verwachting echter niet correct, en was het ook niet de bedoeling om dit te toetsen, maar om te kijken wat je kunt met deze aanname.

In die zin heb ik het rapport verder doorgenomen.

Algemeen:

- Het rapport is uitgebreid, en leest voor een buitenstaander nogal moeilijk; het zou behoorlijk aan toegankelijkheid kunnen winnen door redactie van de tekst, nu de auteurs het even weggelegd hebben
- Bij zo'n redactie verdient het aanbeveling om het engels en de terminologie wat op te schonen: braces = brackets; probing stations = target stations; chance = probability, byname = name, framing tool = …. , etc.; enkelvoud/meervoud,.correct gebruik en weglaten van lidwoorden en van voorzetsels; maar ik erken dat dit geen inhoudelijk punt is
- Figuur 4.1 komt niet in de lijst voor; in de tekst worden veel figuren nog als 2.x aangeduid, waar dit 3.x moet zijn
- In tabel 4.1 hebben we zes parameters: duration T(h), ramp fraction (c), peak speed (u_p), alfa1, alfa2, omega. Dit bevat dezelfde informatie als de zes grootheden in de offerteaanvraag. Zou je niet een zevende parameter verwachten: het moment dat de ruiming inzet? Nu zet de draaiing blijkbaar per definitie in op t=0; zie bijvoorbeeld het geval (24, 100, 260, 360, 45, 45, 1.9, 0.34). Als c=100, hebben we dus nauwelijks invloed vanuit de initiële windrichting; dit lijkt me een te grote beperking voor richtingen zoals 225.
- Er is veel gesimuleerd en gedaan in termen van berekeningen, maar de interpretatie en conclusies zijn nog wat mager, althans niet zo helder verwoord ; dit zou per hoofdstuk moeten gebeuren
- Hoofdstuk 7 zou gebaat zijn bij een korte, puntsgewijze samenvatting van aannames en van de resultaten, e.g. de geïntroduceerde grootheden, de invloed van de gebiedsgrootte, etc. wat we nu echt hebben aan de figuren van hoofdstuk 3, etc.
- Ook is niet erg duidelijk wat we nu bijgedragen hebben aan het verder invullen van de Hydra-K vraag, en hoe we met deze resultaten verder moeten. Met name 7.3.4 geeft wel in erg grote lijnen aan wat we zouden kunnen doen. Is het mogelijk concretere, en behapbare zaken te formuleren.

Specifiek:

- "easternmost province of Friesland"?
- tabel 3.2: Als ik de formule ID = 1- u_{ap}/u_p toepas, kom ik op basis van de eerdere formules en definities op ID = 1-TRROOT(b) en niet op 1-1/(TRROOT(b)). De waarden op de derde rij worden daarmee 0, 2.6, 5.3, 8.8, 11.2, 14.5, 19.1, 22.0, 26.3, 31.3, 37.0
- In de formule in 3.2 heeft OMEGA per definitie een negatief teken; in de tabel 4.1 is OMEGA positief
- Tabel 6.2 en 6.3: "alert scores": dit moet wsh. zijn: maximum excess volumes
- Dezelfde tabellen: zou je niet verwachten dat bij de grootste energie inhoud (e) ook de hoogste "percentage occurrence" voorkomen? M.a.w. moeten de labels van de eerste en derde rij mogelijk omgewisseld worden?

NB; De introductie van de begrippen alert threshold, alert score en excess volume als proxies voor extreme surge waarden vind ik erg goed en practisch: dit maakt het probleem inderdaad meer behapbaar.

Overall conclusie:

- Redactie nodig; wellicht zinvol dat opdrachtnemer en opdrachtgever nog even samen bespreken wat de verwachtingspatronen over en weer waren, en zo tot een eindconclusie mbt. het rapport komen